UPPSALA
UNIVERSITET

Digital Comprehensive Summaries of Uppsala Dissertations from the Faculty of Science and Technology 828

Aqueous Solutions as seen through an Electron Spectrometer

Surface Structure, Hydration Motifs and Ultrafast Charge Delocalization Dynamics

NIKLAS OTTOSSON

ACTA
UNIVERSITATIS
UPSALIENSIS
UPPSALA
2011

ISSN 1651-6214
ISBN 978-91-554-8083-7
urn:nbn:se:uu:diva-151435

Dissertation presented at Uppsala University to be publicly examined in Polhemssalen, Ångström Laboratory, Lägerhyddsvägen 1, Uppsala, Wednesday, June 1, 2011 at 10:15 for the degree of Doctor of Philosophy. The examination will be conducted in English.

Abstract

Ottosson, N. 2011. Aqueous Solutions as seen through an Electron Spectrometer. Surface Structure, Hydration Motifs and Ultrafast Charge Delocalization Dynamics. Acta Universitatis Upsaliensis. *Digital Comprehensive Summaries of Uppsala Dissertations from the Faculty of Science and Technology* 828. 118 pp. Uppsala. ISBN 978-91-554-8083-7.

In spite of their high abundance and importance, aqueous systems are enigmatic on the microscopic scale. In order to obtain information about their geometrical and electronic structure, simple aqueous solutions have been studied experimentally by photo- and Auger electron spectroscopy using the novel liquid micro-jet technique in conjunction with synchrotron radiation. The thesis is thematically divided into three parts.

In the first part we utilize the surface sensitivity of photoelectron spectroscopy to probe the distributions of solutes near the water surface. In agreement with recent theoretical predictions we find that large polarizable anions, such as I^- and ClO_4^-, display enhanced surface propensities compared to smaller rigid ions. Surface effects arising from ion-ion interactions at higher electrolyte concentrations and as function of pH are investigated. Studies of linear mono-carboxylic acids and benzoic acid show that the neutral molecular forms of such weak acids are better stabilized at the water surface than their respective conjugate base forms.

The second part examines what type of information core-electron spectra can yield about the chemical state and hydration structure of small organic molecules in water. We demonstrate that the method is sensitive to the protonation state of titratable functional groups and that core-level lineshapes are dependent on local water hydration configurations. Using a combination of photoelectron and X-ray absorption spectroscopy we also show that the electronic re-arrangement upon hydrolysis of aldehydes yields characteristic fingerprints in core-level spectra.

In the last part of this thesis we study ultrafast charge delocalization dynamics in aqueous solutions using resonant and off-resonant Auger spectroscopy. Intermolecular Coulombic decay (ICD) is found to occur in a number of core-excited solutions where excess energy is transferred between the solvent and the solute. The rate of ultrafast electron delocalization between hydrogen bonded water molecules upon oxygen 1s resonant core-excitation is found to decrease upon solvation of inorganic ions.

The presented work is illustrative of how core-level photoelectron spectroscopy can be valuable in the study of fundamental phenomena in aqueous solutions.

Keywords: Water, Aqueous solutions, Ions, Molecular Hydration, Electron dynamics, Atmospheric Chemistry, Hydrolysis, Acid-Base Chemistry, Interatomic Coulombic Decay, ICD, Liquid Micro-Jet, X-ray Photoelectron Spectroscopy, XPS, Auger Electron Spectroscopy, AES, MAX-lab, BESSY

Niklas Ottosson, Department of Physics and Astronomy, Surface and Interface Science, Box 516, Uppsala University, SE-751 20 Uppsala, Sweden.

ISSN 1651-6214
ISBN 978-91-554-8083-7
urn:nbn:se:uu:diva-151435 (http://urn.kb.se/resolve?urn=urn:nbn:se:uu:diva-151435)

"In general, a scientific account of mythical substances is bound to disappoint. With water, that need not be so. Even when we remove its symbolic trappings, its association with purity, with the soul, with the maternal and with life and youth, when we reduce it to a laboratory chemical or a geological phenomenon, water continues to fascinate. At first glance a simple molecule, water still offers up profound challenges to science."

Philip Ball

"Det värsta man kan servera mig är isvatten. Vatten är giftigt. Det visste redan Jesus. Han förvandlade vatten till vin så fort han fick syn på det."

Sten Broman

Till mina föräldrar

List of Papers

This thesis is based on the following papers, which are referred to in the text by their Roman numerals.

I Photoelectron Spectroscopy of Liquid Water and Aqueous Solution: Electron Effective Attenuation Lengths and Emission-Angle Anisotropy
N. Ottosson, M. Faubel, S.E. Bradforth, P. Jungwirth, and B. Winter
Journal of Electron Spectroscopy and Related Phenomena, **177**: 60 (2010)

II Large Variations in the Propensity of Aqueous Oxychlorine Anions for the Solution/Vapor Interface
N. Ottosson, R. Vácha, E.F. Aziz, W. Pokapanich, W. Eberhardt, S. Svensson, G. Öhrwall, P. Jungwirth, O. Björneholm, and B. Winter
Journal of Chemical Physics, **131**: 124706 (2009)

III The Influence of Concentration on the Molecular Surface Structure of Simple and Mixed Aqueous Electrolytes
N. Ottosson, J. Heyda, E. Wernersson, W. Pokapanich, S. Svensson, B. Winter, G. Öhrwall, P. Jungwirth, and O. Björneholm
Physical Chemistry Chemical Physics (Cover article), **12**: 10693 (2010)

IV Increased Propensity of I^-_{aq} for the Water Surface in Non-Neutral Solutions: Implications for the Interfacial Behavior of $H_3O^+_{aq}$ and OH^-_{aq}
N. Ottosson, L. Cwiklik, J. Söderström, O. Björneholm, G. Öhrwall, and P. Jungwirth
Journal of Physical Chemistry Letters, **2**: 972 (2011)

V The Protonation State of Small Carboxylic Acids at the Water Surface from Photoelectron Spectroscopy
N. Ottosson, E. Wernersson, J. Söderström, W. Pokapanich, S. Kaufmann, S. Svensson, I. Persson, G. Öhrwall, and O. Björneholm
Submitted

VI Molecular Sinkers: X-ray Photoemission and Atomistic Simulations of Benzoic Acid and Benzoate at the Aqueous Solution/Vapor Interface
N. Ottosson, A.O. Ramonova, J. Söderström, G. Öhrwall, O. Björneholm, and M.V. Fedorov
Submitted

VII On the Origins of Core-Electron Chemical Shifts of Small Biomolecules in Aqueous Solution: Insights from Photoemission and Ab Initio Calculations of $\text{Glycine}_{\text{aq}}$
N. Ottosson, K.J. Børve, D. Spångberg, H. Bergersen, L.J. Sæthre, M. Faubel, W. Pokapanich, G. Öhrwall, O. Björneholm, and Bernd Winter
Journal of the American Chemical Society, **133**: 3120 (2011)

VIII An Electronic Signature of Hydrolysation in the X-ray Absorption Spectrum of Aqueous Formaldehyde
N. Ottosson, E.F. Aziz, I.L. Bradeanu, S. Legendre, G. Öhrwall, S. Svensson, O. Björneholm, and W. Eberhardt
Chemical Physics Letters, **460**: 540 (2008)

IX Electronic Re-Arrangement Upon the Hydrolyzation of Aqueous Formaldehyde Studied by Core-Electron Spectroscopies
N. Ottosson, E.F. Aziz, H. Bergersen, W. Pokapanich, G. Öhrwall, S. Svensson, W. Eberhardt, and O. Björneholm
Journal of Physical Chemistry B, **112**: 16642 (2008)

X Interaction Between Liquid Water and Hydroxide Revealed by Core-Hole De-Excitation
E.F. Aziz, N. Ottosson, M. Faubel, I.V. Hertel, and B. Winter
Nature, **455**: 89 (2008)

XI Bond-Breaking, Electron-Pushing and Proton-Pulling: Active and Passive Roles in the Interaction

between Aqueous Ions and Water as Manifested in the O 1s Auger Decay
W. Pokapanich, N. Ottosson, S. Svensson, O. Björneholm, B. Winter and G. Öhrwall
Submitted

XII Cations Strongly Reduce Electron Hopping-Times in Aqueous Solutions
N. Ottosson, M. Odelius, D. Spångberg, W. Pokapanich, M. Svanqvist, G. Öhrwall, B. Winter, and O. Björneholm
Submitted

XIII Charge Dependence of Solvent-Mediated Intermolecular Coster-Kronig Decay Dynamics of Aqueous Ions
G. Öhrwall, N. Ottosson, W. Pokapanich, S. Legendre, S. Svensson, and O. Björneholm
Journal of Physical Chemistry B, **114**: 17057 (2010)

Reprints were made with permission from the publishers.

The following is a list of publications to which I have contributed to but which will not be covered in this thesis.

Extended bibliography

1. pH-Induced Protonation of Lysine in Aqueous Solution Causes Chemical Shifts in X-ray Photoelectron Spectroscopy
   D. Nolting, E.F. Aziz, N. Ottosson, M. Faubel, I.V. Hertel, and B. Winter
   Journal of the American Chemical Society, **129**: 14068 (2007)

2. Pseudoequivalent Nitrogen Atoms in Aqueous Imidazole Distinguished by Chemical Shifts in Photoelectron Spectroscopy
   D. Nolting, N. Ottosson, M. Faubel, I.V. Hertel, and B. Winter
   Journal of the American Chemical Society, **130**: 8150 (2008)

3. Electron Dynamics in Charge-Transfer-to-Solvent States of Aqueous Chloride Revealed by Cl^- 2p Resonant Auger-Electron Spectroscopy
   B. Winter, E.F. Aziz, N. Ottosson, M. Faubel, N. Kosugi, and I.V. Hertel
   Journal of the American Chemical Society, **130**: 7130 (2008)

4. Cation-Specific Interactions with Carboxylate in Amino Acid and Acetate Aqueous Solutions: X-ray Absorption and Ab Initio Calculations
   E.F. Aziz, N. Ottosson, S. Eisebitt, W. Eberhardt, B. Jagoda-Cwiklik, R. Vácha, P. Jungwirth, and B. Winter
   Journal of Physical Chemistry B (Cover article), **112**: 12567 (2008)

5. Solvent Effect of Alcohols at the L-edge of Iron in Solution: X-ray Absorption and Multiplet Calculations
   S. Bonhommeau, N. Ottosson, W. Pokapanich, S. Svensson, W. Eberhardt, O. Björneholm, and E.F. Aziz
   Journal of Physical Chemistry B, **112**: 12571 (2008)

6. Probing the Electronic Structure of Hemoglobin's Active Centre in Physiological Solutions

E.F. Aziz, N. Ottosson, S. Bonhommeau, N. Bergmann, W. Eberhardt, and M. Chergui
Physical Review Letters, **102**: 068103 (2009)

7. Vattnet inpå livet *(Popular scientific paper in Swedish)*
N. Ottosson
Forskning och Framsteg (Cover article), **6**: 43 (2009)

8. Functionalized Nanoparticles in Aqueous Surroundings Probed by X-ray Photoelectron Spectroscopy
J. Söderström, N. Ottosson, W. Pokapanich, G. Öhrwall, and O. Björneholm
Journal of Electron Spectroscopy and Related Phenomena (In press)

9. Ionic-charge Dependence of the Intermolecular Coulombic Decay Time-Scale for Aqueous Ions Probed by the Core-Hole Clock
W. Pokapanich, N.V. Kryzhevoi, N. Ottosson, S. Svensson, L.S. Cederbaum, O. Björneholm, and G. Öhrwall
Submitted

Preface

This doctoral thesis presents a number of soft X-ray-based core-electron spectroscopic studies of simple aqueous solutions. All experiments have been performed between 2007-2011 at the MAX-lab and BESSY synchrotron facilities during my time as a Ph.D. student in the Division of Molecular and Condensed Matter Physics at the Department of Physics and Astronomy, Uppsala University. While future practical applications of some of the presented results are conceivable this work constitutes a piece of fundamental research. Me and my colleagues have been driven by a scientific curiosity, to address long-standing problems in fundamental physical chemistry of the aqueous phase with new spectroscopic tools. Luckily, we have had the privilege to work with some outstanding theoreticians who have both deepened our knowledge and put our experimental findings on solid ground. As a result, the last fours years have been an exciting – at times frustrating – but, all in all, very rewarding journey. On the following pages I have done my best to summarize the essence of all that we have learnt during the way, however knowing it to be a nearly impossible endeavor. Thanks for reading anyway!

Comments on my own participation

The work here presented is the result of cooperative efforts, and I am grateful for the contributions and endless support of my colleagues. The common denominator for all papers is that I have actively taken part in performing the experiments. Generally, my degree of participation is reflected in my position in the author list. For the papers of which I am the lead author I have had the main responsibility for planning the experimental part of the study, performing the experiments and subsequent data analysis as well as writing up the paper. For paper VII I also performed XPS spectrum calculations under the supervision of my more computationally inclined co-authors.

Niklas Ottosson
Uppsala, April 2011

Contents

Preface 11
1 Introduction 15
2 Background and some essential concepts 19
2.1 Some general remarks on the physical chemistry of the liquid phase 19
2.2 Water; the molecule and the aqueous phase 20
2.3 Aqueous solutions: Thermodynamics and microscopic structure 24
2.3.1 Inorganic aqueous salt solutions 25
2.3.2 Aqueous solutions of molecules 26
3 Experimental methods and setups 29
3.1 X-ray photoabsorption, photoionization and some possible pathways of de-excitation 29
3.2 Core-electron spectroscopies 32
3.3 Spectroscopy of liquids using soft X-rays – prospects and challenges 35
3.4 Synchrotron radiation – why it's worth leaving town to get hold of the X-rays elsewhere! 37
3.5 Liquid photoelectron spectroscopy at beamline I-411, MAX-lab 40
3.6 Liquid photoemission at U-41 PGM, BESSY 41
3.7 LIQUIDROM – Liquid NEXAFS at BESSY 42
3.8 Spectral lineshapes and fitting 44
4 Distribution of solutes at the aqueous solution/vapor interface 47
4.1 Why bother about aqueous surfaces? 47
4.2 The Gibbs adsorption equation 48
4.3 The microscopic surface structure of aqueous electrolytes . 50
4.4 How to probe the distribution of solutes at the water surface using photoelectron spectroscopy 53
4.5 XPS studies of inorganic ions at the water surface 56
4.5.1 Effects of anion size and polarizability 57
4.5.2 Effects of ion-ion interactions at higher concentrations 59
4.5.3 Effects of pH 64

4.6 XPS studies of weak organic acids at the water surface . . . 66
4.6.1 Linear mono-carboxylic acids at the water surface . . . 67
4.6.2 Surface conformations of aqueous benzoic acid and benzoate . . . 70
5 Core-electron spectroscopies as probes of molecular protonation state and local hydration structure . . . 73
5.1 Core-level photolines of aqueous solutes . . . 74
5.2 Investigations into the information content in core-level spectra of a small biomolecule in water . . . 76
5.3 Core-electron probes of electronic structure modifications upon hydrolysis of formaldehyde . . . 80
6 Ultrafast electron dynamics in aqueous solutions seen through core-hole de-excitation processes . . . 83
6.1 The Auger process revisited . . . 83
6.1.1 ICD – a peculiar relaxation pathway in the condensed phase . . . 84
6.1.2 *What's the time?* – The core-hole clock and some of its applications . . . 85
6.2 What can O1s core-hole de-excitation in OH^-_{aq} tell about its hydrogen bonding patterns? . . . 87
6.3 Hole- and electron delocalization dynamics in water and aqueous electrolytes . . . 90
6.4 Ultrafast delocalized Coster-Kronig processes in aqueous cations . . . 94
7 Conclusions and Outlook . . . 97
8 Populärvetenskaplig sammanfattning . . . 101
9 Acknowledgments . . . 107
10 Bibliography . . . 109

1. Introduction

Water is as ordinary to the rest of the human race as it is strange to those scientists dedicated to the study of its chemical and physical properties. If it hadn't been for its huge importance for life, the scientific study of liquid water would perhaps just have been an academic trifle. But reality is different – water covers most of the Earth's surface; gaseous in the humid atmosphere, liquid in the lakes and oceans as well as solid in the polar ices and glaciers. Its unusual physical properties to a large extent regulate our planet's complex climate; the large heat capacity makes water act as a global thermostat – cooling during the summer and warming at winter – while its peculiar density variations with temperature keeps the bottom of lakes and oceans from freezing, a necessary condition for aquatic life as we know it. We are so well acquainted with water that most people have a hard time believing that today's chemists and physicists haven't yet got a solid understanding of the microscopic origin of its macroscopic properties. But everyday exposure does not in itself bring knowledge about a material's molecular structure. Neither does the omnipresence of liquid water on planet Earth simplify our scientific investigations of it (except that experimental samples are cheap and easy to come by).

Even though it is the most common chemical compound on Earth's surface, water seldom exists in its pure form; normally it appears as aqueous solutions. We may for example note that the oceans contain $\sim$97% of all the planet's liquid water. Seawater constitutes a complex aqueous electrolyte with an average salt concentration of 0.5 molar – while the dominating solute is NaCl there are other ions in there as well; NH_4^+, Mg^{2+}, Br^- and SO_4^{2-} to mention some of the most abundant. We should also not forget that we ourselves, to a large extent, are made up from aqueous solutions. It is almost a trivial notion that biochemical processes in the human body (as well as those in all other known life forms), such as the folding of proteins to their functional states and ion transport across semipermeable membranes, cannot run 'dry' and are dependent on water's excellent properties as a solvent.

The fact that aqueous systems are both so common and important, but at the same time behave so odd has naturally sparked the interest of many scientists throughout history. Today we know that many of the fascinating properties of liquid water stem from its exceptional ability to form hydrogen (H) bonds, the primary interaction between the constituent molecules. Numerous questions concerning the molecu-

lar structure of aqueous solutions however still remain, at least partly, unanswered: How does various aqueous solutes influence the electronic structure of the solvating water molecules? What are the dominant solvation patterns of water's own ions, H_3O^+ and OH^-, and what is the exact nature of their respective transport mechanisms? What factors determine the propensity of aqueous solutes for hydrophobic surfaces, such as the air/water interface? Questions like these are easy to ask, but represent enormous challenges for both experiment and theory.

Next to various scattering techniques (X-ray diffraction, small angle X-ray scattering, neutron diffraction), spectroscopic methods – NMR, IR/Raman, terahertz time-domain, dielectric relaxation, and pump-probe spectroscopy to name a few – have turned out to be highly useful for studying structural and dynamical properties of aqueous solutions. Photo- and Auger electron spectroscopy represent one further class of powerful experimental techniques that are ideally suited for studying the electronic and geometrical structure of matter. Electron spectroscopy has been successfully applied to gases and solids for decades but since the method requires an evacuated experimental chamber the application to water and aqueous solutions could not be managed for many years – such volatile liquids are simply not vacuum-compatible. However, several important technical advances have been made during later years, overcoming the problems associated with performing soft X-ray-based electron spectroscopy of volatile liquids – the arguably most important breakthrough was the development of the liquid micro-jet technique by Faubel and coworkers (see section 3.3). This thesis can be seen as an exploration of what sort

Figure 1.1: Certain scientists have a complicated relationship to liquid water.

of information the application of electron spectroscopy to the aqueous phase can provide.

The studies reported here can naturally be divided into three categories. In the first part, based on the results of papers I-VI, we utilize the surface sensitivity of electron spectroscopy to study the distribution of inorganic ions and weak organic acids at the water/vapor interface. In papers VII-IX, which serve as the fundament for the second part, we characterize what information core-electron spectroscopies can give about chemical states and hydration structures of solvated molecules. The final part, based on papers X-XIII, explores how ultrafast charge delocalization dynamics in aqueous electrolytes, initiated by either core-level photoionization or resonant photoabsorption, can be probed via Auger electron spectroscopy.

Once through the text, I hope that you, the reader, will have a better understanding of the scientific problems associated with liquid water and aqueous solutions. Even better would be if the text has conveyed a feeling that important progress is being made and that X-ray spectroscopies will play an important role in future explorations of aqueous physical chemistry, even though the road is long and many problems still lie ahead.

Outline of this thesis

Chapter 2 presents some fundamental concepts concerning liquid water and aqueous solutions. Readers already in possession of some insight into the physical chemistry of the aqueous phase might skip this part without missing much. Chapter 3 gives an overview of the core-electron spectroscopic techniques that have been used in the present experiments. The following chapters 4-6 focuses on the respective scientific questions under investigation as described above. Each of these chapters starts by giving an introduction to the problems at hand, defining necessary concepts needed to understand the reported results, which are then described.

2. Background and some essential concepts

This chapter provides a general background to the physical chemistry of the aqueous phase, with focus on the specific systems under investigation. First, a general description of the liquid phase will be given, contrasting it against the way physicists normally describe gases and solid materials. This is followed by a concise description of water, focusing on both the properties of the individual molecule as well as the curiosities of the aqueous phase. The remainder of the chapter deals with the two types of systems that will be studied in this thesis; aqueous solutions of inorganic salts and small organic molecules.

2.1 Some general remarks on the physical chemistry of the liquid phase

A liquid is the intermediate aggregation state of a gas and a solid. Gases are characterized by weak interactions between the gaseous particles (compared to the thermal energy k_BT), which are free to move (almost) independently of each other. In solids, on the other hand, interatomic/intermolecular interactions are so significant that the constituent particles typically are restrained to only slightly move around their respective lattice sites, making most materials exhibit a well-ordered (crystalline) structure. In liquids, the strength of the interaction between the atoms/molecules are comparable to the thermal energy; thus the density is similar to the solid state, while the dynamics resemble that of a gas. This is why so much interesting chemistry takes place in the liquid phase – the reacting atoms/molecules need a high density to get sufficiently close to each other, and the long-range diffusion of the reactants in the liquid is necessary if they are to find each other in significant numbers. As later will become apparent, it is these special characteristics of the liquid phase that makes it so hard to describe in physically rigorous terms. Before turning to the main subject in this thesis – liquid water and aqueous solutions – we will first consider some of the general problems with describing intermolecular interactions in a liquid.

We start by considering how a single-component system with spherically symmetrical particles can be modeled. A first step is to obtain an

accurate description of the pair potential $w(r)$ of the constituent particles, where r is the distance between a pair. In 1903, Mie suggested a general form of a pair potential whose parameters can be adjusted to give a satisfying phenomenological description of different types of particle interactions [1]

$$w(r) = -\frac{A}{r^n} + \frac{B}{r^m} \tag{2.1}$$

Various such potentials have been developed in order to describe different types of interactions, such as the Lennard-Jones potential ($n = 6$ and $m = 12$) which is accounting for attractive Van der Waals interactions as well as Pauli repulsion at short distances [2]. If accurate pair potential parameters can be established for the particles in the gas phase, its macroscopic behavior can be well accounted for, since the low density results in very few many-body interactions. In a liquid however, the collective behavior of the large number of interacting particles become very difficult to model based on pair-potentials. This is because the real potentials often are not additive in a dense medium – the pairwise interactions of two particles can temporarily change their properties which will alter their interactions with all other particles in their vicinity. Any response of the environment will in turn alter the potentials of the initial pair, making the interplay immensely complicated. In so-called *associated liquids*, these types of mutual interactions lead to cooperative phenomena which can produce more spatially extended structures than what could be expected from simple pair potentials. Most liquids consist of non-spherically symmetric particles, making the pair potential a function of three coordinates in order to describe the effect of the relative rotational orientation of an interacting pair, posing further problems in finding a simple description of many-body interactions.

Even though much remains be said about the liquid phase in general terms, the behavior of a specific liquid varies significantly depending on which types of intermolecular interactions that are dominant. The origin of these interactions is to be found in the electronic structure of the molecules themselves. Since this thesis deals with liquid water and aqueous solutions, we therefore cannot avoid having a look at the water molecule itself.

2.2 Water; the molecule and the aqueous phase

Water is a planar molecule of C_{2v} symmetry. It is composed of two hydrogen atoms covalently bonded to an oxygen atom, forming an angle of

104.5° in the gas phase. The electronegativity of the oxygen atom results in a charge displacement over the molecule, and the resulting dipole of 1.854 D lies in the mirror symmetry plane, pointing toward the oxygen site. The ground state electronic configuration is

$$(1a_1)^2 \ (2a_1)^2 \ (1b_2)^2 \ (3a_1)^2 \ (1b_1)^2$$

The origin of the delocalized molecular orbitals from the hydrogen and oxygen atomic orbitals is illustrated in figure 2.1. The character of the molecular orbitals has been the subject of some debate [3]. $1a_1$ is the slightly perturbed O1s orbital. It does not take part in chemical bonding and is highly atomic in character. For this reason it is often referred to as the O1s orbital of the water molecule – a convention that will be used throughout this work. The $2a_1$ and $3a_1$ orbitals are partly bonding and partly non-bonding, even though $3a_1$ is sometimes wrongly referred to as a purely bonding orbital. Together the $2a_1$, $3a_1$ and $1b_1$ make up the oxygen lone pairs. $1b_1$ is a strictly non-bonding orbital while the $1b_2$ is strictly bonding, arising as a linear combination of the O2p and H1s atomic orbitals.

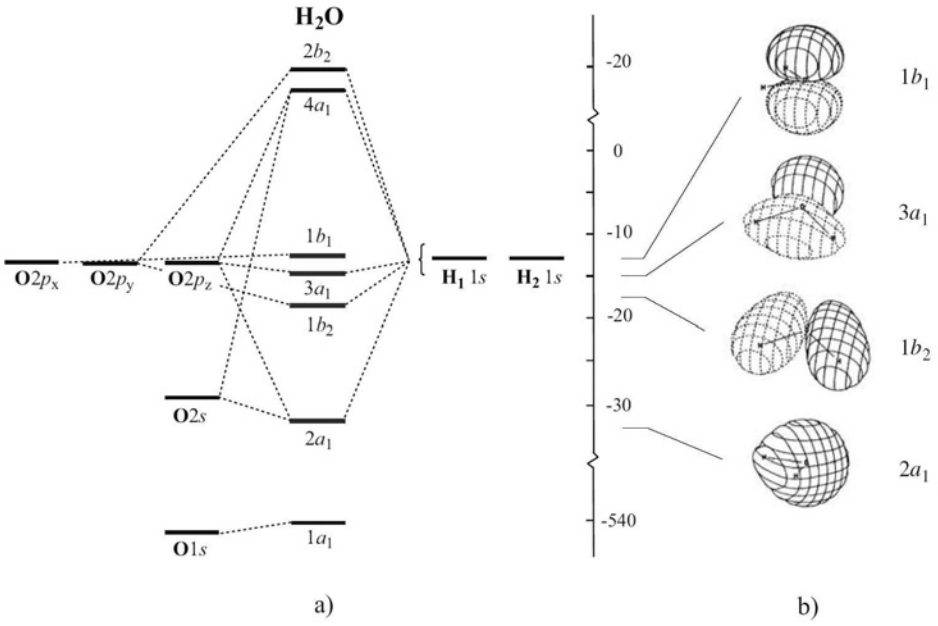

Figure 2.1: Origin of the molecular orbitals of water as a linear combination of the hydrogen and oxygen atomic orbitals [3]. Reproduced with the permission of the publisher.

As explained in the introduction, liquid water is much more complicated to describe than the free molecule. The complication stems from the formation of hydrogen (H) bonds between neighboring water molecules, when a partially positively charged hydrogen end of one molecule is binding toward the negatively charged lone pairs at the oxygen site of another. H-bonding in liquid water was first suggested in 1920 by Latimer and Rodebush [4], formulated in terms of Lewis theory, in order to account for association phenomena. H-bonding between two water molecules is an asymmetric interaction, where one molecule acts as a H-bond *donor* and the other as an H-bond *acceptor* in a nearly linear interaction geometry. Each water molecule can accept and donate two H-bonds, respectively, in a near tetrahedral arrangement. Figure 2.2a shows the water pentamer (the fundamental structural motif in ice I_h), where the center molecule is fully coordinated.

The nature of H-bonding in liquid water has been heavily discussed over the years, and the debate is still lively. While there exists a consensus that the interaction is mainly electrostatic, the relative importance of polarization, electron exchange, dispersion and charge transfer is difficult to establish. The question ultimately boils down to whether covalent contributions are important in water-water H-bonding [5, 6]. While *ab initio* calculations can reproduce H-bonding in small water clusters, and very accurately determine the binding energies, it appears that the answer to this seemingly straight-forward question largely depends on how the energy decomposition is made in the theoretical analysis [7, 8], pointing toward a problem in physically defining H-bonding.

The length of a water H-bond varies significantly with the surrounding, and illustrates another problematic aspect of capturing its essential character. *Ab initio* calculations reveal that the O–O distance of the two molecules in a water dimer is about 2.95 Å, while this distance is shortened by ~ 0.1 Å in the trimer. For larger clusters the value gradually converges toward the ice bulk value of 2.76 Å. Since the H-bond strength has been shown to scale almost exponentially with its inverse length [9], these findings nicely demonstrate the cooperative nature of H-bonded systems – an example of how molecular interaction-potentials typically are not additive in the condensed phase. On an energy scale, H-bonding in liquid water leads to a gain of about 5.56 kcal/mole water molecules, i.e. roughly 20 times weaker than covalent O-H bonding but still significantly stronger than van der Waals attraction.

From a large body of X-ray and neutron diffraction experiments, as well as Raman and infrared (IR) spectroscopic studies, water is commonly thought to be on average close to four-coordinated, in a perturbed ice-like tetrahedral arrangement with additional interstitial wa-

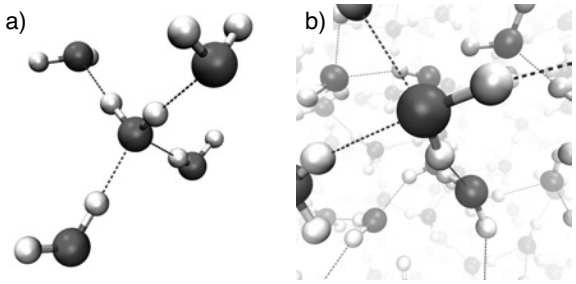

Figure 2.2: a) The water pentamer, $(H_2O)_5$, in which the central water molecules accepts and donates two hydrogen bonds, respectively, to the surrounding in a tetrahedral arrangement. b) A snapshot of liquid water at ambient conditions from a molecular dynamics simulation in which the molecules on average bind in distorted tetrahedral configurations.

ter molecules and some of the four neighbours often missing [10–22]. This picture is also supported by numerous molecular dynamics (MD) simulations [23]; figure 2.2b shows a simulation snapshot of water under ambient conditions. But if this is true, why is liquid water not as stiff as a solid piece of ice? This is because the energy needed to perturb the H-bond of one coordinating H_2O, so that it can be replaced by that of another molecule, is on the order of k_BT, which enables the making and breaking of hydrogen bonds on an ultrafast timescale. Infrared pump-probe studies have revealed significant rearrangement of the H-bonding network on picosecond timescales, resulting in a constant interchange between stable (but short-lived) ice-like configurations [24–26].

This conventional view has recently been challenged, based on X-ray absorption spectroscopy (XAS) measurements at the oxygen K-edge of liquid water. Wernet and co-workers have claimed that liquid water is on average much lower coordinated than ice, with a significant amount of the molecules in ring- and chain-like configurations; each with one broken acceptor and one broken donor bond [27]. The paper has avalanched a discussion as to whether such a structure is compatible with the large body of previous experimental and theoretical results, normally interpreted in favor of the tetrahedral model of liquid water, and if XAS really is a suitable technique to address this question [28–34]. Last year, high-resolution O1s K-edge X-ray emission spectroscopy (XES) measurements of liquid water stirred up the debate once more. The $1b_1$ peak, associated with the fluorescent decay of an electron in the outermost occupied orbital into the oxygen core hole, has now been so well resolved that a doublet structure can be identified. This finding has been interpreted in two radically different ways; either in terms of nuclear dissociation dynamics [35] or as reflecting the existence of two distinct structural motifs

in the bulk liquid – one tetrahedral, ice-like structure and another low-coordinated species [36]. Whether or not calculations of tetrahedrally coordinated water actually can reproduce the experimental XES data seems to depend on how the initial condition for the departing hydrogen atom is formulated [37].

Before heading off on a short tour through the fairyland of aqueous solutions, which is the main subject of this thesis, we must say something about the basis for the fascinating pH-chemistry in the aqueous phase, largely originating from auto-ionization of liquid water, $H_2O \rightleftharpoons H^+ + OH^-$. The hydrated proton has been found to fluctuate between the so-called Eigen [38] and Zundel [39] limiting structures on femtosecond timescales [40]. In the former ($H_9O_4^+$) the central H_3O^+ hydronium ion is strongly solvated by three water molecules whereas in the latter ($H_5O_2^+$) the excess proton is equally shared between two water molecules. A recent X-ray absorption study of concentrated aqueous HCl solutions has shown that the predominant solvation patterns of the excess proton is significantly pH dependent [41]. In the Grotthuss transport mechanism, the ultrafast proton diffusion in liquid water is thought to arise from a nearly barrier-free interchange between the Eigen and Zundel motifs [42]. As will be described in more detail in section 6.2 as well as in paper X, there are serious problems associated with modeling diffusion of the hydroxide anion (OH^-) in a similar fashion. It is becoming increasingly clear that the hydration and diffusion mechanisms of water's two generic ions are not symmetric with respect to the neutral water intermediate. This could for example explain the differences in surface structure of the two ions – a topic currently under intense debate [43–47] which we will return to in chapter 4.

2.3 Aqueous solutions: Thermodynamics and microscopic structure

A solution is a mixture of two or more distinct components, divided into *solutes* and *solvents*. In this thesis, water is the only solvent considered, while the solutes range from atomic inorganic ions to small organic molecules. Thermodynamically, solutions can be considered as mixtures where species-species interactions are significant, i.e. where the solute-solvent interaction is on the order of (or stronger than) the solute-solute and solvent-solvent potentials. Hence, the thermodynamics of solutions is much more complex than that of ideal gases, where all pair-potentials are identical.

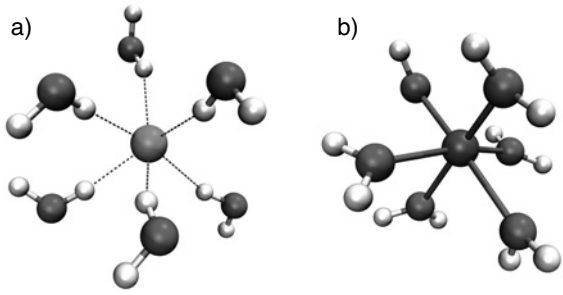

Figure 2.3: Typical first solvation shells of ions in aqueous solutions as obtained from MD simulations. a) shows a dissolved anion, $Cl^-(H_2O)_6$, while b) depicts a hydrated cationic complex, $Mg^{2+}(H_2O)_6$.

Structure-wise, equilibrated solutions are normally considered homogeneous; meaning that they exhibit no inhomogeneities on length scales significantly larger than the size of the constituting particles. The local surrounding of the solutes is however far from chaotic, since solvents form more or less stiff *solvation shells* around them. For simplicity, we will divide the discussion into two cases that are relevant for this thesis: aqueous solutions of inorganic salts and molecules in water.

2.3.1 Inorganic aqueous salt solutions

When salts are dissolved in water the ionic crystal dissociates into simple ions, forming an aqueous electrolyte. This can be thought of as having mainly two reasons. First, the high dielectric constant of water ($\epsilon = 80$) effectively screens charges, which reduces the anion-cation attraction. Secondly, the formation of water solvation shells around the ions maximizes the solvent-solute interaction, thereby minimizing the total energy of the system. Figure 2.3 shows solvated anionic and cationic complexes. The number of coordinating water molecules, as well as the stiffness and lifetime of a specific solvation configuration, heavily depends on parameters such as the charge and size of the ion [48].

Modeling the solvation potential of simple ions is non-trivial, and it is sometimes helpful (but strictly speaking not physically correct) to distinguish classical electrostatic contributions to the hydration energy from those originating from quantum mechanical solvent-solute interactions. In a simple solvation model developed by Max Born, the solvent is treated as a continuous dielectric medium [49]. The change in the Gibbs free energy upon solvation is then given as

$$\Delta G = -\frac{Z^2 e^2}{8\pi\epsilon_0 R}\left(1 - \frac{1}{\epsilon}\right) \tag{2.2}$$

where Z is the charge of the dissolved ion, R its solvated radius, ϵ the dielectric constant of the solvent, and e the elementary charge. Even though somewhat simplistic, the Born model can be used to qualitatively estimate the energetics of solvation. In a pioneering photoemission study of NaI in water, the model was successfully used to rationalize the differences in chemical shifts of cations and anions in the aqueous phase [50]. Newer approaches, such as the polarizable continuum model (PCM) developed by Tomasi and co-workers, treats the solvent as a polarizable dielectric medium [51]. Generally, continuum models can account for interactions between solvents and solutes over sufficiently long distances, typically above 5-10 Å, but have problems describing site-specific interactions in the first solvation shell. The question as to whether covalent contributions are important for ion-water interactions has been intensively discussed in the literature, and today we have good reasons to believe this to be the case [52]. A continuum description of the solvent can never capture such contributions to ion solvation. Still, it offers a good and computationally cheap way to account for long-distance solvation effects in quantum chemical calculations where its only possible to explicitly include the molecules in the first (and potentially the second solvation) shell.

2.3.2 Aqueous solutions of molecules

Given the varying nature of molecules – there are after all quite a lot of them – it is hard to make any generally valid statements about how they behave in aqueous solution. As the least common denominator, all molecular solutes interact with the water solvent by van der Waals forces, originating from electron density fluctuations on one of the sites, giving rise to a weak induced dipole-dipole interaction. Most often, stronger interactions, such as permanent dipole-dipole interactions and/or explicit hydrogen bonding between polar groups of the solute and water are more decisive for the solvation properties.

Solvent-solute interactions in aqueous solutions are normally divided into *hydrophilic* and *hydrophobic* contributions, whose relative importance can vary at different regions around a molecular solute. While hydrophilicity, i.e. the favorable interactions upon strong solute hydration, is easy to intuitively understand, hydrophobic interactions are more elusive. This is because they don't arise from direct solvent-solute interactions but from solute-induced *loss* of solvent-solvent interactions upon the formation of a cavity within the dielectric aqueous medium. On a molecular level, this arises from the need to strain and/or break water

H-bonds in order to accommodate the solute in the water network. Even though hydrophobic hydration phenomena have since long been qualitatively well understood it is only recently that quantitative models thereof have been successfully developed [53].

Molecules with both hydrophobic and hydrophilic parts are called *amphiphiles*. Their dual nature causes them to organize so that the solvent primarily interacts with the hydrophilic parts while the hydrophobic regions tend to either aggregate or adsorb at hydrophobic interfaces. Amphiphilicity is the molecular property that enables detergents to dissolve oil and other hydrophobes in water. Furthermore, it is crucial for the formation and function of numerous biochemical structures, such as lipid bilayers that form the outer cell wall.

The solvation of molecules in aqueous solution can also cause "chemical" modifications of the solute to various extents. Brønsted acids and bases are molecules containing titratable groups which have a propensity to either donate to or accept a proton from the aqueous solvent. This will produce ionic conjugate base/acid residues that are stabilized in the high-dielectric solvent – this is why acid-base reactions are so ubiquitous in water. Another dramatic structural modification upon hydration of molecules occurs through *hydrolysis*, i.e. when water dissociates into its ionic products which are thereafter incorporated into the solvated complex. In papers VIII and IX we for example show that core-electron spectroscopies are sensitive to the hydrolyzation of formaldehyde, the simplest of the aldehydes, where the carbonyl C=O group is converted to OH-C-OH, resulting in methanediole.

3. Experimental methods and setups

The results presented in this thesis are all based on core-level excitations of liquid samples by the aid of synchrotron radiation. This chapter is intended to provide a brief background to the spectroscopic techniques used in the experimental work. Since there already exists a large plethora of literature providing detailed information on all the possibilities and drawbacks of the respective technique, yet another comprehensive presentation thereof would merely be a waste of all parties precious time (and would probably not be as enjoyable to read as those great texts already out there, see e.g. [54, 55]). Instead I shall try to quickly sketch some important physical processes that can be initiated in materials by excitation using X-ray radiation. In the following section we will see how some of these processes can be utilized for spectroscopic purposes. Thereafter the specific problems of performing X-ray spectroscopy of liquids are described and the liquid micro-jet method is introduced. A brief section is then dedicated to the advantages of using synchrotron radiation in our experiments, for reasons such as the large brilliance and photon energy tunability a modern synchrotron facility offers. The remainder of the chapter is intended to introduce the reader to the specific nature of our experiments and to give a flavor of how they were actually conducted in real-life.

3.1 X-ray photoabsorption, photoionization and some possible pathways of de-excitation

All matter – may it be single atoms, molecules, metals, liquids, etc. – absorbs light at certain wavelengths characteristic for a given species. Photoabsorption in the visible range of the electromagnetic spectrum is what gives objects their particular colors. Some materials, like liquid water, do not absorb in the visible range since the lowest energy needed to make an electronic excitation (HOMO to LUMO) lies in the deep ultraviolet range – hence water appears transparent to the human eye.

When a photon is absorbed by an atomic system in its ground state it will remain in an excited state over a limited period of time, after which it will relax to an energetically lower state through various

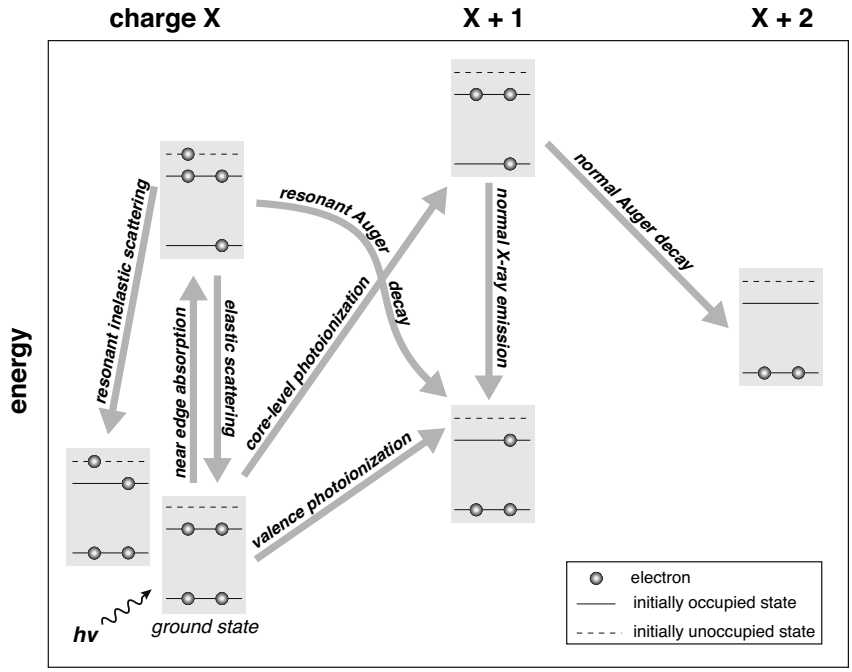

Figure 3.1: Possible excitation and relaxation pathways of an atomic system in its ground state (of charge X) upon absorption of an X-ray photon. Ejection of electrons leads to a +1 increase of the charge of the system.

pathways. The details about how the system absorbs and subsequently de-excites can be used to extract valuable information. An accurate understanding of the physics behind these mechanisms is therefore fundamental to all spectroscopy using electromagnetic radiation as an incident probe. In this thesis we will mostly be occupied by processes initiated by the absorption of X-ray photons by molecules and ions in the liquid phase, i.e. with energies sufficient to initiate ionization of core-electrons. Figure 3.1 schematically illustrates the main possible fates of an atomic system in which one of the electrons absorbs an X-ray photon. For simplicity, we can divide the possible scenarios into two cases, depending on if the photon energy hν is larger or smaller than the electron binding energy (BE) of a specific electron, i.e. the smallest energy needed for the system to expel it into the continuum.

Case A: hν > BE

Photoionization can occur, increasing the initial charge X of the system to X+1. The photoelectron that is expelled will leave the system with a

kinetic energy (KE) according to the photoelectric law [56]

$$\mathrm{KE} = h\nu - \mathrm{BE} \tag{3.1}$$

Either a valence or a core electron can depart in the process, leading to different final states. In the case of *valence photoionization* of the HOMO orbital, the final state is stable and can't relax further[1], while inner valence holes will collapse after a finite lifetime. If *core-level ionization* occurs the system is left in a highly unstable state and after a few femtoseconds the core-hole will decay. The core orbital will may for instance be filled by a valence electron, and the excess energy gained in the decay process can be removed from the system in two principally different ways. If the energy is released as a photon, the charge X+1 remains unaltered, and the system ends up in the same final state as it would upon valence photoionization. This mechanism is referred to as *normal X-ray emission*. For lighter elements, as well as for shallow core levels in heavier elements, the excess energy is much more likely to initiate an auto-ionization event, a so-called *normal Auger decay*. The system then ends up with a X+2 charge, after which it has lost two of its initial electrons. If the holes corresponds to the highest occupied molecular orbital(s) (HOMO) of the initial system it cannot relax further without the interaction with an environment. If further relaxation events are still possible the system can end up in highly charged final states.

Case B: hν < BE

If the photon energy is not sufficient to cause ionization, an absorption event will leave the charge state of the system unchanged. Typically, the onset of core-level X-ray absorption lies only a few, sometime tens of electron volts below the electron binding energy, which is the reason for the common name *near edge absorption*. Within the narrow photon energy span from the absorption onset until the ionization threshold, the absorption cross section varies considerably. This is directly correlated to the local density of unoccupied states at the absorbing site, which can be occupied upon the absorption of the X-ray photon.

If the excited electron itself relaxes to fill the core hole the system returns to the initial state, and an identical photon as that absorbed will be emitted. This process is referred to as *elastic scattering*. If another

[1] In isolation that is – since the charge state, and thus the electron affinity of the system has changed during the process of photoemission the product might be highly reactive in an environment where there are other electrons available on neighboring atoms or molecules.

valence electron fills the core hole, while the initially photo-excited electron still remains in an excited state, the final state is different and a photon of lower energy than the excitation energy will be emitted – this process is called *resonant inelastic X-ray scattering*. Another, and much more likely de-excitation mechanism for the lighter elements is that the system expels an Auger electron. Unlike in the case of normal Auger decay described above this *resonant Auger decay* leaves the system in a X+1 charge state. Hence the kinetic energies of resonant Auger electrons will generally be higher than those resulting from normal Auger decay.

3.2 Core-electron spectroscopies

The processes described above give rise to physical observables that can be utilized to gain information about the system, either about its ground state or the dynamics of the excited states. It is important to realize that spectroscopic measurements always deal with energy differences between initial and final states. In its most general form, this can be expressed through the principle of energy conservation

$$E_{inc.} + E_i = E_f + E_{leav.} \tag{3.2}$$

where E_i and E_f are the initial- and final-state energies of the system, respectively. $E_{inc.}$ and $E_{leav.}$ are the respective energies of the exciting and the leaving particles in the process, may it be photons or electrons (or something else for that matter). In the case of near edge absorption below the ionization threshold, no particle is expelled during the absorption event and hence the energy $h\nu$ of the absorbed photon is equal to the energy difference of the final and the initial state. In *X-ray Absorption Spectroscopy* (XAS) or *Near Edge X-ray Absorption Fine Structure* (NEXAFS) spectroscopy the absorption efficiency is mapped out as function of the exciting photon energy. Since all excitations start from the same initial state this means that the spectroscopy measures the transition probability to final states of varying energies, which is indirectly the same thing as mapping out the partial local density of unoccupied states at the absorbing site [55].

In *Photoelectron Spectroscopy* (PES) the leaving particle is a photoelectron with kinetic energy KE. Combining expression (3.2) with the photoelectric law (3.1) one arrives at

$$\mathrm{BE} = E_f - E_i \tag{3.3}$$

This result might appear trivial, but it is important to realize that electron binding energies are solely determined by the difference in the

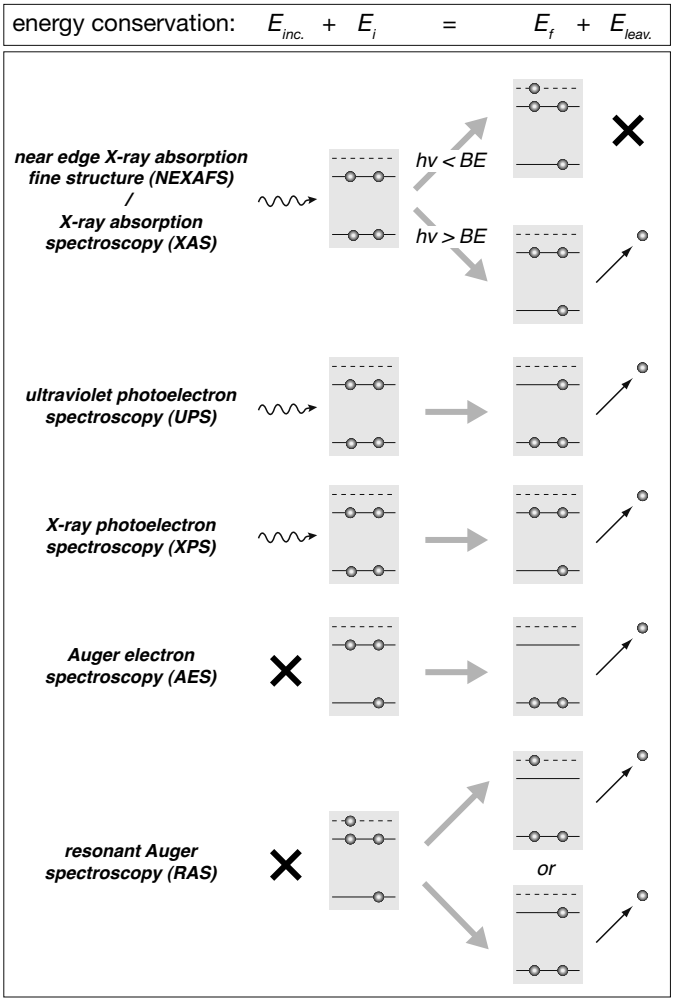

Figure 3.2: Schematic illustration of electron spectroscopic techniques, utilizing the processes outlined in figure 3.1. The principle of energy conservation (top) governs the kinetic energy of the outgoing electron.

system's total initial- and final-state energies.[2] Depending on whether the ionization leaves the system in a valence- or core-ionized state, one

[2]The term binding energy is thus potentially misleading, since it suggests that it is a measure of how tight the electron is bound prior to ionization, which unfortunately can lead one to mix up binding energies with (negative) electron orbital energies. This is the implicit simplification made in Koopman's theorem, in which one assumes that there are no relaxation contributions to the final-state energy. In the condensed phase the final-state polarization screening is however often considerable, making Koopman's theorem a crude approximation.

normally distinguishes between Ultraviolet Photoelectron Spectroscopy (UPS) and X-ray Photoelectron Spectroscopy (XPS), respectively.[3]

In *Auger Electron Spectroscopy* (AES) the kinetic energy of normal Auger electrons are measured. The notation of Auger transitions is made by three capital letters, indicating which shell is involved in the initial ionization event, and in which levels the two final-state holes reside. For example a KLL-Auger event is initiated by the ionization of a 1s electron, and the final state is left with 2 holes in the $n = 2$ shell (where the different combinations $(2p)^{-2}$, $(2s)^{-1}(2p)^{-1}$ and $(2s)^{-2}$ all can result given that they are energetically allowed). As can be seen from figure 3.1, the energy of an Auger electron resulting from a XYZ-decay can be approximated by the binding energy difference

$$\mathrm{KE}_{XYZ} = \mathrm{BE}_X - \mathrm{BE}_Y - \mathrm{BE}_Z - C_{coul.} \tag{3.4}$$

The term $C_{coul.}$ accounts for the Coulomb repulsion resulting from the interaction of the two final-state holes. The magnitude of $C_{coul.}$ thus carries information about the distance between the two holes, and how efficient the system can screen them [57].

A normal Auger process, initiated by a core-ionization event, takes a system of charge X to a final charge of X+2. In Resonant Auger Spectroscopy (RAS) the initial core-hole is not created through ionization, but through resonant absorption, i.e. when the energy of the exciting photon is just right to place a core electron into an unoccupied orbital. This type of spectroscopy is very powerful since it carries information both about the unoccupied states (thus being similar to NEXAFS) but also reveals details about the system's relaxation pathways. In Paper X, where we study the delocalization of final-state holes of the resonantly core-excited hydroxide anion to surrounding water molecules, the energetic distribution of Auger electrons yield structural information about the complex, indicating the existence of a hydroxide hydrogen donor bond.

Finally, one important characteristic of electron-based spectroscopies applied to condensed samples is the considerable surface sensitivity, resulting from the short inelastic mean free path (IMFP) of the emitted photoelectrons. In its most simple form, photoemission signal intensities I from a flat surface at $z = 0$ can be expressed as being proportional to the integral over the atomic density ρ of the target atoms, exponentially

[3]This terminology has historical reasons, but is misleading since it takes the names for the techniques from which type of light sources that were originally used, not from what electronic levels that are actually being studied. A more appropriate terminology would differentiate between valence photoelectron spectroscopy and core-level photoelectron spectroscopy.

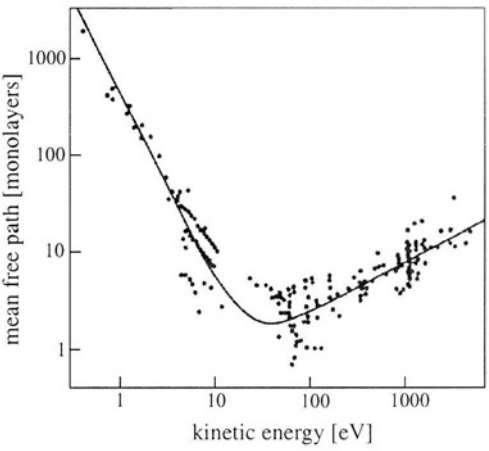

Figure 3.3: The 'universal' electron inelastic mean free path as a function of electron kinetic energy. The solid curve shows the theoretical prediction and the data points are taken from a wide variety of materials [58]. Reproduced with the permission of the publisher.

attenuated by IMFP

$$I = \int_0^\infty \rho(z) \cdot \exp(-z/\mathrm{IMFP})\, \mathrm{d}z \tag{3.5}$$

IMFP varies considerably with the kinetic energy of the photoelectrons, but there is a striking generality in the behavior of the mean free path curve for different materials. For that reason, one sometimes talks about the 'universal' inelastic mean free path curve for electrons in condensed matter, depicted in figure 3.3. The general behavior of the IMFP curve can be utilized in depth-profiling experiments, where the excitation energy is varied so that the emitted photoelectrons from a certain electronic state co-vary in kinetic energy. In paper I we study the specific IMFP curve for liquid water and aqueous solutions, which is experimentally challenging for reasons that soon will become apparent.

3.3 Spectroscopy of liquids using soft X-rays – prospects and challenges

The development of the X-ray spectroscopies outlined above immediately led to rapid development in our understanding of the electronic structure of matter [59, 60]. But there is one catch; the techniques all require an appreciable vacuum in the experimental region. This is because the incident soft X-ray radiation is efficiently absorbed by gaseous particles if

such are present between the light source and the sample. In the case of electron-based spectroscopies, such as PES and AES, the problems are even more severe due to the very short inelastic mean free path of the departing electrons in a dense gas, being on the order of a micrometer at atmospheric pressures. Unless the experimental chamber is evacuated the radiation will therefore barely reach the sample, and the few photoelectrons that are still produced will have no chance to make it to the detector. For solids and dilute gases these problems could be handled quite early on, but liquid samples proved to be a major challenge. Since most liquids are highly volatile, a sample in vacuum will either be consumed by evaporation or frozen into solid within a short period of time, due to evaporative cooling. During this rapid evaporation process the photoelectrons will also have no chance to reach the detector through the dense vapor.

Despite these large difficulties, Hans and Kai Siegbahn reported the first successful PES experiments on liquid formamide in 1973 [61]. Over the coming decade they tried out various experimental approaches. The arguably most successful setup was where the liquid sample was flooded over a rotating metal disc, so that the liquid surface was continuously refreshed. To maintain the required vacuum, either samples with low vapor pressure (such as formamide) were used or the vapor pressure of more volatile liquids was reduced by adding large quantities of salt. In reference [62], Hans Siegbahn formulated an empirical rule of thumb which has to be met in a successful liquid photoemission experiment in order to obtain a sufficient signal; $P \cdot d < 0.13$ mbar mm, where P is the vapor pressure of the liquid and d is the distance to the spectrometer entrance. This put serious doubts to the possibilities of measuring pure water at normal temperatures.

In 1988, Manfred Faubel and co-workers published the design for a novel micro-jet technique [63], which they in 1997 showed could be used to overcome the problems associated with performing electron spectroscopy of water and other volatile liquids [64]. A high backing pressure pushes the liquid through a laser drilled glass nozzle, producing a small cylindrical beam that is injected into a vacuum chamber at a velocity of $\sim$100m/s – see figure 3.4. It can be shown that the effective vapor layer thickness $P \cdot d$ surrounding a liquid jet under such conditions is given by [64]

$$P \cdot d = P_0 R_{jet}(\ln R_{spec} - \ln R_{jet}) \tag{3.6}$$

where R_{spec} is the distance from the center of the jet to the analyzer entrance, R_{jet} is the radius of the jet and P_0 is the vapor pressure of the liquid. Siegbahn's empirical rule of thumb could thus be reformulated into the condition $P_0 R_{jet}(\ln R_{spec} - \ln R_{jet}) < 0.13$ mbar mm. It

Figure 3.4: A liquid micro-jet in action producing a liquid water target in vacuum which allows photoelectons to escape from the surface and reach an electron analyzer. Photo provided by the courtesy of Ev Henke.

is easily seen that the condition can be fulfilled if the system is made small enough – a 10 μm jet of water will do the job. One can qualitatively imagine why shrinking the system solves the problem; if the liquid sample is made very small the evaporation results in few gaseous water molecules surrounding it. This drastically increases the chances for an emitted photoelectron to escape through the vapor and reach the electron analyzer. The high velocity of the jet also ensures that the liquid surface is continuously renewed, thus overcoming the problem haunting many liquid surface experiments. The fast transport of material also reduces the problems of charging the sample in the photoemission process.

In order to perform electron spectroscopy of liquid samples, the challenging task of introducing a liquid jet into vacuum must be ventured due to the extremely short electron mean free path. If we want to measure X-ray radiative decays in liquid samples, e.g. in XES or total fluorescence yield NEXAFS, this problem is not as extreme since soft X-rays have attenuation lengths almost three orders of magnitude longer than electrons. The chamber must still be evacuated but the sample can be contained in a liquid cell, separated from the surrounding vacuum by a micrometer thin membrane, which hence must be able to stand a pressure gradient up to an atmosphere [5, 27, 65, 66]. The membrane material must also not contain the element under investigation, since that would obscure the sample spectrum. The most frequently used materials today are Si_3N_4 and carbon.

3.4 Synchrotron radiation – why it's worth leaving town to get hold of the X-rays elsewhere!

Synchrotron radiation (SR) is the electromagnetic radiation generated when charged particles with relativistic velocities are subjected to cen-

tripetal acceleration. Synchrotrons are superior light sources for most EUV/X-ray experiments, compared to common discharge lamps and X-ray tubes. It offers high photon flux and the photon energy can be varied continuously from the IR- (10^{-1} eV) to the hard X-ray regime (10^5 eV). This flexibility, combined with the high degree of well-defined polarization, makes SR ideal for the types of experiments described in the previous section. In the early days of particle accelerators, synchrotron radiation was merely seen as an unwanted by-product, and the theoretical studies thereof were primarily motivated by the possibility to minimize the problem it posed [67]. Basic characterization was done by a number of researchers during the 1940's, leading to a solid understanding of the phenomenon within the framework of classical electrodynamics and the theory of relativity [68]. Today, many synchrotron facilities, such as MAX-lab and BESSY where the experiments presented in this thesis were conducted, are totally dedicated to the production of radiation for the use in a wide variety of experiments.

As an attractive alternative to the broad Bremstrahlung produced in bending magnets, needed to guide the electrons around the ring, modern 3rd generation facilities have installed *insertion devices* in straight sections of the storage ring. These are commonly divided into undulators and wigglers. All experiments presented in this thesis have been performed using radiation from undulators, and we will therefore quickly review some of its properties.

Undulator radiation is produced when relativistic electrons move through a periodic array of equidistanced magnets with alternating polarity. In theory, an infinitely long undulator would produce completely monochromatic radiation in series of harmonics, defined by the magnetic field set by the undulator gap [69]. A finite undulator (which unfortunately is what we have to be satisfied with in a finite world) will produce broadened peaks. The width of the emitted radiation is, to a good approximation, given by

$$\Delta E = \frac{h\nu}{N_u} \tag{3.7}$$

where N_u is the number of magnetic periods in the undulator [70].

The so-called *beamline* is the place where all the action is, i.e. the place where the X-ray produced in the synchrotron finds its way out to the sample brought by the user for investigation. Figure 3.5 schematically illustrates the important components of a typical beamline. The first thing that differentiates beamlines is the light source (a in figure 3.5), i.e. whether a bending magnet or an insertion device is used – the figure shows an undulator. The non-monochromatized divergent radiation cone

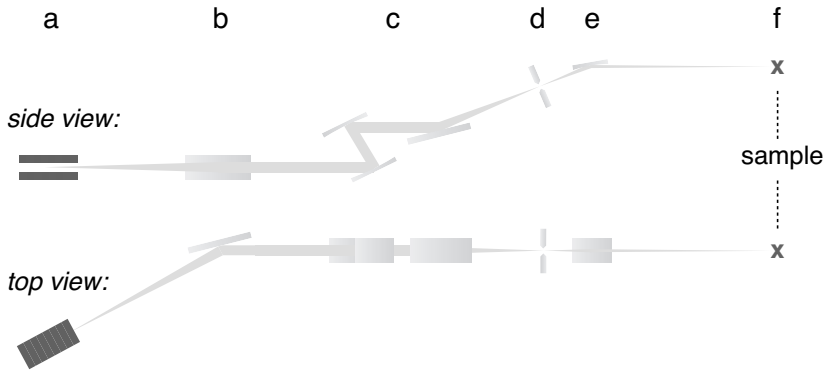

Figure 3.5: Outline of a typical beamline. The letters designates the most important sections which are discussed in the main text.

leaving the undulator is collected by a focusing mirror (b), which directs the radiation toward the monochromator (c). Depending on the energy range delivered by the source as well as the resolution requirements for the intended experiment, monochromators are built after slightly different optical principals. U-41 at BESSY and I-411 at MAX-lab, where we have performed our experiments, both host plane grating mirror (PGM) monochromators based on a design developed at BESSY I, now commercially available by Bestec GmbH. The resolution (at cost of transmission) is determined by the exit slit of the monochromator (d) and can be varied depending on the requirements of a specific experiment. The exact position of the last refocusing mirror (e) can be adjusted to fine-tune the exact path with which the radiation leaves the beamline into the experimental chamber where it hits the sample under investigation (f). Depending on the beamline, the experimental setup must either be brought by the user or a permanently mounted endstation is available.

Due to the wide range of different experiments conducted at a modern synchrotron facility, the desired parameters of the beamlines often vary considerably from user to user. For that reason, beamlines are most often dedicated to a certain type of experiment, e.g. hard X-ray diffraction and soft X-ray spectroscopy experiments require drastically different characteristics of the light. When evaluating a beamline's suitability for a given experiment one will first have to consider the energy range delivered by the source. For core-level spectroscopy of liquid samples, photon energies in the range from 30 – 2000 eV are desirable. This energy range enables one to resonantly probe a wide range of relevant edges from a large number of elements and producing photoelectrons of relatively high kinetic energies for depth profiling experiments. In reality one usually has to

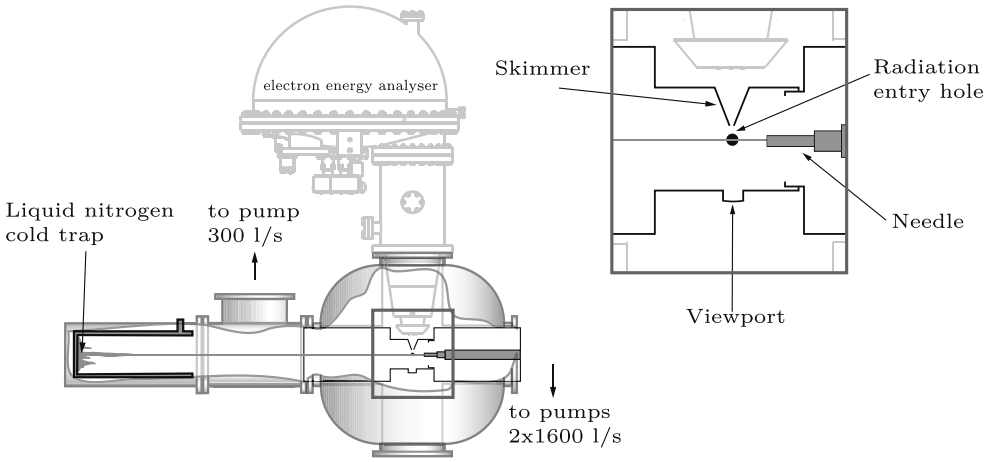

Figure 3.6: Experimental setup for liquid photoemission at beamline I-411 at MAX-lab [72]. Reproduced with the permission of the publisher.

settle for less due to the huge difficulties in producing such a versatile source. Another important parameter is the photon flux delivered at the required resolution, as well as the spot size at the focus point. In liquid-jet experiments the target is typically 10-20 micrometer in diameter and larger spot sizes than that is hence a waste of precious photons. In certain cases it might also be of interest to consider the divergence of the photon beam at the focus if the sample is extending in the direction of the light propagation.

3.5 Liquid photoelectron spectroscopy at beamline I-411, MAX-lab

The liquid photoemission experiments at MAX-lab have been performed using the permanent multi-purpose end station at the I-411 undulator beamline, designed for handling both gases, liquids and solid samples [71]. It is equipped with a high-resolution Scienta R4000 hemispherical electron spectrometer. The main chamber and spectrometer are rotatable around the horizontal plane of polarization, allowing angle resolved measurements in the complete range from zero to 90 degrees. Most often the spectrometer is mounted at 54.7° (the so-called magic angle), due to the simplification in the subsequent data analysis [54].

The experimental station, as modified for the liquid jet experiments, is schematically shown in figure 3.6. The liquid micro-jet source is mounted on a stainless steel rod, which can be moved through the inner cylindrical

compartment, evacuated by two large turbo pumps (each at 1600 l/min). The figure inset shows how the nozzle is placed so that the laminar region of the liquid jet intersects with the synchrotron radiation and the electron spectrometer axis. The departing photoelectrons leaving in the direction of the spectrometer passes through a copper skimmer with a 0.5 mm circular opening, entering a differentially pumped compartment leading up to the R4000 lens system. In this way a sufficient vacuum is maintained in the spectrometer to perform the measurements. The liquid that has passed the ionization region will break up into a train of droplets, which are collected in a liquid nitrogen cold trap.

The liquid jet is provided with samples from a system of beakers connected to a switching cross, which enables switching samples on-the-fly during experiments. The solutions are pressurized by a High Pressure Liquid Chromotography (HPLC) pump that adjusts the pressure to obtain a constant flow rate (Micro-Liquids GmbH [73]). The liquid is lead up to the nozzle through a thin metal tube (stainless steel alt. titanium). To generate a 15 μm jet of water at 100m/s, a pressure of 5-15 bar must typically be applied. When flowing more viscous liquids, such as highly concentrated aqueous solutions of LiCl, the pressure can rise to higher than 100 bar in order to maintain the same flow rate.

3.6 Liquid photoemission at U-41 PGM, BESSY

The experimental setup used for the photoemission experiments at BESSY was constructed by Bernd Winter and Manfred Faubel and has been the model for our own setup at MAX-lab [75–77]. As seen in Figure 3.7, the setup can be divided into four parts: A differential pumping stage (**III**) constitutes an interface between the main chamber (**I**) and the last refocusing chamber at the U41-PGM beamline. The synchrotron light enters through a small opening connecting the differential chamber and the main chamber, with a diameter of 500 μm, while the differential chamber is being pumped (Pfeiffer, 400 l/s turbopump). In the main chamber (**I**) the synchrotron light hits the liquid microjet. The main chamber is evacuated by a high-performance turbopump (Pfeiffer, 1500 l/s). The jet hits a cold trap (**II**) filled with liquid nitrogen. The setup is equipped with a hemispherical electron energy analyzer (Spex Leybold EA10) which is situated on top of the main chamber (**IV**) being pumped by two turbopumps (Pfeiffer, 400 l/s). The skimmer separating the main chamber from the analyzer typically has an opening orifice with a diameter of 0.2 mm.

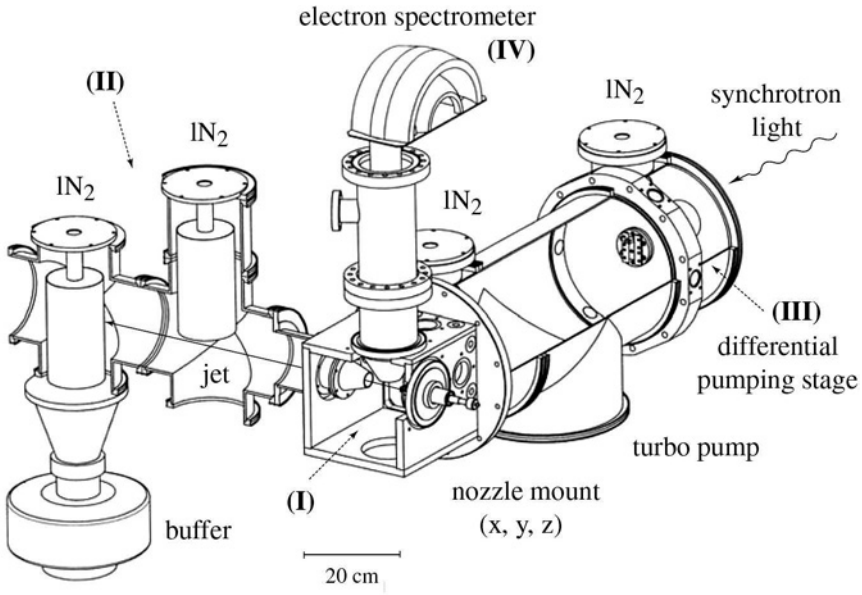

Figure 3.7: Schematic picture of the liquid-jet photoemission setup at BESSY, usually operated at beamline U-41 PGM [74].

Since the setup is not mu-metal shielded, a 0.8 x 0.8 x 0.8 m^3 Helmholtz cage surrounds the main chamber in order to minimize the effect of Earth's magnetic field on the measured photoelectrons. The currents through the coils are set such that the resulting magnetic field in the interaction region is zero, which is measured with a Gaussmeter (LakeShore 450).

3.7 LIQUIDROM – Liquid NEXAFS at BESSY

LIQUIDROM is an experimental end-station in operation at BESSY, constructed by Emad F. Aziz for the study of liquid samples under ambient conditions by means of X-ray absorption spectroscopy [79, 80]. It is mainly operational at the U-41 PGM beamline. The liquid samples can be introduced into the chamber in two principally different ways: either as a micrometer liquid jet in helium atmosphere or in a liquid flow cell behind a 200 μm thick Si_3N_4 membrane in vacuum (see inset in figure 3.8). All measurements made at LIQUIDROM that are presented in this thesis were performed in the latter way, because it enables a larger versatility in the choice of samples. Since X-ray induced sample damage can be considerable in certain cases, an external pump constantly circulates

the liquid samples. In this way the liquid sample is refreshed in the ionization region. In certain rare cases, where sample damage can still be observed, one can choose to dispose of the irradiated sample instead of letting it back into a closed loop.

The absorption cross sections are determined by total fluorescence yield (TFY) using commercial GaAsP photodiodes. These types of detectors have a smooth quantum yield function, extending from the visible range (a few eVs) to the hard X-ray regime (> 2 keV), making them ideal to monitor a large number of parallel radiative decay channels. The spectra measured at U-41 are normalized with respect to the current measured on the last gold plated refocusing mirror, which to a good approximation is proportional to the photon flux.

The synchrotron radiation enters the chamber through a pinhole opening into a differential pumping stage, separating the beamline from the main chamber. As seen in figure 3.8, the radiation then continues through a stainless steel rod extending into the main chamber, up-close to the liquid flow cell. The measuring photodiode can be positioned relative to the sample holder in order to obtain the maximum fluorescence signal. The measurements are normally made at 45° relative to the membrane in the polarization plane of the synchrotron radiation.

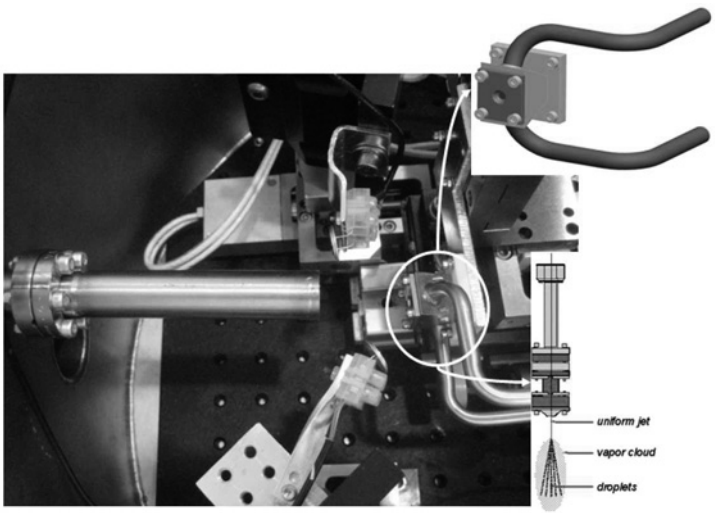

Figure 3.8: Close-up photo of the interaction region in LIQUIDROM, where the soft X-rays from U-41 are guided into the main experimental chamber through a cylindrical tube, hitting the liquid sample flowing in a cell (separately illustrated, top right) behind a Si_3N_4 membrane, allowing passage of entering and leaving radiation [78].

3.8 Spectral lineshapes and fitting

The key to extract information from any spectrum is a correctly performed peak fitting and a subsequent interpretation of the spectral features. While the latter activity is difficult to account for in general terms, peak fitting is an art that is "hands-on" but still requires an understanding of the origin of the spectral features. Generally, absorption spectra are difficult to reliably decompose into individual components since analytical lineshapes aren't easy to come by. Photoemission lines are however well understood and quantitative lineshape parameters that can be extracted from a fit potentially carry valuable information about the sample's electronic structure.

A photoelectron feature is seldom composed of just one line, but shows substructure owing to a superposition of vibrational final states. In the gas phase, these states can often be separated and adiabatic binding energies can thus be obtained, pertaining to excitations into the lowest vibrational final state [54]. In the liquid phase, the vibrational progression is most often smeared out due to overlapping lines, slightly chemically shifted because of the fluctuating environment, and the vibrational profile will only be observed as an unresolved envelope.

Photoemission of deeper lying orbitals than of the HOMO results in spectral lines with an inherent Lorentzian linewidth, due to the finite lifetime of the hole. Major efforts have been put into accurately determining the lifetime widths of important photoemission lines for many elements, done by high-resolved photoemission experiments on molecules in the gas phase, e.g. see the extensive work of H. and S. Aksela. These values can then be used as input for fits of the same atomic lines in other samples. The core-levels studied in this thesis typically have Lorentzian widths of the order of 100 meV, but if Coster-Kronig decay channels are open, i.e. where the initial-state hole and one of the final-state holes belong to the same principal electronic shell [81], the decays are much faster and lifetime widths in the order of eVs can be observed [54].

Another lineshape parameter that can be important at low kinetic energies is the asymmetry arising from post-collision interaction (PCI) [82]. This effect comes into play when the kinetic energy of the photoelectron is smaller than the Auger electron emitted in the subsequent decay of the core-hole – as a result the Auger electron eventually will pass the photoelectron. Thus, the nucleus is screened by one less electron that increases the electrostatic interaction between the departing electron and the ionized core, which in turn retards the photoelectron. Since the Auger decay is a stochastic process, the effect will retard photoelectrons depending on the distance of the ionic residue. Therefore, PCI results in asymmetric line shapes toward the higher binding energy side.

The by far largest contribution to the linewidth of species in the liquid phase comes from Gaussian broadening. This is partly due to "phononic" excitations, arising from vibrational coupling with the environment in the final state [54]. The strongest effect is however thought to arise due to the large number of co-existing fluctuating configurations, each resulting in small chemical shifts [76]. Another part of the Gaussian width originates from the experimental contributions, given primarily by the photon energy bandwidth (set by the monochromator slit) and the electron spectrometer (determined by the pass energy). One usually tries to set the experimental resolution in such a way that the inherent width of the spectral features under investigation dominates the total width. In cases where the photon resolution is of no real importance, e.g. in the study of off-resonant normal Auger, the photon bandwidth can be broadened significantly by opening the monochromator slit, resulting in higher flux on the sample.

All photoemission lineshapes presented in this thesis have been fitted using the SPANCF package by Edwin Kukk [83], available as a plug-in for IGOR Pro by Wavemetrics [84]. The script treats a photoelectron spectrum as the sum of a linear background and optional nonlinear backgrounds (such as Shirley backgrounds, spline interpolation functions etc.) plus a variable number of photoemission lines. The latter are defined by a number of parameters, namely their energy position, intensity (peak height), Lorentzian full width at half maximum (fwhm), Gaussian fwhm and a PCI asymmetry parameter. One can choose to lock any given parameter to a certain value or leave it free in the fit, or link parameters in certain ways, e.g. that two lines should be separated in energy with a certain fixed value (like a spin-orbit splitting) or that the intensity ratio of two features should be constant. Though non-restricted fits always give the best numerical results (which is the essential content of the variational-theorem), proper linking is the key to extract physically relevant data from fits. The more information one has at hand that can be formulated in terms of linking conditions, the more reliable the values of the remaining free parameters will be.

4. Distribution of solutes at the aqueous solution/vapor interface

4.1 Why bother about aqueous surfaces?

In an isotropic medium like liquid water the interactions of a single spherical solute particle with its surrounding are on average identical in all directions in space. Upon diffusion in an infinite box of water there is therefore no spatial region that is preferred nor avoided; for the solute all places look the same. When the solute approaches an interface, i.e. the boundary between the aqueous solution and an adjacent phase, the forces acting on the particle become spatially asymmetric. For the sake of simplicity we can assume that the surface is planar and infinite in the two dimensions x and y which are parallel with the surface. The surface potential of mean force, describing the variation in the free energy as function of a particle's position relative to the surface, will thus be a function of the z-coordinate, and so will the residence time at finite temperatures. All places don't look the same anymore; some are more preferred than others!

A useful concept when talking about varying solute densities near an interface is that of *density profiles*. The density profile $n_i(z)$, describing the local concentration of the i:th solute with bulk concentration n_i at a distance z from the interface, is related to the particle's surface potential of mean force $w_i(z)$ via the expression

$$n_i(z) = n_i \cdot \exp\left(\frac{-w_i(z)}{k_B T}\right) \tag{4.1}$$

Therefore, when we in the following will discuss different energetic contributions to the surface potential of various solutes it should be clear how this governs the surface propensities of the particles.

The surface potential of mean force of a solute particle greatly depends on the nature of both the particle and the interface, i.e. whether they are charged, polar, amphiphilic, hydrophobic, etc. Other factors, such as solute-solute interactions, whose importance will vary with concentration, can also alter the surface affinity of a given species. The variable space determining the distribution of a given solute at a given interface is hence enormous and represents several large areas of active research in modern physical chemistry; it is therefore not possible to cover all that in this thesis. Here we will be more modest and only concern ourselves

with two types of solutes, inorganic ions and weak organic acids, and study their propensities for the aqueous solution/vapor interface, which we in the following will merely refer to as the "water surface".

Beyond being of fundamental interest in aqueous physical chemistry the surface distribution of ions and amphiphiles have been found to be crucial for numerous atmospherically relevant chemical reactions [85, 86]. These can occur either continuously or under the influence of solar radiation at natural aqueous interfaces, e.g. at the surface of aqueous aerosols, and are often crucial for the production, reduction/oxidation and dissociation of essential compounds in the troposphere. Aqueous chloride is of particular importance in this context, since it acts as a precursor in photolysis reactions leading to the formation of chlorine gas. Knipping and co-workers have shown that the surface distribution of Cl^- in aqueous aerosols is important in these photolysis reactions since the occurrence of aqueous chloride ions in the outermost surface layers seems to be rate limiting [87]. Chlorine is an oxidizing agent and has been found to significantly reduce the lifetime of atmospherical pollutants [88, 89].

Before turning to the physics associated with any specific interface we will briefly review some thermodynamical relations which are crucial for understanding the relation between microscopic surface phenomena, such as ion-specific surface adsorption, and macroscopic manifestations thereof, such as surface tension variations.

4.2 The Gibbs adsorption equation

In thermodynamical language, an infinitesimal variation of the Gibbs free energy of a liquid system with a surface can be written as

$$dG = -SdT + VdP + \sum_i \mu_i dn_i + \gamma dA \tag{4.2}$$

where S is the entropy of the system, T is the temperature, V is the volume, P is the pressure and μ_i is the chemical potential of the n_i:th particle [90]. γ is called the *surface tension* of an interface with area A joining two phases. In a molecular picture, γ originates from the difference between the attractions and repulsions felt by molecules situated in the asymmetric surface layer compared to those in the symmetric bulk.

It was early noted that the introduction of a solute in pure water changes the surface tension and that concentration plays a crucial role. In a systematic study by Wagner in 1924 it was concluded that all inorganic salts raise the surface tension of water [91]. It is therefore reasonable to conclude that the surface distribution of solutes is related to the surface

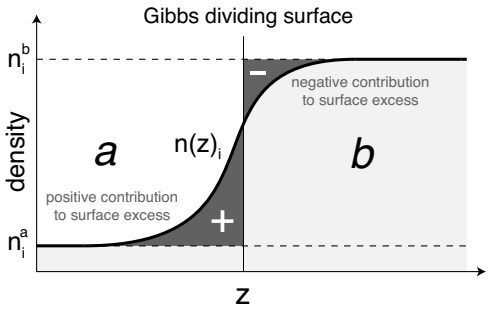

Figure 4.1: Illustration of how the surface excess n_i^α of a component i at the interface of two phases a and b depends on the respective bulk concentrations n_i^a and n_i^b together with the position of the Gibbs dividing surface.

tension. However, equation (4.2) provides no such information. In the late 19th century Josiah Willard Gibbs developed a powerful formalism relating the surface tension of a solution to the *surface excess* of the solutes [90].

The surface excess n_i^α of the i:th component of a multi-component system is defined relative to the *Gibbs dividing surface* joining two phases a and b (depicted in figure 4.1), and the bulk concentrations n_i^a and n_i^b of the i:th component in the respective phase:

$$n_i^\alpha = \int_{\text{phase } a \text{ up to Gibbs surf.}} (n_i - n_i^a) dV + \int_{\text{phase } b \text{ up to Gibbs surf.}} (n_i - n_i^b) dV \tag{4.3}$$

It should be noted that the value of n_i^α depends on the position of the Gibbs dividing surface. When treating solutions it is conventional to define the Gibbs surface such that surface excess of the solvent is zero. If the solvent component is indexed with $i = 1$ and the solutes as $i = 2, 3, 4...$, it is convenient to refer to the solute *surface excess concentration* defined as

$$\Gamma_1^i = \frac{n_i^\alpha}{A} \tag{4.4}$$

where A is the area of the surface considered. Γ_1^i is thus a measure of the amount of component i that is adsorbed at the interface per unit area. The *Gibbs adsorption equation* can then be written as

$$\Gamma_1^i = -\left(\frac{d\gamma}{d\mu_i}\right)_{T,\mu_{i\neq j}} \approx -\frac{1}{RT}\left(\frac{d\gamma}{d\ln n_i}\right)_T \tag{4.5}$$

This equation implies that the surface tension of solutions with a net positive surface excess concentration decreases when adding the solute –

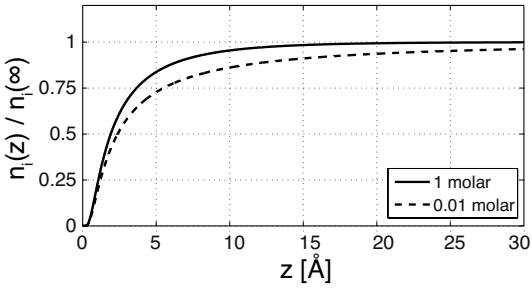

Figure 4.2: Surface density profiles for two concentrations of a 1:1 Debye-Hückel electrolyte as predicted by the Onsager-Samaras model at T = 300 K. Note that the outermost surface layer is completely void of ions.

this is the case for organic surfactants. Analogously, the net surface excess concentration must be negative for solutions with solutes that raise the surface tension, e.g. inorganic salts. This is an important result relating the macroscopic surface tension of the solution to the microscopic distribution of the solutes in the interfacial region.

4.3 The microscopic surface structure of aqueous electrolytes

Many attempts have been made to derive models for the detailed microscopic surface structure of aqueous electrolytes, i.e. to find expressions for the density profiles of ions near the water/vapor interface. Even though equation (4.5) puts some restraints on what the interface can look like in order to conform with surface tension data, it should be clear that infinitely many different solute distribution functions satisfy the equation.[1] Some other assumptions must hence be made if the exact surface structure of a solution is to be inferred. In 1934, Onsager and Samaras published a paper, presenting a model based on classical electrostatics, where ions in the interface region are treated as point charges and the liquid/vapor surface is modeled as a sharp interface between two continuous dielectric media [92]. By assuming that the interaction of an ion with its own image charge, located at the other side of the interface, is the only factor contributing to the surface potential of mean force they could derive an analytical expression for the solute density profile

$$n_i(z) = n_i \cdot \exp\left(-\frac{q^2 \exp(-2\kappa z)}{16\pi\epsilon\varepsilon_0 k_B T z}\right) \tag{4.6}$$

[1] Even though these distributions are equivalent with respect to surface tension of the electrolyte, they may result in radically different chemical properties of the surface.

where q is the charge of the ions, ϵ is the dielectric constant of water and the exponential damping factor κ comes from the ionic screening in the solution, derived from Debye-Hückel theory. Equation (4.6) is plotted in figure 4.2 and shows how the solute density is predicted to drop near the interface, resulting in a negative surface excess in accordance with the Gibbs adsorption equation (4.3).

Even though the Onsager-Samaras model reasonably well reproduces the general surface tension behavior of dilute aqueous solutions it fails to account for experimental data at higher concentrations. What is worse is that the model cannot account for the significant *ion specificity* in the surface tension behavior of aqueous electrolytes, e.g. an aqueous solution of 0.1M NaCl has different surface tension than 0.1M of LiI [91].

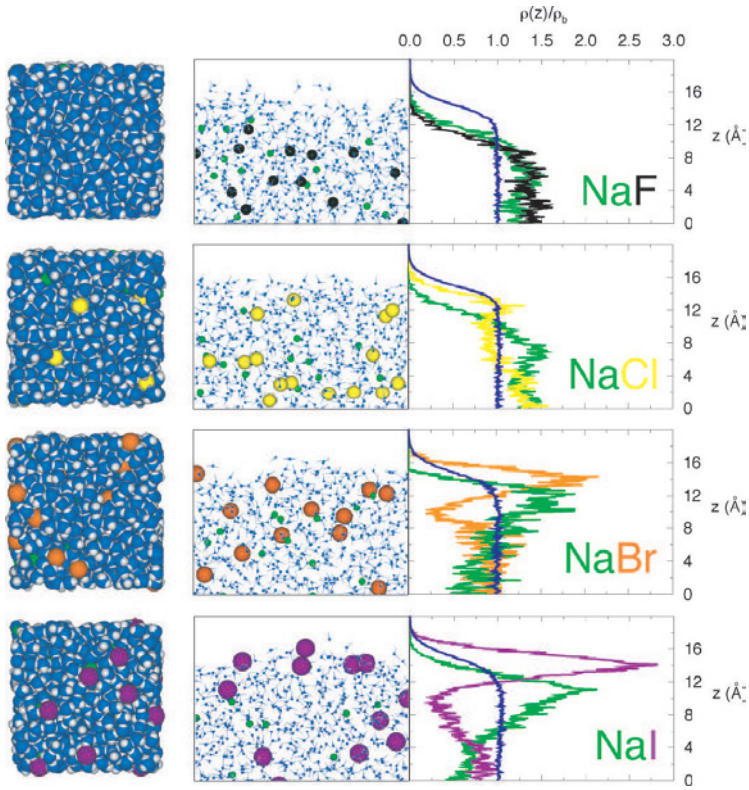

Figure 4.3: Top- and side-view snapshots as well as converged density profiles from classical MD simulation of various alkali-halide solutions employing polarizable force fields [93]. Small hard anions, such as F^-, are repelled from the solution interface while large polarizable anions such as I^- have an increased propensity to exist at the surface. Reproduced with the permission of the publisher.

A drastically different picture of the aqueous solution interface from that given by the Onsager-Samaras model has recently emerged from MD simulations employing polarizable force fields, including ion specific polarizabilities [94–96]. Jungwirth and Tobias have shown that such simulations predict solute-specific density profiles, and can reproduce many of the ion-specific phenomena observed in experiments [93]. Small ions with low polarizability such as Li^+ and F^- (referred to as *hard* ions) exhibit density profiles similar to what is predicted by the Onsager-Samaras model (see the MD simulations of an aqueous NaF solution in the top panel in figure 4.3). In contrast, large and polarizable (soft) anions exhibit a very different behavior near the water surface, and for NaBr and NaI (two bottom panels in figure 4.3) the ions can actually be enhanced in the outermost layers. This enhancement, contributing with a positive part to the surface excess, can still be compensated for by a larger subsurface depletion, which results in a net negative surface excess. Hence, it should be clear that this type of non-monotonous ion distribution can still be compatible with the Gibbs adsorption equation.

Recently, a new class of analytical models have been developed that capture essential parts of the behavior revealed in MD simulations [97, 98]. While earlier electrolyte theories have modeled solvated ions as hard spheres, with the charge located at the center of the sphere; Levin and co-workers have explicitly included the effects of asymmetric charge distributions over the ionic spheres in the calculation of the electrostatic surface potential, arising from the induced polarization near the interface. In general, this is a tricky problem to solve but it is enlightening to have a look at the special case where a perfectly polarizable anion is situated right in the interface, i.e. with one of its hemispheres submersed in water and the other sticking out in air. The ratio between the occupancy of the excess electron in the two phases is then given by $q_{water}/q_{air} = \epsilon_{water}/\epsilon_{air}$. This means that only 1.25% of the electron charge will be exposed to the low-dialectric phase. Compare this with the analogous situation for a rigid ion, where 50% of the electron cloud will lack solvation, and you may start to understand why polarizability can be a key factor for driving anion-specific surface adsorption.

Beyond removing part of the energy penalty associated with incomplete screening of the negative charge of surface-bound anions, polarization also enables the formation of stabilizing surface-dipoles – this contribution can even cause a surface enhancement [93]. Taking an ion from the bulk to the surface is also associated with the reduction of another energy term, namely the free energy cost of forming a cavity within the dielectric aqueous medium, as was discussed in section 2.3.2. This contribution is not large compared to the free energy of solvation of the ionic charge

itself[2] but can be important for the energy differences between bulk and surface solvation motifs – this is after all why hydrophobes are enriched at the water surface. Only recently have electrolyte models been developed which explicitly take aspects of hydrophobic hydration into account [99]. As an illustrative example of how hydrophobic effects influence the surface coverage of aqueous ions, Horinek et al. have recently shown that MD simulations with bulk-parameterized non-polarizable force fields predict a weak enhancement of I^- for the water surface [100].

4.4 How to probe the distribution of solutes at the water surface using photoelectron spectroscopy

Later in this chapter we will discuss a number of studies in which we have used photoelectron spectroscopy to probe the distribution of ions and molecules near the water surface. Before going into the details of any specific system we should first stop and contemplate how the method can be used to gain this sort of information. We will utilize the high (but variable) surface sensitivity in UPS and XPS, owing to the short inelastic mean free path of electrons transversing in condensed matter; this was briefly touched upon in section 3.2. In so-called *depth profiling* photoemission experiments of condensed samples one utilizes the fact that IMFP varies as function of kinetic energy of the photoelectrons. The general qualitative behavior of the IMFP curve has been found to be quite similar for a wide range of different materials, characterized by a minimum of about 5-10 Å in the 50-100 eV KE range, with a steep increase toward the low energy side, and a steady but slower increase for higher KEs. This has led to the useful concept of an 'universal' mean free path function, common to all materials [54]. This is however only a first approximation, and measurements have revealed significant material dependence.

Since the inelastic mean free path governs the information depth in depth-profiling photoemission experiments, quantitative determination of solute density variations in the surface region are limited by an uncertainty in the IMFP function. But the interest in more exact determinations of the IMFP function in aqueous systems extends well beyond the specialized interests of the electron spectroscopic community. For example, electron inelastic scattering events of secondary electrons generated in cancer radiotherapy are responsible for the creation of highly

[2] Which is why it e.g. can be left out of the Born model and it still works pretty good.

toxic water radicals [101–103]. Knowledge about electron energy loss in the aqueous phase, potentially leading to the formation of secondary tumors, is hence important for minimizing radiation induced damage and can have implications for proper patient dose planning.

In paper I we experimentally address electron attenuation in the aqueous phase. IMFP is defined as the average distance an electron has travelled in a material before it inelastically scatters, measured *along* the trajectory, which is nearly impossible to determine directly through experiments. A related quantity is the electron effective attenuation length (EAL) which is the (shortest) distance from a point A to point B, at which the initial electron signal is reduced to 1/e [104]. As sketched in the left panel of figure 4.4, the IMFP can be significantly larger than EAL if elastic scattering is efficient in the medium. In the case of weak elastic scattering, IMFP and EAL are almost identical, as depicted in the right panel of figure 4.4. Experiments can determine EAL values, but cannot easily distinguish between inelastic and elastic scattering contributions to the total signal attenuation, i.e. we cannot extract the corresponding IMFP value from an EAL measurement. It should however be noted that EAL often is the important quantity, e.g. for determining the distribution of toxic water radicals in the volume surrounding an irradiated tumor as well as governing the information depth in photoemission experiments. Also note that IMFP is a much more common concept in the literature and that it is often used in the sense of EAL (which is also the case for many papers in this thesis).

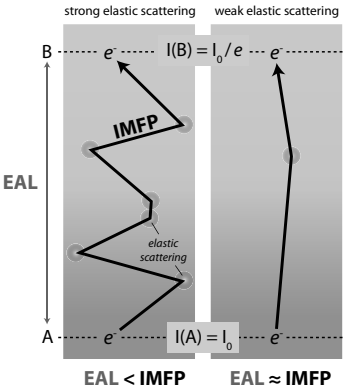

Figure 4.4: Relationship between the electron inelastic mean free path (IMFP) and the electron effective attenuation length (EAL).

In paper I we utilize the fact that the recorded signal intensity of a photoemission line is dependent on the EAL at a given photoelectron kinetic energy. PE signals can generally be expressed as the integral over the density function, $n_i(z)$, associated with a molecular or atomic species i, exponentially attenuated with the effective attenuation length EAL. The PE emission density $I(z)$ from a depth z in the sample is proportional to the density of the emitting species. Since the electron attenuation length, to a good approximation, is inversely proportional to the integrated particle density from an emission depth z [105], the total recorded photoelectron signal I_i from a species i, can be expressed

as

$$I_i = \alpha F \sigma T \int_0^\infty n_i(z) \cdot \exp\left(-\frac{1}{\mathrm{EAL_{jet}}} \int_0^z \frac{n_{tot}(y)}{n_0}\, dy\right)\, dz \qquad (4.7)$$

where $n_{tot}(z)$ is the sum of density profiles for all species and n_0 is the average density in the bulk, i.e. $n_{tot}(\infty) = n_0$. σ is the photoionization cross-section, F is the total photon flux and α is an experimental alignment factor, which is determined by the illuminated area of the sample and the entrance aperture solid angle of the electron analyzer. Finally, T is the transmission function of the electron analyzer.

In the case of pure water there is only one molecular species, hence $n_i(z) = n_{tot}(z)$. If we define $\alpha' = \alpha n_0$ and make the variable substitution

$$z' = \frac{1}{\mathrm{EAL_{jet}}} \int_0^z \frac{n_i(y)}{n_0}\, dy \quad \longrightarrow \quad dz' = \frac{1}{\mathrm{EAL_{jet}}} \frac{n_i(z)}{n_0}\, dz \qquad (4.8)$$

equation (4.7) transforms into the much simpler

$$I = \alpha' F \sigma T\ \mathrm{EAL_{jet}} \int_0^\infty \exp(-z')\, dz' = \alpha' F \sigma T\ \mathrm{EAL_{jet}} \qquad (4.9)$$

meaning that the measured photoemission signal I is proportional to the electron effective attenuation length EAL; just the quantity we want to determine. If we can account for the other factors in equation (4.9), we can thereby derive the relative EAL(KE) values from O1s PE intensity measurements in pure water as function of kinetic energy. α' remains constant over the measurement series and T as well as F can be determined, individually.

Two significant problems remain: First, there exists no good molecule-specific photoionization cross section values σ for O1s of water which remains to be accounted for in equation (4.9), a problem that is extensively discussed in paper I. Secondly, even if we derive *relative* EAL values from water O1s intensity measurements, an *absolute* length scale must still be determined, which needs to be done independently. Here we pursue the strategy to determine the missing scaling factor from depth-profiling measurements of ions residing in the interfacial region of a 4m NaI aqueous solution. As discussed above, MD simulations show that the soft and polarizable iodide is significantly enhanced compared to the small and hard sodium cation. The structured interface can thus function as a "ruler" on the molecular scale and the comparison of experimental PE data with MD simulations yields the missing proportionality factor, anchoring the relative EAL values on an absolute length scale. The experimentally estimated EAL function for liquid water and aqueous solutions is shown in figure 4.5.

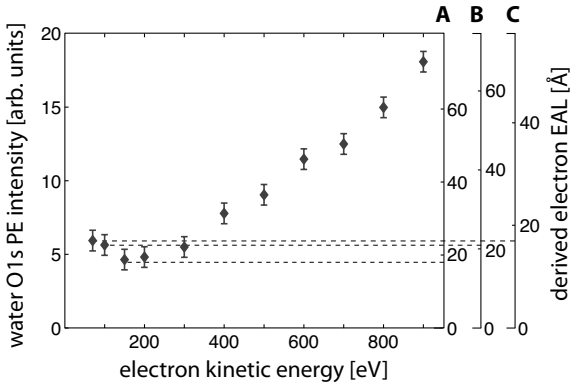

Figure 4.5: Experimental EAL curve for water derived from O1s PE intensity measurements of pure liquid water (left y-axis). The (right-hand side) absolute length scale **A** was determined through comparing experimental and simulated ion density profiles from a 4m NaI aqueous solution. **B** and **C** are the length scales obtained when using ice calibration points (see paper I for details).

Even though it would be highly useful to have complete control over the EAL values and photoionization cross sections for the components of a certain solution we are investigating it must be confessed that there are large uncertainties associated with the approach just outlined. First of all, it is obviously risky to use tabulated atomic cross to account for the corresponding solvated ionic species; if the difference in surface affinity between the species compared is small, the cross section errors might dominate the result. Furthermore, we are most often not primarily interested in explicitly depth profiling a given solution, but rather to see how the surface structure evolves with composition of the solution, e.g. solute concentration or pH. For these reasons, we typically choose a photon energy so that the resulting photoelectrons have kinetic energies near the minimum of the inelastic mean free path curve and monitor *relative* changes in the spectra as function of the variable of interest. In this way, both the EAL and cross-section values remain (approximately) constant throughout the measurement series and the intensity evolution of a certain component can be evaluated without the explicit correction for these factors.

4.5 XPS studies of inorganic ions at the water surface

The following section deals with three studies we have conducted concerning the surface coverage of inorganic ions, and which are reported in

papers II-IV. They can be seen as complementary, exploring the effect of three different parameters on the surface structure of electrolytes: anion size/polarizability, concentration, and the pH of the solution. In the following we will go through these, one at a time, building up a more and more nuanced picture of the forces governing the surface structure of aqueous salt solutions.

4.5.1 Effects of anion size and polarizability

In simulations of atomic systems, computational scientists are not necessarily limited by what systems actually exist in reality – in the computer they can study how a system with a given set of parameters would behave *if* it existed, and thereby isolate the effect of a certain parameter on one or several of the system's properties. By varying the size of a solvated ion and by switching on and off the polarizabilities of the water solvent and the solute in MD simulations, Vrbka et al. have predicted that the anion surface coverage should increase with its size and polarizability [93, 96], in accordance with the discussions in section 4.3. However, few experiments have been able to directly measure the surface coverage of inorganic ions at the water surface. Cheshnovsky and co-workers found evidence that I^- is surface-solvated from photoemission studies of small water clusters [106], while Hemminger and co-workers showed that I^- is surface enhanced relative to its counter ion in KI crystals, wetted to the deliquescence point [107]. While these experiments were crucial for lending credibility to the MD simulations of Jungwirth and Tobias they were only model systems of aqueous solutions. Liquid-jet experiments, however, such as those reported in this thesis, concerns the "real thing".

In experiments we typically cannot vary a single property of a solute, such as its size, without at the same time changing other parameters. As outlined in the previous section we also have to take other practical aspects into account if we are to do a successful photoemission experiment, e.g. each species must exhibit a suitable photoline, and their respective intensities must be comparable in some meaningful way. Searching for a suitable set of ions to study experimentally we came across the oxychlorine anions, ClO_n^-, $n = 1-4$, which are appealing for the intended study. Going from the simple chloride anion to perchlorate (ClO_4^-) the charge is unaffected while both the size and polarizability increases. From a spectroscopic point of view they are also ideal since they all contain chlorine; meaning that they appear in the same core-level spectral regions, e.g. Cl 1s and Cl 2p. The lines can also be expected to be shifted relative to

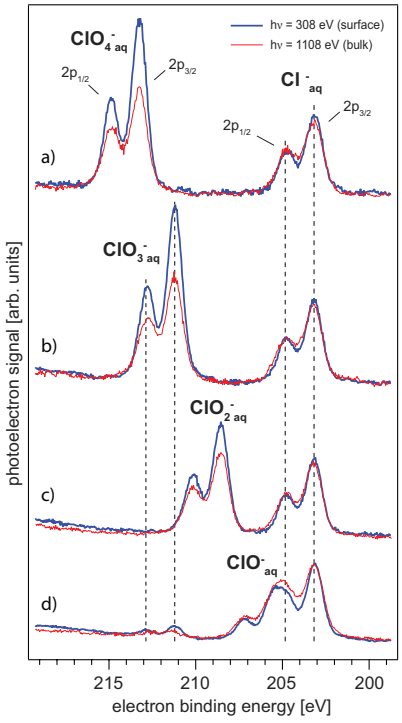

Figure 4.6: Cl 2p photoemission spectra from aqueous solutions of 1m $NaClO_n$ co-dissolved with 1m NaCl; $NaClO_4$/NaCl (trace a), $NaClO_3$/NaCl (b) and $NaClO_2$/NaCl (c) and NaClO/NaCl (trace d).

each other (making them quantitatively distinguishable) given the large variation in oxidation number throughout the series.[3]

In paper II we report a depth profiling study of various $NaClO_n$ salts (n=1-4), co-dissolved with NaCl in water. For each solution we compare the oxychlorine anion Cl 2p photoemission signal relative to that of chloride, as function of excitation energy. Chloride thus serves as a reference point, and the surface propensities of the different ClO_n^- ions are monitored relative to, and in co-solvation with, Cl^-. This type of measurement does not in itself provide information about the absolute distribution of the oxychlorine anions in the interfacial region, since the density function of the chloride reference is not independently measured. However, we can monitor differences in the propensities of the oxychlorine anions for the aqueous surface, depending on the oxygen coordination number. Importantly, the fact that we are only comparing relative photoelectron

[3]The chloride anion has oxidation number -1. This value is increased by 2 for the Cl atom as function of each oxygen added to the oxychloride anions, meaning that the Cl atom in perchlorate has oxidation number +7.

intensities from core-levels of the same element leads to the cancelation of many problematic factors discussed in the previous section. This is because the localized and highly atomic character of the Cl 2p orbital makes changes in photoionizaion cross section largely independent of chemical environment at kinetic energies sufficiently far above threshold, i.e. higher than 50-70 eV [54].

Figure 4.6 shows the Cl 2p PE spectra of NaCl co-dissolved with $NaClO_4$ (a), $NaClO_3$ (b), $NaClO_2$ (c) and NaClO (d), measured at two different photon energies. The blue trace, taken at hν = 308 eV, corresponds to photoelectrons of approximately 100 eV KE, resulting in high surface sensitivity due to the short electron inelastic mean free path in this energy range. This is contrasted against the red trace, taken at hν = 1108 eV, resulting in less surface sensitive electrons with kinetic energies of about 900 eV. All spectra have been normalized to the intensity of the chloride Cl 2p feature. Variations in intensity of the respective oxychlorine photoemission line with excitation energy therefore reflect relative differences in the surface coverage of the ions.

Our study shows that the oxygen coordination number n has a large effect on the surface coverage of the oxychlorine anions – perchlorate has the highest propensity, followed by chlorate and chlorite – inferred from the decrease in their respective intensities at the higher photon energy. These conclusions are further qualitatively corroborated by the MD simulation of the 1m $NaClO_4$ / 1m NaCl system reported in paper II, employing polarizable force fields for water and all ions. Our results thus indeed indicate that the surface propensity of anions for the water surface increases with size and polarizability of the solute.

4.5.2 Effects of ion-ion interactions at higher concentrations

Until now we have only talked about how the inherent properties of an ion affects its affinity for the water surface. In doing so we have implicitly neglected the role of ion-ion interactions; a contribution that varies with the concentration of the electrolyte. In paper III we therefore directly address the question of how the surface coverage of polarizable anions is altered with total concentration. The first part of this work deals with *simple* solutions, i.e. where a single inorganic salt has been dissolved in water. Experimentally, we have chosen to work with LiBr and LiI as model systems for concentration dependent surface effects of simple solutions. The reason for this choice is two-fold: First, the iodide and bromide anions are thought to have the highest surface affinity of all atomic ions while Li^+ is considered to be surface repelled, based on the

considerations outlined earlier in this chapter. Secondly, and purely practical from a spectroscopic standpoint, we can utilize the fact that highly suitable core-level photolines from all these species (Li1s, I4d and Br3d) fall within a narrow BE range (52-78 eV). This means that both cations and anions can be probed in the same spectra and have approximately the same kinetic energy.

Figure 4.7a shows the Li1s and I4d photoelectron spectra from aqueous LiI solutions, allowing us to monitor the respective anion and cation signals as function of concentration. Panel b shows the anion/cation ratio from the integrated PE peaks, normalized to the values at the lowest concentration (0.25 M) for LiI (open circles) and LiBr (filled squares). While no clear effect is observed for LiBr the relative amount of I^- in the surface appears to decrease compared to the Li^+ counterions in concentrated LiI solutions. Assuming that the iodide anion is surface enriched relative to its cation in the dilute limit – what effects could explain these observations? We can identify at least three, closely connected reasons as to why the surface affinity of the anion should gradually decrease, i.e. that the anion surface concentration should grow sub-linear relative to its bulk concentration, while the cation surface affinity instead should increase slightly. First of all, the self-repulsion in the respective anion- and cation-enriched interfacial regions will increase if the density profiles of the respective components are simply re-scaled with concentration. Therefore, the anion/cation surface separation will tend to decrease in stronger electrolytes. If the anion is preferentially adsorbed at lower concentration it can further display a saturation behavior at higher concen-

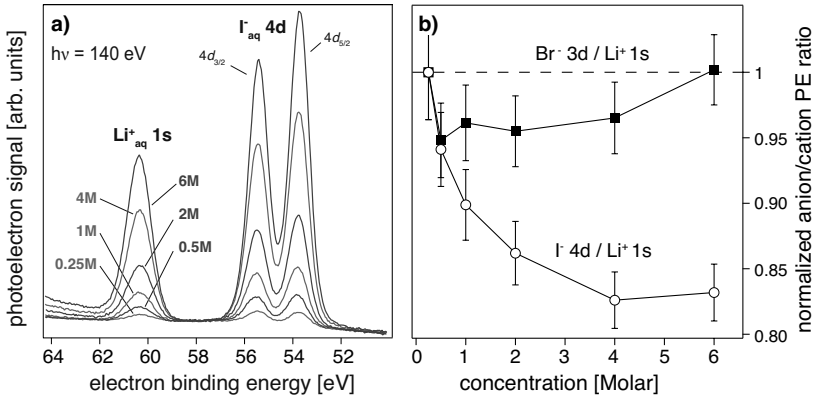

Figure 4.7: a) Surface sensitive photoelectron spectra of aqueous LiI solutions at concentrations ranging from 0.25 to 6 M. b) Concentration dependence on the integrated anion/cation PE ratios for LiI (open circles) and LiBr (filled squares) normalized to the value at 0.25 M.

tration, due to the limited number of available surface "sites". Finally, the electrostatic screening length is reduced at higher concentrations. In Debye-Hückel theory it takes the form

$$\kappa^{-1} = \sqrt{\frac{\epsilon\varepsilon_0 k_B T}{2N_A e^2 I}} \tag{4.10}$$

where

$$I = \frac{1}{2}\sum_{i=1}^{n} n_i z_i^2 \tag{4.11}$$

is the ionic strength of the solution, in which n_i and z_i are the concentration and charge of the i:th component, respectively.[4] This means that the electric field arising from the interface is more rapidly screened in the sub-surface. As a result, the cations (which are more strongly surface repelled than the anions) can move further out at higher concentrations.

In paper III we compare the concentration dependent photoelectron spectra of alkali-halide solutions to MD simulations, employing polarizable force fields. We conclude that all the effects discussed above contribute to the concentration-induced weakening of the structured interfacial layer. The agreement between experiments and simulations further corroborates the notion that soft polarizable anions are preferentially adsorbed at the water surface and furthermore illustrates the importance of ion-ion interactions in determining the exact surface structure.

Using the same methodology as just described we have also looked at the surface structure of *mixed* alkali-halide solutions, more precisely mixtures of NaCl and NaBr with the former as the majority component, as function of total concentration. This type of mixture is interesting as a model system for naturally occurring aqueous solutions of seawater origin; while the dominant solute is NaCl, about 1 out of 650 solvated anions is Br^- [108].

We have looked at mixed NaBr/NaCl solutions with a fixed Br^-:Cl^- ratio of 7:100, in order to obtain a reasonable spectral contrast between the different solutes. Investigating the surface structure of these solutions we have found a phenomenon which, at first sight, seems to contradict the conclusions just drawn from the simple systems: As seen in figure 4.8 the Br^- PE signal now *increases* relative to the Na^+ cations with concentration. But didn't we just learn that the anion surface coverage should decrease with concentration? This apparent paradox is resolved once we realize that the present system contains two different anions,

[4]It should be noted that Debye-Hückel theory is only valid near infinite dilution, i.e. not in the concentration range we are here considering. However, the model still provides a qualitative understanding for the problem at hand.

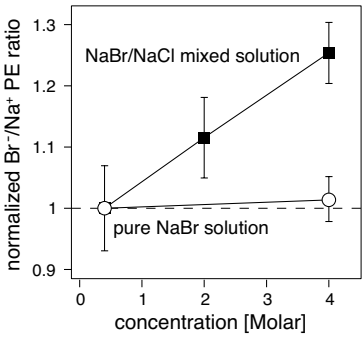

Figure 4.8: Concentration dependence on the integrated Br^-/Na^+ PE ratios for mixed NaCl/NaBr solutions, in which Br^-:Cl^- = 7:100. The values have been normalized to lowest concentration, i.e. 0.25 M.

Br^- and Cl^-, each associated with its own density profile that do not have to be identical.

In mixed systems like these it is important to distinguish between the distribution of negative charge carriers (the sum of the anion density profiles) and that of a specific type of anion. The distinction is schematically illustrated in figure 4.9. The top trace shows the *total* anion density profile $n_{total}(z)$ in the interface region at a given concentration – this is the distribution which is partially governed by the electrostatic effects discussed above. We now assume that the electrolyte contains two different types of anions, A and B, at equal concentrations. Traces a-c in figure 4.9 show three different ways these can be partitioned: In a, both anion distributions are identical, i.e. $n_A(z) = n_B(z) = \frac{1}{2}n_{total}(z)$. In trace b, anion A is more strongly surface enriched than B, while trace c shows the

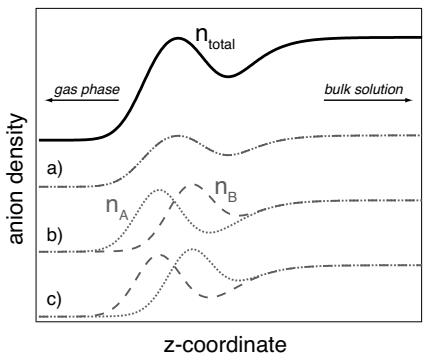

Figure 4.9: Principle sketch showing the partitioning of anions A and B (each with same bulk concentration) in three radically different ways, all fulfilling the condition $n_{total}(z) = n_A(z) + n_B(z)$.

reversed situation. Since all cases satisfy the overall anion distribution requirement ($n_{total}(z) = n_A(z) + n_B(z)$) this illustrates that electrostatic effects is not uniquely determining the distributions of the co-solvated anions. This stems from the simple fact that the surface enrichment of a particular anion does not necessarily imply a net surface charge redistribution if compensated for by an equivalent depletion of another anionic species in the same spatial region.

It is hence natural to interpret the present experimental results as originating from Br^- being "salted out" towards the water surface by Cl^-, i.e. that the former gradually gets surface enriched at higher concentrations. This must be balanced by a depletion of chloride, restoring the interfacial charge balance. The MD simulations presented in paper III, employing the same polarizable force fields as for the simple solutions, supports this interpretation.

We are still left with the crucial question; *why* is Br^- "salted out" by Cl^-? We can look at this question from either a thermodynamic or microscopic perspective, providing complementary pictures. First, it is known that the excess free energy of mixing equimolal solutions of sodium chloride and sodium bromide is slightly positive for 1 M solutions, and further increases at higher concentrations [109]. This reveals that there is a weak unfavorable anion-anion interaction in the bulk region, even though the entropy gain upon full bulk mixing is the dominating contribution to the total free energy. There thus exists an energetic incentive for anion partitioning in the interface region; if Br^- is enriched in the surface layer while Cl^- preferably occupies the subsurface region (compare figure 4.9) the unfavorable interaction upon mixing is minimized. The inherent differences in surface propensities of the two anions will further come into play when the two are mixed: The energy will be lowered if the more strongly hydrated species, i.e. Cl^-, is preferentially in the bulk enabling full hydration. Populating the hydration-wise less favorable surface sites preferentially with the more weakly hydrated but polarizable Br^- (which reduces its surface energy, see section 4.3) therefore both lowers the total bulk free energy and leads to a more favorable surface configuration. Naturally, these effects become more important at high concentrations, at which the different anionic species starts to effectively compete for the solvent molecules, in agreement with the experimental findings.

In summary, we have shown that Cl^- is "salting out" Br^- from the bulk of mixed NaCl/NaBr solutions to the surface – an effect that becomes more and more important at higher concentrations. This again illustrates how ion-ion interactions are crucial for determining the microscopic surface structure of aqueous electrolytes. The here observed "salting out" effect may well be a contributing factor to the anomalous

importance of bromide chemistry in the atmosphere, a topic which has stimulated quite some research during recent years [86].

4.5.3 Effects of pH

Another parameter that varies in naturally occurring aqueous systems is pH. A wide range of strong acids/bases are abundant in the troposphere [85] and will readily dissociate in aqueous aerosols of seawater origin. The natural question arises: how will the availability of free hydronium and hydroxide ions influence the ionic surface structure of the resulting solution?

Since most atomic inorganic ions are not themselves titratable, the addition of a strong acid or base (such as HCl or NaOH) to a simple aqueous 1:1 electrolyte will not cause any structural modifications of the original solutes. The resulting acidic and alkaline electrolytes can hence be seen as as mixtures of two types of cations and two anions, with higher ionic strength than the original solution. The problem at hand is thus similar to that discussed in the previous section, i.e. how a given anion will be distributed in the surface region of a mixed electrolyte. There is however one important difference: H_3O^+ and OH^- don't behave like any other ions in water.

Recently, the propensities of hydronium and hydroxide for the water surface have been under intense debate [43–47]. The solvation patterns of hydronium and hydroxide are complicated, largely originating from their unique ability to form directional H-bonds with the water solvent, and cannot be inferred from that of other aqueous solutes. Traditionally, the H-bonding motifs of the two water ions have been thought of as each other's mirror images, where H_3O^+ only can donate three bonds while OH^- only accepts three [110]. This picture has recently been questioned, a topic to which we will return in section 6.2. Briefly, *ab initio* calculations indicate that while the negative charge on the H_3O^+ oxygen site is too weak to enable a proper acceptor H-bond, the hydrogen of OH^- is sufficiently positive for the ion to donate a bond to the aqueous solvent [111]. While OH^- therefore fits rather well into the tetrahedral water network, the asymmetric binding motif of hydronium gives it an amphiphilic nature. In 2004, Voth and co-workers showed that classical MD simulations indeed predict an enhancement of H_3O^+ in the top layer of the water surface, where it can orient its "hydrophobic" oxygen side away from the solution and still donate three H-bonds to water molecules in the subsurface [112]. On the other hand, several molecular calculations show that the strongly hydrated OH^- instead avoids the water surface [113, 114]. These results have resulted in the notion that

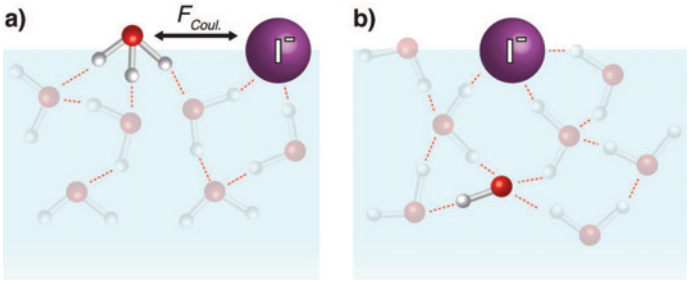

Figure 4.10: Schematic illustration of the proposed mechanisms causing the surface enhancement of I^- in non-neutral aqueous solutions.

the surface of neat water is "acidic".[5] Interestingly, this molecular-scale picture is in grave conflict with the interpretation of ζ-potential measurements of the water surface as well as electrophoretic and titration measurements in terms of strong adsorption of hydroxide [47, 115]. While these macroscopic measurements clearly show the presence of a negative charge on the water surface, the microscopic interpretation in terms of OH^- adsorption lacks a reasonable mechanistic rationale.

In paper IV we experimentally study 0.5 M LiI aqueous solutions, following the I4d/Li1s photoelectron spectrum as function of pH. The measurements are accompanied by MD simulations, in order to validate the interpretation of the PES data and provide further mechanistic insight into the driving forces for ion-specific adsorption in these solutions. It is found that the I^- surface coverage is weakly increased in *both* acidic and basic solutions. While this result is of interest in its own right, since it shows that pH variations will further drive the surface enhancement of large polarizable anions at atmospherically relevant surfaces, we have primarily been interested in understanding what it tells us about the surface propensity of H_3O^+ and OH^-. From simple electrostatic arguments and by analysis of the MD simulations in paper IV we argue that these findings are in accord with the recently proposed picture of a weak enhancement of hydronium and a weak repulsion of hydroxide at the water surface. The argument is schematically illustrated in figure 4.10: In acidic solutions, depicted in a), the surface enrichment of H_3O^+ leads to an electrostatic "pull" on iodide toward the interface. In the basic solution, shown in b), OH^- avoids the surface and is therefore replaced by I^-, i.e. the latter is "salted out" from the bulk to the surface region by hydroxide according to the same mechanism as was discussed in the

[5]This terminology is somewhat confusing as pH is defined as the negative logarithm of the proton *activity*, which by definition is the same throughout the solution at thermodynamic equilibrium. We should thus rather talk about the surface *concentration* of H_3O^+ when discussing this phenomenology.

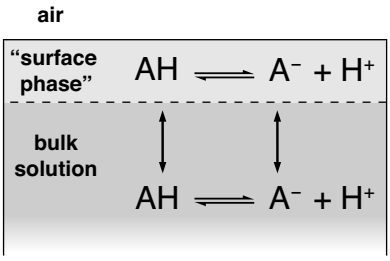

Figure 4.11: Principle sketch of how the energetics of a "surface acid-base reaction" can be related to the surface propensities of the reactants and products.

previous section. Note that the opposite behavior would be expected if the surface affinity of OH^- was larger than that of I^-.

4.6 XPS STUDIES OF WEAK ORGANIC ACIDS AT THE WATER SURFACE

In our studies of simple inorganic ions we have so far only been concerned with the spatial distribution of the particles at the water surface, not their "chemical state", given that no real chemistry takes place in these simple systems. When we now turn our attention to weak organic acids at the water surface things get more complex. Brønsted acids can dissociate in water, resulting in a hydrated proton and an anionic conjugate base form of the acid – these ionic fragments are stabilized in the high-dielectric aqueous medium.[6] The equilibrium reached between the acid and its conjugate base in the bulk solution at a given pH (which can be formulated as an acid equilibrium constant K_a) thus reflects the energy difference between the neutral molecular state and that of the ionic fragments upon dissociation. We now pose the seemingly simple question: How should we think about the acid-base reaction at the water surface?

The problem at hand is schematically illustrated in figure 4.11 in which we consider the equilibrium between an acid AH and its ionic fragments A^- and H^+ in two idealized "phases"; the bulk solution and the solution "surface phase" – the latter being in contact with air (or just water vapor if one rather prefers). If we choose the bulk solution as our thermodynamical reference state it is important to realize that the *activities* (described by the acid equilibrium constant K_a) is the same throughout the system [116]. However, the *concentrations* of the reactants and products might

[6] The lack of such electrostatic screening is naturally the reason why acids typically don't dissociate in air.

be very different in the surface and bulk phases at the same pH. The respective equilibria $AH \rightleftharpoons A^- + H^+$ in figure 4.11, thought of in terms of concentrations, might thus be very different in the two phases. What will determine the equilibrium in the surface phase, which we can think of as describing the "apparent surface acidity" of the molecule? This will ultimately depend on the surface propensities of the respective components, as illustrated by the vertical arrows crossing the phase boundary in figure 4.11. Thought of in this way, the present problem strongly resembles what we already have dealt with in the studies of inorganic ions at the water surface.

Given the sensitivity of XPS to local binding environments we are able to spectroscopically distinguish the protonation states of acids. In the following we will use this sensitivity to quantify the abundances and surface conformation of the respective charge state of a number of important weak organic acids.

4.6.1 Linear mono-carboxylic acids at the water surface

Linear mono-carboxylic acids, in which a carboxylic group (COOH) is attached to the end of a linear alkyl chain, represents the simplest class of organic acids. Due to the hydrophilic nature of the carboxylic group, forming weak hydrogen bonds with the aqueous solvent, and the hydrophobic character of the carbon chain, these systems are suitable model systems for studying amphiphilic molecular hydration. With increasing chain length, the hydrophobic interactions gradually govern the hydration patterns of the molecule, resulting in an increased surface activity at hydrophobic interfaces. Carboxylic acids are weak acids, dissociating into carboxylate ions ($R\text{-}COO^-$) upon release of the proton. The carboxylate group is a strong H-bond acceptor, shifting the ampiphilic balance toward hydrophilicity upon dissociation, which favors bulk hydration of the anionic conjugate base form. These considerations suggest that the surface occupancy of a carboxylic acid and its carboxylate at a given pH may be radically different from that in the bulk (i.e. that its apparent "surface acidity" is different from that in the bulk), forming the motivation for the experimental investigations reported in paper V.

Figure 4.12 shows surface sensitive C1s photoelectron spectra of 1 M acetic acid at different pH. Since we know the pK_a value, 4.57 (obtained from titration measurements, shown at the top-right inset in the figure), the bulk proportions between the acid and the acetate anion can be tuned to a desirable ratio by addition of a strong acid or base. In order to aid the fitting of photoelectron spectra from solutions where both the acid and

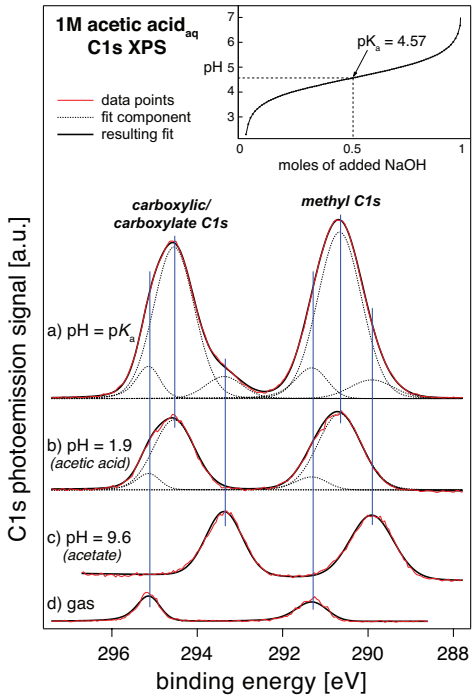

Figure 4.12: Carbon 1s photoelectron spectrum of acetic acid in water at various pH values at 1M total concentration. Note that the relative intensity scale of the different traces is not the same.

base forms are present, we have recorded the C1s spectra of pure acetic acid (trace b, pH = 1.9) and pure acetate (trace c, pH = 9.6). Since the acid form is rather volatile and evaporates from the solution surface, we have also recorded the C1s spectra of acetic acid in the gas phase (trace d). Equipped with fits of these three pure cases, trace a) shows how the spectrum at the equivalence point (i.e. pH = pK_a) can be decomposed, resulting in an excellent fit. As is immediately clear from this spectrum, the surface composition of the solution is radically different from the bulk; the $COOH/COO^-$ signal ratio obtained from the fits of Fig. 1a) is ∼7.3, i.e. much larger than unity, which is the bulk proportion at the pK_a value.

How can we make quantitative sense out of this result? Obviously, it does *not* mean that the surface occupancy of the acid is 7.3 times larger compared to the acetate at 1 M total concentration. The real value must instead be even larger since the photoemission signal contains bulk contributions from the respective components (yielding identical values). We therefore need some type of model to interpret the photoemission data. In our studies of the surface coverage of inorganic salts, described in

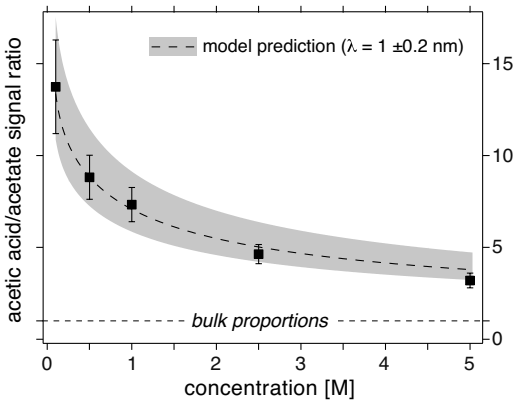

Figure 4.13: Comparison between the concentration dependent acetic acid/acetate PE signal ratios (filled markers) and the corresponding model predictions. The dotted line shows the model predication for $\lambda = 1$ nm while the grey shaded area shows the span between 0.8 nm and 1.2 nm. Higher ratios correspond to smaller values of λ.

the previous sections, the results from photoemission experiments were compared to converged density profiles from MD simulations. In order to make the connection between theory and experiments explicit we there employed simple attenuation models to simulate the photoemission response from the calculated profiles. Here we have chosen a different approach: The concentration dependent surface excess of small carboxylic acids and their corresponding carboxylates, which provides information about the surface affinity of the respective form, have been extensively studied in the literature [117, 118]. Under the simplest possible approximation, namely that the molecules contributing to the surface excess Γ_i are restricted to an infinitesimally thin layer in the outermost surface region of the solution, we can derive the following simple model expression for how the respective photoemission signal of the acid and carboxylate anion should vary with concentration

$$I = \Gamma_i + n_i\lambda \tag{4.12}$$

where λ denotes the assumed electron mean free path. By comparing the experimental results with the predictions of equation 4.12 we can thus investigate the validity of our model assumptions, i.e. if such a direct microscopic interpretation of the thermodynamic surface excess data is valid.

The concentration dependent acetic acid/acetate PE signal ratios as function of concentration is shown in figure 4.13, together with the corresponding model prediction. The dotted line shows the model ratios for

$\lambda = 1$ nm while the grey area spans out a region of ± 0.2 nm, i.e. between $\lambda = 0.8$ and 1.2 nm. As is clear from figure 4.13 the model well captures the overall trend in the experimental ratios between the acid and base forms. In paper V we also show that the absolute signal from the respective component is gradually deviating from the concentration dependent model signal, revealing that the excess molecules are on average located deeper inside the solution at higher concentrations.

4.6.2 Surface conformations of aqueous benzoic acid and benzoate

While it is clear from the previous section that the degree of dissociation of an acid at the water surface can be quite much smaller than in the bulk, we have not yet discussed the possible interfacial binding mechanisms of acids and their conjugate base forms on the molecular scale. In exploring such phenomena we have focused at benzoic acid, since it might show strong orientational effects at the water surface depending on its charge state. Such a behavior could have implications for our understanding of the molecule's reactivity and chemical function at numerous interfaces, not just the free water surface [119].

Benzoic acid is the simplest aromatic acid, made up from a carboxylic group attached to a benzene ring. It dissociates in water into the benzoate anion upon release of its proton. This makes it ideal to study with

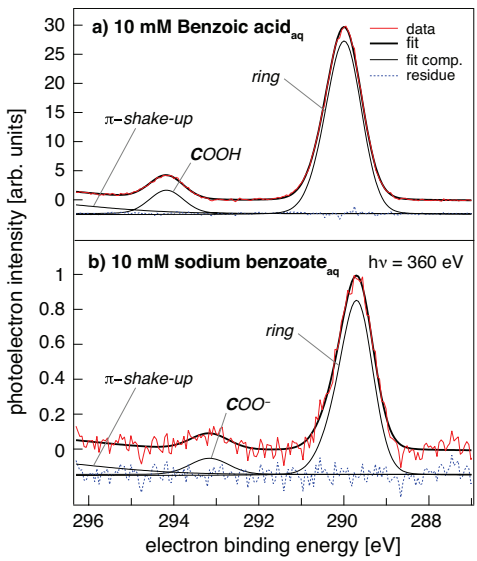

Figure 4.14: C1s photoelectron spectra of a) 10 mM benzoic acid and b) 10 mM sodium benzoate recorded with 360 eV photon energy.

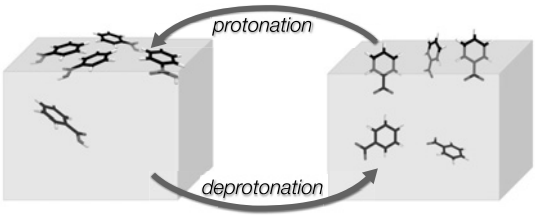

Figure 4.15: Schematic illustration of the proposed conformations of benzoic acid and benzoate at the water surface, based on XPS measurements and MD simulations.

XPS along the same lines as described in the previous section. The C1s spectrum yields two distinctly separated regions; one for the ring carbons and one for the carboxlic group – the latter is furthermore characteristically red-shifted by ∼1.2 eV upon deprotonation, as was seen for acetic acid in section 4.6.1. Panels a) and b) in figure 4.14 show photoelectron spectra from 10 mM benzoic acid and 10 mM sodium benzoate, respectively. By comparing the relative intensity of the two spectral regions for each charge state we can obtain information about whether the two forms display any difference in preferential surface orientation. Furthermore, the differences in total photoemission signal between the two charge states carries information about their respective surface activity.

By comparing the C1s photoemission spectra with the MD simulations reported in paper VI a consistent picture emerges, and which is summarized in the cartoon shown in figure 4.15: The hydrophobic ring of the neutral acid to a large extent drives the molecule to the interface region. There, its binding pattern is highly ordered; the weakly H-bonding carboxylic group causes a small tilt of the molecule with the COOH group pointing into the solution. At the same time the ring is lying nearly flat on the water surface, due to the favorable interaction of the polar solvent with the ring's π-system achieved in such conformations. This situation, which is depicted on the left side of figure 4.15, results in a strong PE signal even at the low concentration of 10 mM and is consistent with measured ring/COOH PE ratio of 7.8, i.e. slightly larger than the stoichiometric value 6. When the acid dissociates into the benzoate anion the carboxylic group, however, can form strong hydrogen acceptor bonds with the solvent. Since these are not possible to satisfy in a fully parallel geometry with the surface the deprotonation causes a flip of the molecule, so that the carboxylic group points downwards into the aqueous phase. Since the amphiphilic balance is shifted the molecule is now better bulk hydrated and the surface activity decreases – see right part of figure 4.15. This causes a pronounced decrease of the PE signal

upon deprotonation and a strongly non-stoichiometric ring/carboxylate C1s PE ratio of 10.1.

In summary, while the benzoic acid molecule acts as a surfactant, lying nearly flat on the water surface, the carboxylate group of the benzoate anion shows a sinker-like behavior. At the same time the aromatic ring acts as a buoy, minimizing unfavorable interactions of the hydrophobic part of the interfacial molecules with the aqueous solvent. The strong hydration of the carboxylate group also causes a considerable fraction of the ions to move into the bulk solution.

5. Core-electron spectroscopies as probes of molecular protonation state and local hydration structure

Even though the specialized spectroscopist sometimes likes to think differently, different spectroscopic techniques are good at different things. In the previous chapter we for example exploited the advantageous surface sensitivity of photoelectron spectroscopy to study the distribution of solutes near the water surface. When it comes to determining structure of molecules in bulk solutions, nuclear magnetic resonance (NMR) and infrared/Raman spectroscopy are however normally the tools of the trade, yielding high-resolved chemical information about the solutes bonding patterns down to minute concentrations.

Core-level photoelectron spectroscopy can also provide quantitative chemical information about inequivalent sites of hydrated molecules with elemental specificity. In sections 4.6.1 and 4.6.2, we saw examples of how the protonation state of the carboxylic group in carboxylic acids can be resolved in the C1s photoelectron spectrum, and how the $COOH/COO^-$ photolines are clearly separated from those of the ring and chain carbons in the same molecule. Up till now we have taken these shifts for granted, not addressing the underlying physics causing them. In this chapter we will therefore ask questions like: What are the origins of the core-level shifts in the aqueous phase? How much of the shift upon protonation/deprotonation of a hydrated molecule comes from "structural modifications", i.e. connected with internal electronic rearrangements associated with the covalent bond to the proton, and what comes from the interactions with the aqueous solvent? How is the core-level lineshape dependent on the hydrogen bonding pattern of the solute? What types of observables can solvent-induced chemical reactions give rise to in associated core-electron spectra?

We will not be the first to ask these types of questions, even though the relevant literature is very limited. During the 1980's Hans Siegbahn, in collaboration with Hans Ågren conducted a number of studies of how electronic structure effects upon solvation is manifested in the electronic spectra of solutes [120, 121], yielding valuable insight that partly will form the theoretical foundations of our present investigations. The recent advances which has enabled photoelectron spectroscopy to be applied to a broad range of aqueous solutions is an important step forward, but the

full realization of XPS to become a standard tool to access important site-specific chemical information from complex solutes in aqueous solution, complementary to standard tools, such as NMR and IR spectroscopy, is yet (if ever) to come. This will ultimately depend on how useful the information contained in these spectra are, how well we can characterize this information (which still needs to be considerably improved), as well as to what extent we can *extract* the available information content from experimental spectra in practice.

In this chapter we will first review some basics in the theory of core-level shifts in the aqueous phase. Thereafter, experimental studies of two small organic molecules, glycine and formaldehyde, in aqueous solution will be presented, hand-in-hand with theoretical efforts to understand and model the core-electron spectra. This will hopefully be illustrative of the potential of these novel spectroscopic applications.

5.1 Core-level photolines of aqueous solutes

When a solute is dissolved in a polar liquid like water, its spectral response to electromagnetic radiation changes in various ways; lines shift, broaden or even disappears while new ones may take their place. Understanding the origins behind these *solvent effects* in the electromagnetic spectra is of fundamental interest in physical chemistry as it contains information about the chemical state of the solute, and the nature of the solvent-solute interactions. In the present context we are interested in understanding solvent effects on the core-level spectra of solvated species. The most obvious thing to address first is the chemical shift upon solvation, which is defined as

$$\Delta \mathrm{BE} = \mathrm{BE}_{\mathrm{liq}} - \mathrm{BE}_{\mathrm{vac}} = (\mathrm{E}^{\mathrm{f}}_{\mathrm{liq}} - \mathrm{E}^{\mathrm{i}}_{\mathrm{liq}}) - (\mathrm{E}^{\mathrm{f}}_{\mathrm{vac}} - \mathrm{E}^{\mathrm{i}}_{\mathrm{vac}}) \qquad (5.1)$$

Typical values for core-level peaks are -1 to -2 eV upon hydration in the aqueous phase. The O1s peak of the water molecule itself is for example red-shifted 1.8 eV – from 539.9 eV in the gas phase to 538.1 eV in the aqueous phase [122]. This can be rationalized as being primarily a final-state effect; the cationic final state is screened in the liquid phase by the induced polarization of the surrounding, which lowers the BE.

There are other ways to rationalize core-level chemical shifts upon solvation. In so-called thermochemical models, ionization energies are related to thermodynamical quantities [123]. Using a Born-Haber cycle [54], as shown in figure 5.1, we can estimate the core-level chemical shifts based on solvation energies. If a solute of charge q is core-ionized at the

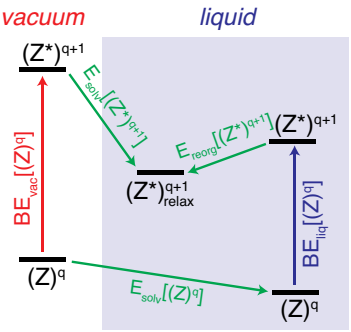

Figure 5.1: Born-Haber cycle relating thermodynamic solvation energies to photoemission binding energies.

site of an element Z, equation 5.1 can be written as:

$$\Delta\mathrm{BE} = (\mathrm{E}[(\mathrm{Z}^*)^{\mathrm{q+1}}_{\mathrm{liq}}] - \mathrm{E}[(\mathrm{Z})^{\mathrm{q}}_{\mathrm{liq}}]) - (\mathrm{E}[(\mathrm{Z}^*)^{\mathrm{q+1}}_{\mathrm{vac}}] - \mathrm{E}[(\mathrm{Z})^{\mathrm{q}}_{\mathrm{vac}}]) \tag{5.2}$$

If we make the equivalent core-approximation, i.e. that Z*=Z+1 [54], and re-arrange this expression we end up with

$$\begin{aligned} \Delta\mathrm{BE} &= (\mathrm{E}[(\mathrm{Z}+1)^{\mathrm{q+1}}_{\mathrm{liq}}] - \mathrm{E}[(\mathrm{Z}+1)^{\mathrm{q+1}}_{\mathrm{vac}}]) - (\mathrm{E}[(\mathrm{Z})^{\mathrm{q}}_{\mathrm{vac}}] - \mathrm{E}[(\mathrm{Z})^{\mathrm{q}}_{\mathrm{liq}}]) \\ &= \mathrm{E}_{\mathrm{solv}}[(\mathrm{Z}+1)^{\mathrm{q+1}}_{\mathrm{liq}}] - \mathrm{E}_{\mathrm{solv}}[(\mathrm{Z})^{\mathrm{q}}_{\mathrm{liq}}] - \mathrm{E}^{\mathrm{Z+1}}_{\mathrm{reorg.}} \end{aligned} \tag{5.3}$$

Here $\mathrm{E}_{\mathrm{reorg.}}$ is the solvent reorganization energy in the core-ionized state, i.e. the difference between the adiabatic energy where the environment is fully relaxed, which is what the thermodynamic solvation energies measure, and the vertical energy reached upon photoionization where the solvation geometry is frozen to that of the ground state. Upon the approximation $\mathrm{E}^{\mathrm{Z^*}}_{\mathrm{reorg.}} = \mathrm{E}^{\mathrm{Z+1}}_{\mathrm{reorg.}}$, equation 5.3 can therefore be used to derive solvent reorganization energies for solvated species via photoemission experiments – a quantity that is hard to measure but can be of importance to understand the energetics in various redox reactions [124, 125].

Photoemission line widths are often dramatically increased upon hydration, owing to *configurational broadening* in the aqueous phase. The vertical BE should thus be viewed as the ensemble average of the individual binding energies of a large number of inequivalent solvation configurations, while the width of the line carries information about the spread around this average. Configurational variations can for example encompass the same species with different local coordination numbers (e.g. different number of hydrogen bonds) or variations in the bonding geometry with its nearest neighbors. To model the configurational contribution to the core-level linewidth analytically is difficult (if not

impossible!) and we typically have to resort to molecular simulations to obtain information regarding a specific system. As we will see in the next section, one can still extract some general rules of thumb for what factors that contribute, e.g. the charge state if the ionized group and the initial-state charge localization.

Instead of going deeper into the general theory of core-level shifts in the aqueous phase we will instead have a look at a few specific aqueous solutions of small organic molecules, namely glycine and formaldehyde, that will serve as our playground for exploring solvent-induced effects on the solute core-electronic spectra. By means of theoretical calculations we can rationalize the experimental findings, providing insight that has much broader implications than for just the specific system under investigation.

5.2 Investigations into the information content in core-level spectra of a small biomolecule in water

We have performed an extensive experimental and computational study of the C1s and N1s photoelectron spectra of glycine (NH_2CH_2COOH), the most fundamental of the amino acids, in liquid water. While the molecule is deceivingly simple it can take three distinctly different forms in the aqueous medium, namely in the shape of a cation ($NH_3^+CH_2COOH$), zwitterion ($NH_3^+CH_2COO^-$) or anion ($NH_2CH_2COO^-$), depending on the pH of the solution. These are all different from the structure in the gas phase. Figure 5.2 shows the respective aqueous form including its first hydration sphere (together with a neutralizing counter-ion in the net-charged cases) in relation to the gas phase structure. The protonation/deprotonation of the functional groups significantly alter the internal electronic structure of the molecule and leads to pronounced effects on its hydration properties. Therefore, glycine is an ideal model system for studying electronic structure effects upon biomolecular hydration. Also, the understanding gained can potentially be applicable in future studies of larger biomolecules.

While we won't go into the gory spectroscopic details here (they are described in sufficient detail in paper VII for the interested reader) we will instead focus on the underlying philosophy of our study and have a quick look at some of the results on a conceptual level. Let us for the moment accept that the C1s and N1s regions of aqueous glycine show pronounced shifts upon variation of pH, and that the photolines are

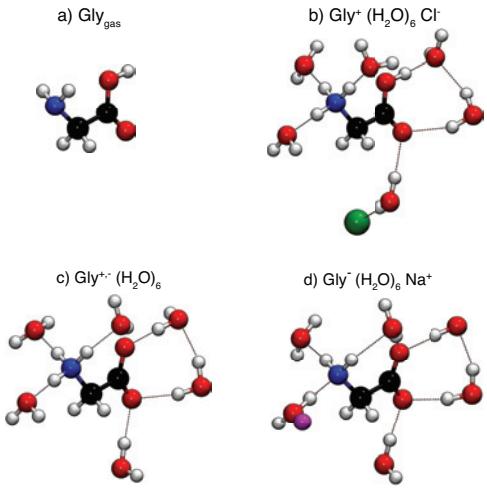

Figure 5.2: Stuctures of glycine: a) shows the molecule in the gas phase while b-d) show first solvation shell structures of anionic, zwitterionic and cationic glycine in aqueous solution, respectively. Neutralizing counterions are included for the anion (Na^+) and the cation (Cl^-).

significantly broader than in the gas phase (if you doubt it, have a look at figure 2 in paper VII). Especially noteworthy is that the N1s lines of zwitterionic and cationic glycine are very broad (∼1.4 eV full width at half maximum), which is ∼0.2 eV broader than that of the anion. What can we learn from these spectra? Our approach in paper VII has been to try to calculate the core-electron spectra of glycine in different charge states using models based on hybrid density functional theory (DFT) in which we model the molecular solvation with increasing complexity. By comparing with the experimentally determined shifts we thereby can learn what aspects need to be incorporated in the computational model in order to capture the main spectral features. Thereby we gain some insight into which factors that are most decisive for the molecule's electronic structure in solution.

Starting with simple PCM models that treat the solvent as a structureless polarizable continuum, into which the bare solute (i.e. anionic, zwitterionic or cationic glycine) is placed, we find these models unable to reproduce the characteristic spectral features. Including neutralizing counterions, Na^+ and Cl^-, into the cavity together with the respective anionic and cationic forms somewhat helps but the agreement with experiment is still poor. The inclusion of an explicit first hydration shell greatly improves the results, from which we conclude that the explicit H-bonding with the aqueous solvent has direct bearing on glycine's electronic structure in aqueous solution. The basis set and DFT-functional dependence

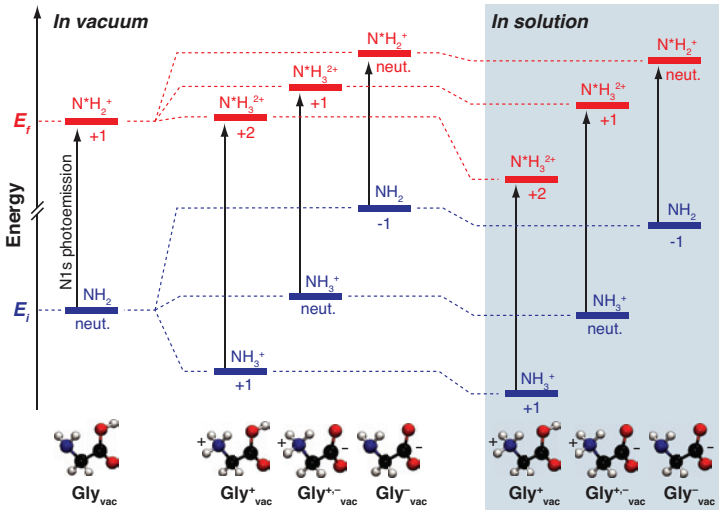

Figure 5.3: Energy diagram for the N1s photoionization process of glycine in various charge states, as obtained from *ab initio* calculations.

is further studied and we show that the highest level of theory used (B3LYP/aug-cc-pVTZ) is robust for the present calculations of N1s and C1s core-level binding energies.

In order to get an intuitive feeling for the energetics determining the directions and magnitudes of the core-level shifts in glycine in the various charge states, we have decomposed the calculated N1s shifts into initial- and final-state contributions, as is shown in figure 5.3. Here, the energy diagram of the gas-phase molecule is shown to the left while those of the solvated forms are shown to the right. In the middle, the calculated initial and final-state energies of the ionic structures in vacuum are shown, forming hypothetical intermediates between the gas-phase and aqueous forms – note that these are not stable in the real world. By studying how both the net charge of the molecule, the local charge of the amino group as well as the solvation affects the respective energies we can partially separate "structural" contributions to the chemical shift, i.e. caused by protonation/deprotonation of the functional groups, from solvent-induced effects which are primarily due to different degrees of polarization screening in the initial and final states.

Figure 5.3 contains tremendous amount of information which we won't try to decipher in detail at this point. To learn from an illustrative example we can instead just look at how the energy levels shift when the gas-phase molecule is converted into a zwitterion in vacuum, and thereafter placed in water. The initial-state energy (E_i) of the zwitterion in vacuum is naturally higher than that of the gas-phase form, due to the

unshielded local charges of the functional groups. When placed in water, the zwitterion is greatly stabilized by charge-diplole interactions, lowering the energy below that of the neutral gas-phase molecule in vacuum. Turning to the final-state energies (E_f) it is found that ionization of the ammonium group of the zwitterion in vacuum causes a state significantly higher in energy than the corresponding ionization of the amino group of the gas-phase structure. This is understandable, given the localized dicationic charge on the nitrogen site in the final state of the zwitterion. This causes a significant positive chemical shift in the N1s BE (given by the differences in length of the corresponding arrows in figure 5.3) compared to the gas phase. The final state, being net-cationic and displaying a considerable charge asymmetry, is significantly lowered in energy in the aqueous phase, also lowering the BE. However, we can conclude that this negative solvent-induced polarization screening contribution to the chemical shift is smaller in magnitude than the positive shift caused by the proton-rearrangement upon formation of the zwitterion. As a result, the N1s BE of solvated zwitterionic glycine is higher than of the neutral molecule in the gas phase, in accord with the experimental findings in paper VII.

In the second part of paper VII we address the question of how the H-bonding patterns of glycine in water are correlated with the core-level electron spectra of the different forms. Our approach in answering this question (at least partly) has been to perform MD simulations of zwitterionic glycine and extract a large number of uncorrelated snapshots. From these structures we have calculated vertical N1s and C1s BEs using the best computational method as described in the previous paragraph (explicit water solvation shell + PCM). The BE histogram from these calculations indeed well captures the main features of the experimental photoelectron spectrum – in particular the substantially broader N1s feature compared to the two C1s lines. We can therefore perform a structure-to-spectrum correlation analysis with certain faith in the results. Given the large number of geometrical degrees of freedom in the hydration shell of glycine it is not obvious how these should be related to the ionization energies. Furthermore, we observed that both the structural parameters (the independent variables) and the three BEs (the dependent variables) show a large degree of co-variance amongst themselves, making multi-dimensional univariate types of analysis unsuitable, i.e. correlating the BEs with individual structural parameters. Under these circumstances, multivariate approaches are much more suited [126], and in paper VII we perform a partial least square (PLS) regression analysis. One of the main results is that the N1s BE shows a much stronger correlation with the hydration geometry of the ammonium group (NH···O H-bond dis-

tances and angles) than do the other BEs. This is found to be primarily a final-state effect, which can be understood intuitively: Core-ionization of the the nitrogen atom in NH_3^+ leads to a highly unstable $N^*H_3^{2+}$ state. Screening by the lone-pair on the acceptor side of the solvating water molecules will thus have a substantial effect on lowering the total energy. As an effect, the geometric configuration space spanned in the ground state (determined by the available thermal energy k_BT) will project onto a large energy space in the core-ionized state, given the large variation by the screening ability of the solvation shells in each geometry. This causes, at least partially, the substantial increased width of the N1s line of cationic and zwitterionic glycine observed in experiments.

5.3 Core-electron probes of electronic structure modifications upon hydrolysis of formaldehyde

As was briefly outlined in section 2.3.2, the structural modifications of solute molecules can be quite pronounced upon introduction to the aqueous phase. The incorporation of solvent molecules into solute complexes constitutes a broad class of chemical phenomena, known as *solvolysis*. In the special case when the ionic fragments of water, i.e. H^+ and OH^-, is included into the solutes one normally talks of *hydrolysis* [116]. Hydrolysis is of general importance in the aqueous phase, not at least in affecting active sites of biological macromolecules. As an example, it has recently been suggested that the active form of oxoalanine, an aldehyde playing an important function in sulfatase enzymes, is not really an aldehyde in aqueous solution. Evidence instead indicate that the oxoalanine carbonyl group is hydrolysed into a diol, which could be influential for the enzyme function [127].

As mentioned in the beginning of this chapter, structural determination of solutes in aqueous solution is most often made using NMR or IR spectroscopy. Since the local electronic structure at the site subjected to hydrolyzation will be influenced – both in the occupied and unoccupied states – the core-electron spectroscopic techniques employed in this thesis should also be sensitive to these types of reactions.

Papers VIII and IX presents a combined XPS and NEXAFS study of the hydrolyzation of formaldehyde in water. A reason for choosing formaldehyde as a model system is because it is the simplest of the aldehydes and is known to be subject to hydrolysis in aqueous solution [128]. Two pathways for the hydrolysis of formaldehyde into methanediol is sketched in figure 5.4. The top reaction is base-catalyzed, where the

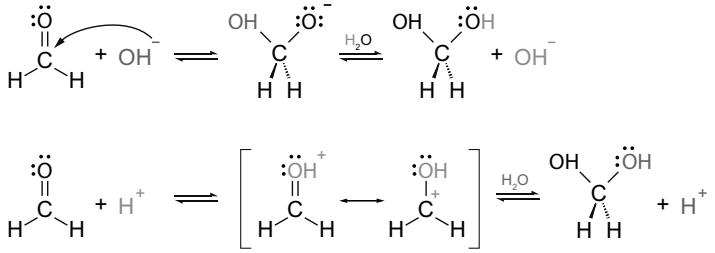

Figure 5.4: Two chemical pathways for the hydrolysis of formaldehyde to methanediol. The top trace shows the base-catalyzed nucleophilic attack of hydroxide on the keto carbon. The lower trace shows a reaction which is instead initiated by a proton attacking the carbonyl oxygen.

nucleophilic hydroxide anion is attacking the keto carbon. The intermediate anionic form is unstable and will break a solvent water molecule to obtain the missing proton needed to form the stable methanediol. In the acid-catalyzed reaction shown in the bottom trace of figure 5.4, an electrophilic proton is attacking the double bonded oxygen, forming a resonance-stabilized carbocation. A water molecule then donates an OH^-, resulting in methanediol. Due to the high electron density around the double bond of formaldehyde, this type of reaction is very likely. Molecules in which the hydrogens that are binding to the central carbon are replaced by more electronegative sidegroups should hence be less reactive. For that reason, we have made a comparative study of formaldehyde, formamide and urea in water – the structures of which are shown in figure 5.5. These molecules all exhibit the central carbonyl group which can lead to hydrolysis according to the schemes in figure 5.4.

What core-electron spectroscopic observables would the hydrolyzation of these molecules give rise to? Double bonded carbonyl groups show distinct O1s $\rightarrow \pi^*$ and C1s $\rightarrow \pi^*$ absorption resonances, which is well established in the literature [129–131]. The NEXAFS spectra of hydrolyzed forms (diols) must thus be very different from the intact molecules, retaining their carbonyl group. This gives an elegantly simple way to determine whether a molecule with a single keto bond is completely hydrolyzed or not, since the former leads to a complete lack of the π^* resonances. Whether or not partial hydrolyzation has occurred is however more difficult to infer from a X-ray

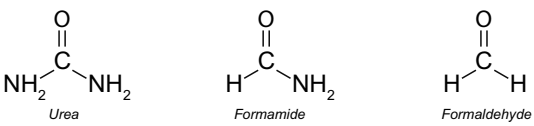

Figure 5.5: Lewis diagrams of urea, formamide and formaldehyde.

absorption spectrum alone. The DFT calculations presented in paper IX show that the co-existence of hydrolyzed and non-hydrolyzed forms give rise to two C1s photoemission lines, separated by about 1.0 eV, which makes PES sensitive to partial hydrolyzation.

We find that formaldehyde is near completely hydrolyzed in aqueous solution while urea and formamide remain intact. This is rationalized in terms of the difference in electronegativity of the carbon side groups. In formamide and urea the amino groups significantly reduces the electron density on the keto bond, and thus the reactivity in the aqueous phase, which is confirmed by a Mulliken population analysis from the DFT calculations.

6. Ultrafast electron dynamics in aqueous solutions seen through core-hole de-excitation processes

All experiments presented in this thesis are based on single-photon excitations of aqueous samples and are thus *stationary* probes, i.e. we do not follow the evolution of spectral features directly in the time-domain, in contrast to e.g. two-photon pump-probe experiments where the delay time between two light pulses is varied as an experimental variable. This does *not* mean that no dynamical information is contained in stationary core-level spectra. While the core-electron photoabsorption/photoionization process to a good approximation can be considered instantaneous the subsequent Auger decay is delayed by the characteristic lifetime of the core-hole. During this time, the environment interacts with the residue and both electronic and nuclear re-arrangements can occur which affects the energy of the core-ionized state as well as of the various final states reached in the Auger decay. This makes AES and RAS sensitive probes of dynamics in molecular systems in the low femtosecond regime, where explicit time-domain experiments are extremely challenging to perform.

In this chapter we will explore what type of information this unique feature of core-electron spectroscopies can yield about aqueous solutions.

6.1 The Auger process revisited

In chapter 3 we briefly discussed Auger decays and spectroscopy thereof in very general terms. Before turning to the detailed results forming the basis for papers X-XIII we need to say a few more words about Auger processes in order to make the following discussion understandable. Auger decay occurs spontaneously – the final states reached must all be lower in energy than the core-hole state, since no excess energy is provided to the system. The final states are most often numerous, given that the two final-state holes (upon normal Auger decay) are permuted through the available electronic levels, creating broad and complex spectral structures. As will become obvious later in this chapter, analysis of Auger spectra often means studying the branching ratios of contributing final states. This, among many other things, can yield information

about ultrafast relaxation mechanisms on the timescale of the core-hole lifetime.

To extract such information we must be able to spectroscopically separate different types of final states. In section 3.1 we mentioned how normal Auger decay produces two-hole final states, whereas decays from resonantly excited states at which the excited electron remains localized, result in singly ionized final states. These are typically distinguishable spectroscopically as the screening of the excited electron lowers the energy of the system; as a consequence these states appear at higher KE in the resulting Auger spectrum. As we will see next, other types of final states may appear in the Auger spectrum of condensed samples, which we need to be aware of. Thereafter we will have a look at ways to analyze Auger spectra to extract dynamical information.

6.1.1 ICD – a peculiar relaxation pathway in the condensed phase

In the final state of a normal Auger process the system is left with two additional valence holes relative to the ground state electronic configuration. In the gas phase, these two holes will naturally be located on the same species as was subject to the initial core-ionization. In the condensed phase, where the core-ionized atom or molecule is close to neighboring particles, this is not the only conceivable type of final state though. One or both of the final-state holes can delocalize into the surrounding. The probability for this to occur naturally depends on the electronic coupling between the constituent particles. In a metal, where the valence electronic structure is delocalized throughout the whole sample, the delocalization of the final-state hole[1] upon Auger decay is typically complete. But what about weakly bonded systems that retain much of their molecular character, such as hydrogen bonded liquid water? Given the small degree of electronic overlap between the different centers, one could expect the probability for forming delocalized two-hole states to be minute.

In 1997 Cederbaum et al. made the unexpected theoretical prediction that inner valence-ionized states of hydrogen-bonded clusters should relax rather efficiently to delocalized two-hole final states [132] – the decay mechanism was given the name Interatomic or Intermolecular Coulombic Decay, or ICD in short. A few years later, ICD was even predicted

[1] Note I here say hole and not holes since the intermediate state in the Auger decay upon core-ionization of a grounded metal will be completely screened (neutralized), given the infinite bath of electrons available from the ground, resulting in single-hole final states upon spectator/participator decays.

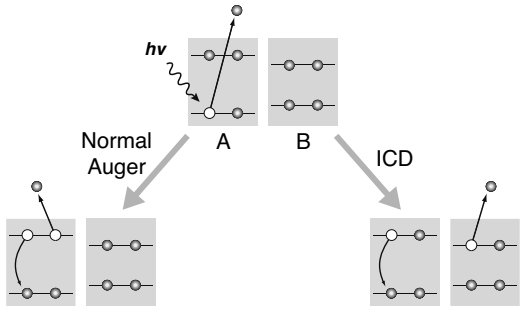

Figure 6.1: Schematic illustration of how normal Auger decay and ICD can produce different final states following core-ionization of site A. Normal Auger produces a localized two-hole valence state on A whereas one of the holes have delocalized to the neighboring site B upon ICD decay.

to occur even in weakly van der Waals-bonded clusters [133], suggesting that the phenomena is of general importance in the condensed phase. In 2003, ICD was experimentally demonstrated by Marburger et al. when they found a feature in the decay spectrum of neon clusters following 2s ionization that could not be explained by local two-hole valence final states of a single Ne monomer and which was interpreted as a fingerprint of an ICD decay [134]. Subsequent work has shown that the ICD rate strongly depends on the local coordination number of the ionized site, which lowers the ICD efficiency at free surfaces [135]. In 2005, Öhrwall et al. showed the existence of an ICD-like mechanism following O1s ionization of large water-clusters [57] and recently the analogous phenomena was demonstrated following inner valence-ionization [136]. Figure 6.1 contrasts normal Auger decay against the ICD mechanism for two inequivalent neighboring sites A and B (atoms or molecules), following core-ionization of A.

In our Auger studies of aqueous solutions we have found various phenomena, reminiscent of ICD. In papers X, XI and XIII analysis thereof is used to study the electronic coupling between aqueous solutes and the water solvent.

6.1.2 *What's the time?* – The core-hole clock and some of its applications

If two competing mechanisms that result from the same initial excitation are at work in a molecular system, and which give rise to distinguishable spectral signatures in the associated decay spectrum, the ratio between

the respective decay time-constants, τ_1 and τ_2, can be deduced from their relative spectral intensities, I_1 and I_2, using the simple relation

$$\frac{\tau_1}{\tau_2} = \frac{I_2}{I_1} \tag{6.1}$$

This means that if one of the time-constants is known in advance, the other can be derived from analysis of the intensity distribution in the spectrum. In 1992, Björneholm et al. demonstrated that such an analysis can be applied to characterize charge-transfer times from a substrate to a core-ionized adsorbate molecule [137], utilizing the known time-constant of the normal core-hole Auger decay τ_{CH}. This type of analysis from which characteristic time-scales of ultrafast electron phenomena can be extracted has become known as the core-hole clock method, and has been used in numerous studies thereafter [138–140]. Föhlisch et al. explicitly confirmed the quantitative nature of the core-hole clock method when they probed the same electron transfer process from an adsorbed sulphur atom to a ruthenium surface utilizing different core-holes of the sulphur atom with distinctly different lifetimes, yielding the same electron transfer time-constant [141]. They also demonstrated the possibility of probing such processes on the attosecond timescale [142].

If you are having a hard time understanding how the core-hole clock works, imagine a molecule, being core-ionized at t = 0, adsorbed on a surface "willing" to donate electrons to the adsorbate in order to neutralize the cationic charge. If $\tau_{\mathrm{CH}} \to 0$ there would be no time for electrons to jump from the substrate to the adsorbate, and the Auger spectrum would exclusively contain normal two-hole final states. If instead $\tau_{\mathrm{CH}} \to \infty$ all the molecules would be screened before the decay occurred, only producing singly charged final states, appearing as either spectator or participator lines in the Auger spectrum. It should thus be clear that the core-hole clock method is ideal to analyze processes that happens on the same timescale as the core-hole decay – if the two time-constants are identical then so will also the normal and resonant contributions to the resulting Auger spectrum be.

As we will see in some of the following examples, the core-hole clock can be used to derive information about the efficiency for various charge-delocalization processes in aqueous solutions. Since the spectroscopic details are described in their respective paper, we shall here primarily focus on the underlying motivations and the main results obtained in the respective study.

6.2 What can O1s core-hole de-excitation in OH^-_{aq} tell about its hydrogen bonding patterns?

The transport of water's two generic ions hydronium (H_3O^+) and hydroxide (OH^-) is abnormally fast compared to, for example, inorganic salt ions moving through the water H-bond network. Historically, the diffusion of hydronium has been explained in terms of the so-called Grotthuss mechanism (also referred to as "structural diffusion"), suggested in 1806 by Theodor de Grotthuss [42]. Figure 6.2 schematically illustrates the modern view on the mechanism, offering a beautifully simple explanation to the anomalous speed; it is not the intact hydronium ions that move, but only hydrogen atoms involved in the H-bonding between the ions and the neighboring water molecules. This is possible since H_3O^+ is intimately connected to water through H_2O auto-ionization, in contrast to other types of aqueous ions.

Structure **i** in figure 6.2 shows the solvated $H_3O(H_2O)_3^+$ Eigen complex, with a full-coordinated hydronium cation at site **A**, donating three H-bonds to the surrounding water molecules. The water molecules are in turn each full-coordinated, i.e. both donating two and accepting two H-bonds (not completely shown in the figure). In the Grotthuss transport scheme, the hydronium transport from site **A** to **B** is initiated by a perturbation in its second water solvation shell, when an acceptor H-bond of the water molecule at site **B** is broken – compare figure 6.2**i** and **ii**. This water will thus no longer be fully coordinated and is hence more reactive. The hydrogen involved in the H-bonding between the water molecule (**B**) and the hydronium (**A**) will then start to drift, forming the Zundel complex $H_5O_2^+$ (shown in figure 6.2**iii**). In **iv** the hydrogen has been completely transferred, resulting in a fully coordinated H_3O^+ at site **B**, surrounded by four-coordinated water molecules.

In the so-called "proton-hole" picture, it is assumed that the migration of OH^- can be modeled by an analogous scheme, shown in figure 6.3 [143]. The hydroxide Grotthuss mechanism is actually identical to that of the hydronium under inversion of the hydrogen bond polarities, since

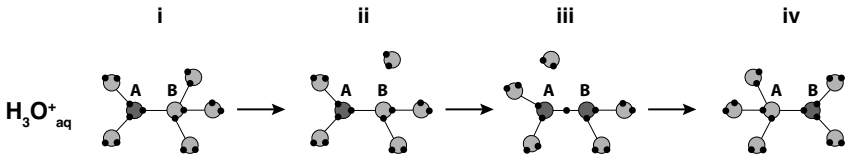

Figure 6.2: The Grotthuss transport mechanism of H_3O^+ in liquid water. **i** and **iv** show the Eigen $H_3O(H_2O)_3^+$ complex while **iii** is the Zundel cation, $H_5O_2^+$.

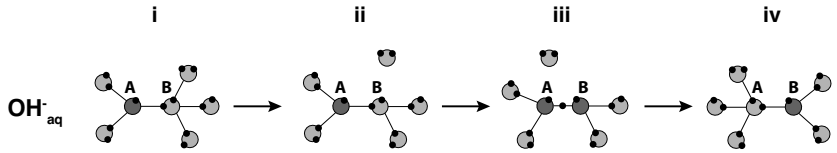

Figure 6.3: The Grotthuss transport mechanism of OH^- in liquid water.

H_3O^+ is assumed to be exclusively donating three H-bonds while OH^- is assumed to only be donating the same number. A mirror-symmetry of water's generic ions relative to that of the neutral intermediate is thus assumed, providing an elegant and simple theory.

Infrared/Raman measurements of concentrated NaOH solutions have been reported which have turned out to be difficult to interpret in terms of the proton-hole picture of hydroxide [144]. Also, neutron diffraction experiments indicate that $OH(H_2O)_4^-$ actually is the most common hydration structure [145], not $OH(H_2O)_3^-$ that is assumed in the Grotthuss scheme. Furthermore, it is puzzling why the OH^- transport is about a factor of two slower than that of hydronium. These types of observations, indicative of an asymmetry in the hydration and migration of water's two generic ions, have motivated substantial theoretical effort. In 2002, Tuckerman and co-workers suggested a radically different transport mechanism of aqueous hydroxide based on Car-Parinello MD simulations [146]. Their calculations show that aqueous OH^- most often accepts four H-bonds in a nearly planar configuration – see figure 6.4**i**. The OH^- transport is initiated by a fluctuation in its first solvation shell, when one of the H_2O–OH^- bonds is broken, see 6.4**ii**. The change from the symmetrical $OH(H_2O)_4^-$ complex to the reactive $OH(H_2O)_3^-$ leads to a high probability for the formation of a transient OH^- donor bond, see subfigure **iii**. The hydroxide (at site **A**) now has a hydration structure similar to that of a water molecule, which activates proton transfer from a neighboring water molecule (at site **B**), see figure **iv**. In this transient state, the water molecule at **B** is being 'prepared' to become a bulk sol-

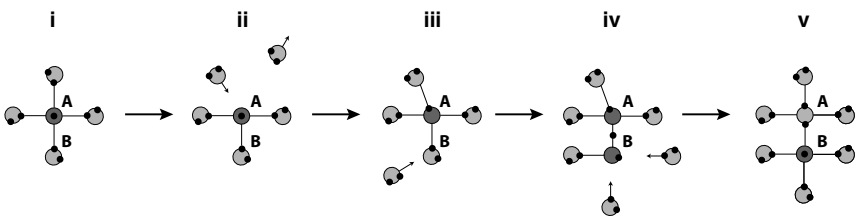

Figure 6.4: Transport mechanisms of OH^- in liquid water as suggested by Tuckerman and co-workers, involving a hydroxide donor bond to water.

vated OH^-, as two H-bond donating waters approach site **B**. When the migration is complete, as shown in figure **v**, the water molecule at **A** is tetrahedraly coordinated while the hydroxide at site **B** symmetrically receives four hydrogen bonds.

There are important differences between the OH^- diffusion scheme suggested by Tuckerman and co-workers compared to the Grotthuss structural diffusion mechanism. As already pointed out, the newly suggested mechanism is driven by fluctuations in the *first* solvation shell of the hydroxide anion, while the Grotthuss mechanism starts with a *second* solvation shell perturbation. Further, the predicted OH^- donor bond lacks an analogue (acceptor bond) in the case of the hydronium transport. In reference [146], up to 50% of the hydroxide anions at a given instance is predicted to be engaged in H-bond donation.

We have conducted a resonant Auger study of concentrated aqueous NaOH solutions in order to investigate the hydration and diffusion patterns of hydroxide in water, and this is the subject of paper X. As previously reported by Cappa and co-workers, the hydroxide anion exhibits a distinct oxygen K-edge absorption band around 532 eV [147], well separated from all water absorption features. By resonantly exciting this band, we thus selectively core-excite the hydroxide anions. Through the observation of lines in the Auger spectrum, owing to delocalized final states in the valence electronic structure of neighboring water molecules, which originates from an ICD-like mechanism, we have concluded that a large fraction of the aqueous hydroxide anions must indeed be involved in H-bond donation. As mentioned in the introduction, the available relaxation pathways of hydrogen bonded complexes might be very different from that of the isolated molecules, which is the reason why these spectra are sensitive to the OH^- H-bonding.

The spectroscopic details are rather complex, and are explained more in detail in paper X, but our conclusion is based on the following line of reasoning: The Auger spectra of resonantly core-excited aqueous hydroxide show that a large fraction of final states involves holes on neighboring water molecules. Resonant core-excitations of aqueous halide anions (H-bond acceptors only) on the other hand only result in local decays, showing spectator shifts due to that the excited electron resides in a Charge-Transfer-To-Solvent (CTTS) orbital, stabilized by the polar solvent [148]. OH^- is also CTTS active and shows a similar optical CTTS spectrum as the isoelectronic fluoride anion. As demonstrated in paper X, the core-excitation of hydroxide apparently opens up a different de-excitation channel, effectively competing with the localized spectator Auger decay. This is assigned to ultrafast energy transfer to neighboring water molecules through an OH^- donor bond, leading to the ionization

of the water valence band. This explains the radically different behavior of hydroxide compared to halides upon resonant core-excitation, owing to a difference in H-bonding patterns.

6.3 Hole- and electron delocalization dynamics in water and aqueous electrolytes

We have just discussed an example of how core-excitation of an aqueous solute, OH^-, caused solvating water molecules to take place in an ICD-like auto-ionization process. The natural question arises what type of decay channels are available upon O1s excitation of the water molecules themselves in aqueous solutions. In exploring various aspects of this question we have focused our attention on simple aqueous electrolytes, primarily aqueous alkali-halides and ammonium-halides. In paper XI we investigate the branching in the Auger decay upon O1s ionization of water molecules, where we identify new delocalized final states with valence holes on both water molecules and the ionic solutes. In paper XII we instead study the O1s Auger spectra upon resonant excitations of water molecules in solution. By comparing to the analogous spectra of pure water we can study the influence of the solute ions on the fate of the excited electron during the core-hole lifetime, which is indeed found to be significant.

We will start with the off-resonant case. Figure 6.5 shows a pictorial representation of how the conceivable final states reached in auto-ionization processes following decay of the $O1s^{-1}$ state of a water molecule depends on its local surrounding. Panel i) shows a core-ionized molecule, W^{c-1}, in vacuum; due to the lack of neighbors the only possible electronic decay path available is via a normal Auger decay, indicated by the branch **a**, producing a local two-hole final state W^{v-2}. In liquid water (panel ii in the figure), where the core-ionized molecule typically is donating two and accepting two H-bonds, the local channel **a** is still dominating [149]. As shown in reference [57] an additional minority branch, here denoted as **b**, is further available where the two final-state charges have delocalized over two water molecules – we here label this state as $W^{v-1}W^{v-1}$.

In paper XI we study how the decay pathways for water molecules residing in the first solvation shell of hydrated ions are influenced by the solutes. As expected, we find that the local channel **a** still dominates the Auger spectrum of aqueous solutions. We also show that the efficiency for forming $W^{v-1}W^{v-1}$ states is reduced in the solutions. The reason for this becomes obvious upon comparing the final states reached through

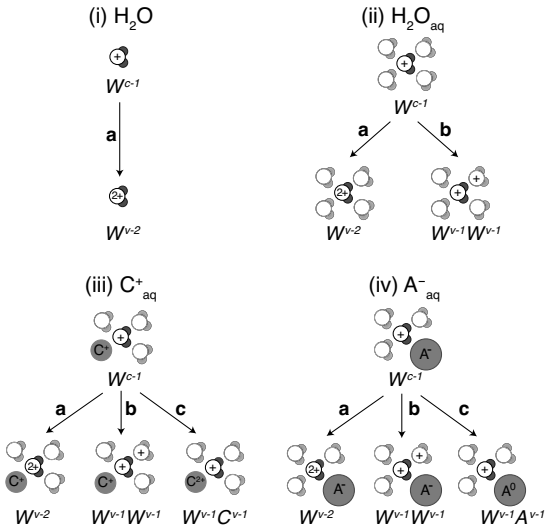

Figure 6.5: Schematic illustration of possible localized and delocalized two-hole final states can be reached in the O1s Auger decay of a water molecule, depending on its surrounding.

channel **b** in panel ii, iii and iv; since the average number of nearest water neighbors of a water molecule is reduced in the solution (and partly replaced by ions) the probability for forming pair-wise $W^{v-1}W^{v-1}$ states also decreases. This can be described as arising from a "passive role" played by the solutes in the Auger decays of water molecules in aqueous solutions. A less obvious finding reported in paper XI is that solvated anions also play highly "active" roles in the water core-hole decay, resulting in final states where one of the valence state holes resides on the solvated anion, i.e. the $W^{v-1}A^{v-1}$ states reached through channel iv**c** in figure 6.5. We have, however, found no spectral signatures of any analogous states involving cations, i.e. such as the $W^{v-1}C^{v-1}$ states depicted in iii**c** of figure 6.5.

The hydration strength of the halides, and hence also the ground state electronic overlap with the water molecules, decreases from F^- to I^-. One could therefore expect that the probability of forming a delocalized final state involving the anion upon decay of the water-core hole would follow the same order. This is, however, just the opposite of what is experimentally observed – the efficiency increases in the order $F^- < Cl^- < Br^- < I^-$. We therefore argue that the decay probability is rather correlated with the anion polarizability than with ground state charge transfer. During the excited state lifetime electron density from the anion will be "pulled" towards the cationic core-ionized water molecule,

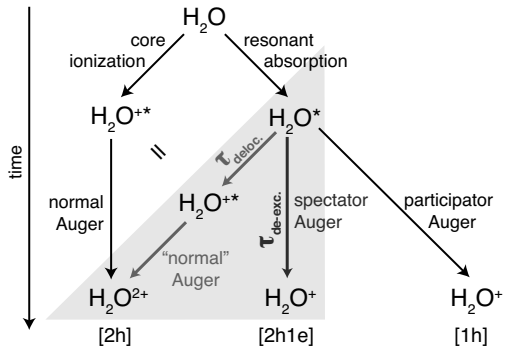

Figure 6.6: Flow diagram of how O1s core-ionization/resonant absorption in liquid water and aqueous solutions produce core-excited states that can decay to various different final states, distinguishable in the Auger spectrum.

residing in its first solvation shell, which increases the probability for forming delocalized $W^{v-1}A^{v-1}$ states.

In paper XII we turn our attention to resonant O1s excitations in aqueous electrolytes. Previous RAS studies of pure liquid water [149, 150] have resolved clear spectator-shifts of the Auger lines throughout the O1s near-edge absorption spectrum, indicating a certain degree of localization of the excited electron upon the various excitations [54]. The first O1s resonance (commonly denoted as the "pre-edge" following ref. [27]) displays a strong excitonic character in which the excited electron remains nearly fully localized on the parental molecule during the core-hole lifetime. Upon excitations into higher excited states (which are spatially more diffuse) the probability for the electron to delocalize into the H-bonded surroundings has been found to greatly increase. For the sub-ensemble where the electron has delocalized prior to the core-hole decay the Auger spectrum will thus be identical to the normal Auger spectrum. Figure 6.6 schematically illustrates the dominating pathways relevant for the present discussion. By use of the core-hole clock analysis described in the beginning of this chapter, the observed branching between the spectator and normal contributions to the resulting Auger spectrum can be used to extract the electron delocalization time, labeled $\tau_{\text{deloc.}}$ in figure 6.6. Using this approach Nordlund et. al. estimated that the electron delocalization time must be less than 500 attoseconds upon post-edge excitation in pure water [150].

We have investigated how the introduction of ionic solutes affects the efficiency for electron delocalization at various excitations in the water O1s near edge absorption fine structure, by performing a RAS study of LiBr and $MgBr_2$ aqueous solutions. The interpretation of the spectra is rather complicated but we will just have a brief look at the main results

in paper XII: We find that the pre-edge spectrum is hardly influenced by the ions, i.e. a near complete localization of the excited electron (yielding spectator shifted lines) is observed for the solutions, similarly as in pure water. At the main- and post-edge the branching of the O1s core-hole decays of H_2O molecules in the solutions and neat water, however, differ substantially: a considerable fraction of the normal Auger intensity is redistributed into the spectator channel in the solutions, signifying localization. This means that the introduction of ions in water slows down the ultrafast electron delocalization dynamics. While this phenomenology shows no dependence on the exact nature of the anion (as was the case for the H_2O-anion ICD process discussed above) we find that the charge of the cation strongly influences the electron hopping-time. From a core-hole clock analysis we find that $\tau_{\text{deloc.}} = 1.9$ and 1.5 fs for post-edge excitations of 3m $MgBr_2$ and 6m LiBr aqueous solutions, respectively, i.e up to a four-fold increase in the former case compared to neat water.

The interpretation of the RAS data in paper XII is further supported by electronic structure calculations of snapshots obtained from MD simulations, allowing a deeper understanding of what causes the observed effects. More specifically, we have compared both the occupied and unoccupied density of states of p-charachter (PDOS) of different classes of water molecules in the aqueous solutions, i.e. "water-like" molecules which only coordinate other waters and those which coordinate the ions in various ways. The cation-coordinated waters are especially found to energetically mismatch the surrounding molecules, both in the occupied and the unoccupied electronic structure. This decreases the overlap between these species and the surrounding, reducing the probability for the excited electron to delocalize on the time scale of the core-hole lifetime.

We can also identify another reason as to why the delocalization time is reduced from cation-coordinated waters. From simple considerations the electron is expected to jump along the donor H-bond of the excited molecule [150]. If a core-excited water molecule is situated in the first solvation shell of a cation, the excited electron will therefore be "back-polarized" towards the cationic charge, situated on the other side of the molecule's oxygen atom. As a result, the spatial overlap of the electron with orbitals of the neighboring H-bond accepting molecules will be reduced, thereby localizing the electron to its parental molecule. This effect should scale with the charge of the cation, in agreement with our experimental findings.

6.4 Ultrafast delocalized Coster-Kronig processes in aqueous cations

In this chapter we have so far investigated hole- and electron-delocalization processes initiated by either resonant or off-resonant core-excitations of the hydroxide anion and water molecules. These species display a relatively weak charge-transfer to and from other water molecules in liquid water in the ground state. The timescales for the observed ICD processes in these systems have typically been on the order of tens to hundreds of femtoseconds (which is still pretty fast!). Upon investigating atomic cations (Na^+, Mg^{2+} and Al^{3+}) we have, however, found an intermolecular decay mechanism following 2s core-ionization that extends down to the attosecond time domain. This finding was not made by observation of the secondary electrons in the Auger spectrum directly from the delocalized decay but from a line-shape analysis of the cation 2s photoelectron spectrum (remember that the finite lifetime of core-ionized state leads to a Lorentzian broadening of the photoline with the characteristic lineshape parameter $\Gamma = \hbar/\tau$).

In order to distinguish Lorentizian line width contributions from the 2s cation spectra from Gaussian ones we simultaneously recorded 2p spectra. Given that both the instrumental and configurational (Gaussian) linewidth contributions to these photolines are the same, this can be formulated as a constraint in the simultaneous fitting of the two spectra (see section 3.8). From such analysis, we could in paper XIII extract lifetimes of the $(2s)^{-1}$ state of 3.1, 1.5, and 0.98 fs for Na^+, Mg^{2+} and Al^{3+}, respectively. These values are actually similar to those observed for metallic Na, Mg and Al [151].

What causes this extremely efficient hole-delocalization into the aqueous surrounding? First of all, water molecules solvating cations form stiff hydration spheres in which they donate part of the their electron density from their oxygen lone-pairs to the solute ion, an effect that increases with the charge of the cation. This (initial-state property) increases the probability for delocalizing one of the valence final-state holes onto a water neighbor upon core-ionization. Since the cationic charge is increased by one unit in the ionization process, the electronic coupling between the solute and the aqueous solvent is further strengthened in the intermediate state of the Auger process.

In the corresponding metallic systems the conventional explanation to the ultrafast decay rate is that the two-hole (local) final states, e.g. $(2p)^{-1}(3s)^{-1}$, has a hole in the same principal shell as the intermediate $(2s)^{-1}$ core-hole state [151]. This dramatically increases the overlap and

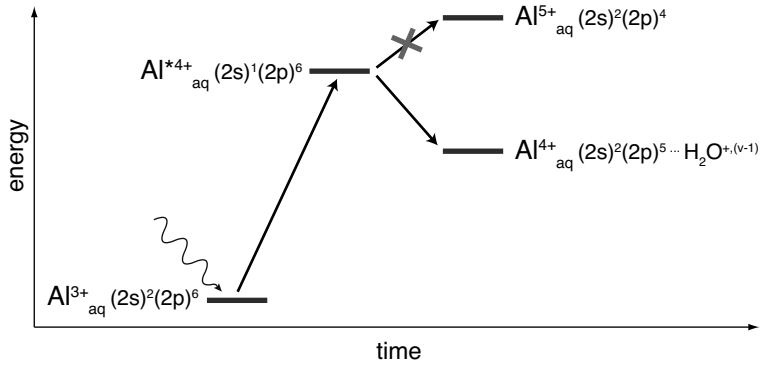

Figure 6.7: Schematic energy diagram, showing why the ultrafast Coster-Kronig decay of the 2s core-hole in the aqueous Al^{3+} ion must involve intermolecular energy transfer, causing an ionization of a solvating water molecule. This is because the local two-hole final state of aluminum that is lowest in energy, i.e. $(2s)^2(2p)^4$, is still higher in energy than the core-ionized intermediate state.

thus the transition rate to such a degree that it has been given its own name; Coster-Kronig (CK) decay, after its discoverers [81]. So, why do we believe that the ultrafast decay of the 2s hole in aqueous cations signifies an ICD mechanism involving the water solvent, and not just an internal CK decay of the ion, similar to that in the metal? This is because the local CK-channel is energetically forbidden in these systems, due to that the outermost electrons (i.e. 3s, and in the case of Al also one from the 3p shell) have been donated to the counterion(s) in forming the counterion pair. As a result, the $(2s)^2(2p)^4$ state, which is the energetically lowest possible local two-hole state relative to the $(2s)^2(2p)^6$ ground state, is *higher* in energy than the $(2s)^1(2p)^6$ core-hole state. Hence, all electronic decays must involve the water solvent. Figure 6.7 shows a schematic energy diagram of the proposed Coster-Kronig ICD mechanism for the hydrated aluminum ion. As shown to the right, an $Al^{4+}(2s)^2(2p)^5$ configuration can be reached through auto-ionization if one hole delocalizes to the valence electronic structure of a solvating water molecule, denoted as $H_2O^{+,(v-1)}$.

Even this state is not much lower in energy than the intermediate $(2s)^1(2p)^6$ core-hole state, meaning that the kinetic energy of the secondary electron is close to zero. Therefore we have not been able to detect them directly, given the highly unfavorable circumstances of having a weak, probably rather spread-out, signal on top of a huge and structured zero-background, totally dominated by water contributions.

7. Conclusions and Outlook

Recently, core-electron spectroscopy could be applied for the study of volatile liquid samples, such as aqueous solutions. This was made possible through a number of ingenious technical innovations over the last decades – most importantly the liquid micro-jet technique developed by Faubel and co-workers. As a consequence, new and exciting possibilities have opened up for studying fundamental properties of aqueous systems and I have been lucky enough to be part of this exciting development at an early stage.

In this thesis we have explored three aspects of core-electron spectroscopy of aqueous solutions. First, we have utilized the considerable surface sensitivity of the technique to probe the distributions of aqueous solutes near the water/vapor interface. We have evaluated the role of properties inherent to various ionic solutes – such as their size and polarizability – for their surface propensity. The effects of ion-ion interactions, depending on parameters such as concentration and pH of the electrolyte, were also studied and were found to be significant. In studying the surface behavior of weak organic acids it was demonstrated that XPS is sensitive to the degree of dissociation of the interfacial molecules (which is considerably lower than in the bulk at the same pH) as well as their surface orientations. In the second part we explored what type of information chemical shifts and line-shape analysis of photoelectron and X-ray absorption spectra can give about the chemical state and hydration patterns of molecules in aqueous solution. Core-electron spectroscopy has been shown to be a sensitive probe of the local protonation state of functional groups in small biomolecules and the widths of the photolines were found to be dependent on the range of local H-bonding motifs. In the third and final part we have studied how various ultrafast charge-delocalization phenomena, initiated by either core-ionization or resonant core-excitation, are manifested in Auger spectra. Beyond providing fundamental insights into electronic coupling mechanisms between hydrated solutes and the aqueous solvent, such data could be used to identify elusive structural motifs in solutions, e.g. the existence of a weak OH^- hydrogen donor bond.

Even though the results here presented are illustrative of the potential of core-electron spectroscopy to unravel microscopic details of aqueous systems, it should be stressed that the field is still young and much (or most things!) remains to be explored. Put it in the words of Winston

Churchill: "This is not the end. It is not even the beginning of the end. But it is, perhaps, the end of the beginning."

How can core-electron spectroscopy of water and aqueous solutions help advance modern chemical physics?

Pick up any textbook on general chemistry and you will find that very few results therein originate from core-electron spectroscopic measurements on liquid systems. But maybe that is about to change; the near instantaneous nature of the photoabsorption/ionization process and the subsequent femtosecond time window set by the core-hole lifetime, combined with the localized nature of core orbitals make these techniques superior to conventional chemical spectroscopies in capturing ultrafast snapshots of the local electronic structure at chemically active sites. PES can for example probe the individual forms in systems undergoing picosecond tautomeric proton hopping, recently demonstrated for imidazole in aqueous solution [152], which would be impossible with NMR due to the nanosecond nuclear spin relaxation times. In combination with the development of computational power, allowing for *ab initio* electronic structure calculations of larger and larger systems, it can be anticipated that X-ray based spectroscopic techniques applied to liquid systems will play an increasingly important role in the making of future chemistry.

What happens next?

The future for liquid core-hole spectroscopy looks bright and promising. Even though the exact lines of investigation ultimately will depend on the imagination of each individual researcher, it should by now be clear that the field has emerged through technical innovation. And the current instrumental development is indeed rapid; VG Scienta has recently developed the HiPP pre-lens system for their electron spectrometers, which enables measurements at background pressures up to 20 mbar, i.e. about the vapor pressure of liquid water at room temperature. Such instrumentation will surely play a key role in the success of new end-stations dedicated to photoemission studies at ambient pressures that is currently being built or planned at several of the worlds leading synchrotron facilities. The resolution of soft X-ray spectrometers is also constantly pushed to new limits, a development that has turned out to be important for discussions about the microscopic structure of liquid water (review section 2.2). The construction of new light sources, including free electron lasers, is also opening up for new possibilities in the study of liquid sys-

tems. The construction of the MAX-IV laboratory in Lund is presently taking off, meaning that Sweden will have a world-leading synchrotron facility within the next four years. Hopefully, this will lead to a dramatic increase in the number of X-ray spectroscopic studies on liquid systems conducted on Swedish territory.

Who knows what the future will bring in terms of specific results, but we will surely see liquids investigated by ultrafast laser/X-ray or even X-ray/X-ray pump-probe spectroscopy, we will learn about chemical reactions at aqueous surfaces through photoemission studies of liquids in equilibrium with a background gas and hopefully we will see further progress in the quest for the elusive microscopic structure of liquid water.

8. Populärvetenskaplig sammanfattning

Denna doktorsavhandling handlar om flytande vatten och vattenlösningar. Det kanske inte låter så spännande för lekmannen, men vattens fysikaliska egenskaper på den molekylära nivån har fascinerat och förbryllat forskare så länge man vetat att det faktiskt handlar om molekyler[1] och fortsätter att göra så även i våra dagar. Trots att flytande vatten är den vanligaste substansen på jordytan beter den sig nämligen märkligt i fysikers och kemisters ögon. För att byggas upp av en så liten molekyl, H_2O, är det till exempel förvånande att vatten kokar först vid en så hög temperatur som 100 grader Celsius. Och hur kan vi förstå dess oväntat höga värmekapacitet, det vill säga dess goda förmåga att lagra värme, jämfört med andra substansers? Ett annat förbryllande faktum är att vatten *expanderar* när det fryser till is och har högst densitet vid 4 grader. Hade vatten bettet sig som det ”borde”, alltså krympt när temperaturen minskat, hade jordens hav och sjöar bottenfrusit på vintern istället för att toppfrysa. I så fall skulle livet härpå jorden inte kunnat ha utvecklas på det sätt det gjort. Den som trott att dessa vattens egenskaper inte påverkar vanliga människor (dvs. icke-forskare) bör alltså tänka om!

Men *varför* beter sig flytande vatten på detta vis? Sanningen är att vi bara delvis vet svaret på denna mångfacetterade fråga. I grova drag kan vi dock beskriva vad som försiggår: Även om vattenmolekylen som helhet är elektriskt neutral är området kring syreatomen negativt laddat medan väteatomerna är positivt laddade – H_2O är vad man kallar en *polär* molekyl. I den flytande fasen, då molekylerna kommer nära varandra, attraherar därför väteänden av en molekyl syreänden av en annan. Då bildas en speciell typ av medelstark kemisk bindning, en s.k. *vätebindning*. Den starka benägenheten att bilda vätebindningar leder till en starkt geometrisk strukturering av molekylerna i flytande vatten och anses delvis vara den bakomliggande drivkraften för många av dess avvikande egenskaper. Idag vet vi att att vätebindingarna mellan H_2O-molekyler ständigt bryts och ombildas på en ultra-snabb tidsskala

[1] Fram till det att Lavoisier 1783 gjorde den banbrytande upptäckten att vatten både gick att sönderdela till och syntetisera av sina beståndsdelar, väte och syre, och därmed visat att det faktisk är en kemisk förening hade vatten åtnjutit statusen av ett *element*, dvs. man hade trott att det var en av de fundamentala enheter som bygger upp världsalltet. Den moderna bilden av molekyler som konstellationer av atomer blev dock allmänt accepterad först i början av 1900-talet.

av några pikosekunder[2] – detta möjliggör att materialet förblir *flytande* trots att bindningarna mellan molekylerna är relativt starka. Att studera dessa fenomen är en utmaning, då de flesta analysmetoder vi har inte är känsliga för detaljerna i molekylära vätebindningsmönster. Saken blir inte mindre komplicerad när vi vill förstå den molekylära strukturen av vattenlösningar, dvs. vatten i vilken någon kemisk substans lösts upp. Hur beter sig vattenmolekylerna runt den lösta kemikalien? Hur påverkas elektronfördelningen hos vattenmolekylerna och kemikalien beroende på den senares laddning, t.ex. om det är en laddad saltjon? Hur kommer de lösta kemikalierna bete och fördela sig vid vattenytan? Frågorna är många men tyvärr lättare att ställa än att svara på.

Det som fysiker och kemister ägnar sig åt när de försöker skapa sig en grundläggande förståelse för vatten och vattenlösningar kan närmast liknas vid en utdragen brottsutredning: Bilden är hela tiden fragmenterad och delvis motsägelsefull. Utredarna känner till vissa basfakta men en rad kritiska pusselbitar saknas för att få ihop helheten. Vissa i kåren ägnar sig åt att på analytisk väg skapa modeller som i bästa fall kan hjälpa till att beskriva hur ”gärningsmannen” fungerar, denna sorts forskare kallas för teoretiker. Det finns även en viss teknisk bevisning (de som samlar in sådan kallas experimentalister) som pekar åt ett visst håll. Tolkningen är dock sällan entydig. Vad som är ännu värre är att vissa nya ”bevis” förefaller motsäga andra man redan samlat in. Men genom att utredarna delar med sig av resultaten av sina respektive undersökningar (i formen av vetenskapliga publikationer) och ibland träffas och diskuterar sina senaste fynd vid internationella konferenser faller då och då nya pusselbitar på plats och utredningen tar ett språng framåt. Om fallet skall lösas måste dock nya analysmetoder utvecklas vilka kan generera nya sorters bevis – ingen enskild metod kommer ensam göra jobbet men det måste till nya infallsvinklar!

Okej, denna analogi bör inte dras alltför långt men för att ge läsaren en bild av hur detta avhandlingsarbete passar in i ett större sammanhang skulle man kunna säga att jag och mina kollegor testat ut ett relativt nytt angreppssätt: fotoelektronspektroskopi applicerat på vattenlösningar. Detta har medfört att jag här kan rapportera om ett antal nya fynd rörande den molekylära strukturen av vattenlösningar. Vi har så att säga ”återvänt till brottsplatsen” utrustade med nya hjälpmedel.

Vad är då fotoelektronspektroskopi, vad kan vi lära oss med dess hjälp och varför är det först nyligen som forskare börjat använda det i studiet av vatten och vattenlösningar? Metoden bygger på den *fotoelektriska effekten* vilken upptäcktes av Heinrich Hertz 1887 och fick sin teoretiska förklaring av Albert Einsten 1905 (vilket bl.a. gav honom Nobelpriset

[2] 1 pikosekund = 10^{-12}, eller 0.000000000001 sekunder

i fysik 1921). Fenomenet möjliggör att man kan *jonisera*, det vill säga slå ut elektroner från ett material om man bestrålar det med tillräckligt högenergetiskt ljus såsom UV- eller röntgenstrålning. Under 1950-talet utvecklade Kai Siegbahn vid Fysiska Institutionen i Uppsala en ny spektroskopisk metod, fotoelektronspektroskopi, i vilken man mäter hastigheten av de elektroner som frigjorts vid fotojonisation (vilket även gav honom Nobelpriset i fysik 1981). Om man vet fotonenergin av den joniserande strålningen kan man således ”räkna baklänges” och på så sätt få reda på hur hårt bundna elektronerna är i materialet. Detta var ett stort genombrott då man plötsligt direkt kunde undersöka olika materials *elektronstruktur*, vilken är avgörande för dess kemiska egenskaper. Men när man ville undersöka vattenlösningar på det viset uppstod dock ett stort problem. Metoden kräver vakuum i experimentkammaren, men flytande vatten är inte kompatibelt med vakuum. Ställer man in ett vattenglas och försöker pumpa ut luften runt det så ångar vattnet så mycket att ett tillräckligt vakuum aldrig uppnås. Dessutom kyls det ner i förångningsprocessen vilket inom kort förvandlar det flytande vattnet till is. Detta problem löstes först i slutet av 1990-talet då Manfred Faubel vid Max-Planckinstitutet i Göttingen visade att man kan injicera en tunn vätskestråle, en s.k. mikro-jet i vakuum och därigenom upprätthålla de nödvändiga villkor som krävs för att mäta elektronspektra från vätskor med högt ångtryck. Det är denna metod vi här använt oss av för att studera vattenlösningars mikroskopiska struktur på nya sätt. När nu läsaren på ett ungefär förstår hur våra verktyg fungerar, skall vi ta en kort titt på de problem som behandlas i denna avhandling samt vad vi kommit fram till.

Dagens forskare har ännu en ofullständig bild av hur vätskeytor är sammansatta och beter sig, inte minst av hur lösta saltjoner och molekyler fördelar sig vid gränsskiktet mellan vatten och luft på den molekylära längdskalan. Eftersom två tredjedelar av jordens yta upptas av en gigantisk och komplex saltvattenlösning, som vi i vardagstal kallar haven, måste detta rimligen betraktas som ett ganska stort hål i kunskapen om vår direkta omgivning. Dessutom är den totala ytan av alla vattendroppar i atmosfären ovanför våra huvuden enorm; dess totala area övergår världshavens med mer än en faktor tusen![3] Men, kan man invända, det är ju ändå en försvinnande liten del av molekylerna som sitter i gränsskiktet mot luften jämfört med de som befinner sig inne i vätskan! Spelar dessa vattenytor egentligen någon praktisk roll? Jo, de är faktiskt viktiga för en lång rad atmosfärskemiska reaktioner – eftersom det är vid

[3]Kom ihåg att förhållandet mellan ytarean och volymen av en sfärisk partikel med radien r, såsom en liten vattendroppe, skalar med $1/r$. Det betyder att andelen molekyler som befinner sig i ytskiktet blir större och större ju mindre partikeln blir.

Figur 8.1: Hur ser ytan av en saltvattenlösning ut på molekylär nivå? Det visar sig att vissa sorters saltjoner är bortstötta från de yttersta ytlagren medan andra har möjligheten att ta sig hela vägen ut till ytan.

ytorna som salter och molekyler lösta i vattnet kan komma i kontakt med molekyler i den omgivande luften och reagera med dessa. Det var dock först i början av 2000-talet som forskare fick upp ögonen för ett antal oväntade reaktioner vid vattenytor vilka är av stor vikt för atmosfärens kemiska sammansättning. Till exempel bildas det klorgas, Cl_2, i förvånande stora mängder ovanför haven när solen skiner. Detta måste innebära att klorsalter i ytan av havsvattnet och av havsvattensdroppar reagerar med gasmolekyler i luften under ljusets inverkan. Men detta borde inte vara möjligt enligt klassiska teorier, vilka förutsäger att saltjoner skall vara bortstötta från de yttersta molekyllagren i vattenlösningar (se tex. beskrivningen av Onsagers och Samaras klassiska modell i avsnitt 4.3). Denna spänning mellan experimentella resultat och klassisk teori har genererat en fascinerande utveckling under de senaste åren. Det har visat sig att våra tidigare teorier om hur joner beter sig nära vattenytan varit allt för enkla och forskare börjar nu bli eniga om att vissa saltjoner, framförallt stora och negativa joner såsom jodid, I^-, kan ta sig ut till ytan och kanske rent av anrikas där. Andra joner, som den mindre natriumjonen, Na^+, beter sig däremot mer som man tidigare trott. Man har med andra ord upptäckt att olika sorters joner har olika ”personlighetsdrag” vid vattenytan, vilket gör dess fysik och kemi mycket rikare, mer spännande men också betydligt mer komplicerad än man tidigare kunnat föreställa sig. Denna typ av fenomen kallas jonspecificitet, ett återkommande begrepp i denna avhandling.

Genom att utnyttja fotoelektronspektroskopins imponerande ytkänslighet har vi undersökt hur olika faktorer påverkar sammansättningen av vattenlösningars ytor. Till exempel har vi funnit att ytfördelningen av saltjoner påverkas av den totala saltkoncentrationen på ett icke-trivialt

sätt. Detta beror på att partiklarna är elektriskt laddade och att deras inbördes växelverkningar blir allt viktigare vid högre salthalter, vilket även påverkar deras beteende vid vattenytan. Vi har även funnit att olika sorters salter ibland skiktar sig i ytlagren om de blandas i samma vattenlösning, en effekt som kan vara viktig för en rad atmosfärskemiska reaktioner vid havsvattenytan. Vi har också studerat hur styrkan av syror förändras när de befinner sig nära vattenytan jämfört med inne i vätskan – det visar sig att dom i regel är mycket svagare vid ytan.

Ett annat mål i denna avhandling är att karaktärisera vilken typ av information fotoelektronspektroskopi kan ge om kemiska tillstånd och vätebindningsmönster av molekyler lösta i vatten. Det finns idag ett antal etablerade spektroskopiska metoder, såsom infrarödspektroskopi (IR) och kärnmagnetisk resonansspektroskopi (NMR), som rutinmässigt används för att undersöka strukturen av lösta molekyler. Dessa har sina respektive för- och nackdelar beroende på vilken egenskap man är intresserad av att undersöka. Genom att utnyttja det *kemiska skiftet* i en molekyls fotoelektronspektrum, vilket energimässigt särskiljer atomer i en molekyl med olika lokala omgivningar, visar vi här att metoden är känslig för den lokala laddningen av lösta molekylers funktionella grupper. Detta kan bland annat användas för att karaktärisera hur syra/baseegenskaperna av specifika grupper förändras beroende på externa faktorer. Det visar sig även att fotoelektronspektra är känsliga för de lokala vätebindningsmönstren runt de olika delarna av lösta molekyler. Vår slutsats är att fotoelektronspektroskopi är en lovande kandidat för kemisk karaktärisering som kan ge komplementär information till redan etablerade tekniker när det gäller molekyler i vattenlösning.

Den sista delen av denna avhandling behandlar laddningsöverföringar i vattenlösningar på tidsskalan av några få femtosekunder, dvs. 10^{-15} sekunder. Detta är verkligen ultra-snabba processer som är väldigt svåra att studera genom experiment. Fotoelektronspektroskopi med röntgenljus ger oss dock möjligheten att använda ett trick. Föreställ dig elektronstrukturen i ett material som ett korthus där de olika våningarna representerar olika hårt bundna elektroner. De lättast bundna elektronerna, *valenselektronerna*, är på våningen längst upp. Dessa kan vi ta bort utan att något kort på någon annan våning påverkas. Om vi har tillräckligt hög energi på vårt ljus kan vi dock hastigt och lustigt ta bort *core-elektroner*, dessa motsvarar korten på de lägre våningarna. Eftersom vi då skapat ett väldigt instabilt tillstånd kommer elektroner från högre nivåer falla ner i detta core-hål. För korthuset tar denna process någon tiondels sekund men i molekyler går detta istället på några femtosekunder, det vill säga just den tidsskalan vi är intresserad av. Överkottsenergin som frigörs vid kollapsen av core-hålet kan med stor sannolikhet slå ut en annan elektron

i det som kallas en Augerprocess. Genom att studera Augerelektronernas spektrum kan vi således lära oss om diverse elektroniska processer på svindlande korta tidsskalor. Vi har bland annat använt denna metod för att studera hur elektronhopp mellan vattenmolekyler påverkas av den lokala omgivningen, t.ex. om de binder till lösta saltjoner.

Sammanfattningsvis behandlar denna doktorsavhandling något så till synes vardagligt som vatten och vattenlösningar. Med hjälp av fotoelektronspektroskopi, en kraftfull metod som endast nyligen kunde appliceras på dessa system, har jag och mina kolleger utforskat en rad svårfångade fenomen, t.ex. hur olika saltjoner fördelar sig vid vattenytan. Vissa av våra resultat är spännande i sig, andra är mer lovande för möjliga framtida tillämpningar. Jag har i alla fall gjort mitt bästa för att utreda vad detta nya verktyg kan erbjuda kemister och fysiker i deras framtida forskning.

9. Acknowledgments

First and foremost I would like to thank my supervisors: Svante Svensson, Olle Björneholm and Gunnar Öhrwall. Svante is truly a source of inspiration and his enthusiasm for science seems to know no limits. I am most grateful for his never-failing support, which started right from the first day I got to Uppsala. Olle is what one can call an ideal stealth-supervisor; not once during the last four years have I felt that he has directly told me what to do. But by always being there when I have had questions and through our everyday discussions – often over lunch or a cup of coffee – I have learned tremendous amounts from him. Gunnar is also an extraordinary guy who has taught me a great deal about electron spectroscopy and experimental physics in general. Beamtimes have definitely been more enjoyable thanks to him and his good spirits.

In practice I have had yet another supervisor, namely Bernd Winter. From that I started my diploma work with him in 2006, he has continuously taught me endless things; about doing experiments, about writing papers, and about generally getting things done. Most importantly, he early on managed to convey to me a feeling that what we are doing is important; something that really sparked my interest for experimental physics and for which I will be forever grateful!

Manfred Faubel should be acknowledged for many things. Besides inventing the liquid micro-jet (which made this thesis work possible!) he has also been a great collaborator and mentor, always willing to share interesting physical insight or just a good story. As a result, I have many good memories from the long and intense beamtimes we did together!

I would also like to take the chance to thank Emad F. Aziz; for the good moments at the U-41 beamline and for our numerous successful projects together.

Special thanks goes to Pavel Jungwirth for an enjoyable and most fruitful collaboration that has run like a red thread throughout my PhD studies. I also want to thank all the members of Pavel's kick-ass group, for our numerous joint projects and for always making me feel welcome during my visits in Prague: Robert, Lukasz, Honza, Ondrej and the rest of the guys in the Canon-building. Erik Wernersson is especially acknowledged for his many valuable comments on drafts of this thesis. Knut Børve has taught me a lot about electronic structure and spectrum calculations for which I am grateful. Daniel Spångberg is also gratefully acknowledged for our many stimulating discussions throughout the years,

for his constructive comments on this thesis as well as for providing me with structures from his MD simulations, which I have used for producing some of the pictures in chapter 2. Thanks to Micahel Odelius for our numerous enlightening and creative chats, I'm so glad that we managed to produce such a nice paper in the end! Thanks also to Maxim Fedorov and Anastasia Romanova for a most effective and fun collaboration!

Greetings to my colleagues at the Ångström laboratory in Uppsala – fellow Ph.D. students, former group members and diploma workers with whom I have had the pleasure to work with on a daily basis: Susanna Kaufmann, Henrik Bergersen, Nina Shariati, Ronny Knut, Davide Ragazzon, Stefan Plogmaker, Andreas Schaefer, Rebecka Schölin, Andreas Lindblad, Torbjörn Rander, Aldana Rosso, Oksana Travnikova, Zhuo Bao, Pål Palmgren, Johan Forsberg, Håkan Hollmark, Paw Kristiansen, Johan Vegelius, Ev Henke, Ioana Bradeanu, Sébastien Legendre as well as the senior research staff. Special thanks goes to Wandared Pokapanich who has been my office mate and liquid-jet companion through the years and Johan Söderström who has been a good friend and colleague. Also, my regards to the dynamic trio down in Lund; Maxim, Thomas and Chaofan!

Thanks to Robert Seidel and Stephan Thürmer for all the help at BESSY and for providing a nice atmosphere when I visit you guys. Keep up the good work, both of you!

Science isn't everything though, and I am grateful to all my friends who constantly remind me of that! An homage goes to Vier Brillen; Olle, Stoffe, Peo, Joen, Krille and Ödman, for still letting me join in on the guitar whenever I'm in Göteborg! Special thanks to Joen who provided me with the marvelous illustrations for chapters 1 and 8. I'm also grateful to Martin and the rest of Johansson och det starka bandet for musical adventures extraordinaire – let's get back on the road at some point, I miss it!

All my love goes to my dear family that I constantly miss here in Uppsala; Mom and Dad, Myrra and Pia, Magnus, Elisabeth, Stina and Gunnar, Kristina and Mats, as well as Karin and Tobbe.

And Bessa, my love, thanks for just making life great!

10. Bibliography

[1] G. Mie, Ann. Physik **11**, 657 (1903).

[2] J. Lennard-Jones, Proc. Phys. Soc. London **43**, 461 (1931).

[3] M. A. Henderson, Surf. Sci. Rep. **46** (2002).

[4] W. M. Latimer and W. H. Rodebush, J. Am. Chem. Soc. **42**, 1419 (1920).

[5] J. Guo, Y. Luo, A. Augustsson, J. Rubensson, C. Såthe, H. Ågren, H. Siegbahn, and J. Nordgren, Phys. Rev. Lett. **89**, 137402 (2002).

[6] T. K. Ghanty, V. N. Staroverov, P. R. Koren, and E. R. Davidson, J. Am. Chem. Soc. **122**, 1210 (2000).

[7] H. Umeyama and K. Morokuma, J. Am. Chem. Soc. **99**, 1316 (1977).

[8] A. D. Buckingham, J. E. D. Bene, and S. A. C. McDowell, Chem. Phys. Lett. **463**, 1 (2008).

[9] E. Espinosa, E. Molins, and C. Lecomte, Chem. Phys. Lett. **285**, 170 (1998).

[10] R. C. Dougherty and L. N. Howard, Biophys. Chem. **105**, 269 (2003).

[11] A. K. Soper, Chem. Phys. **258**, 121 (2000).

[12] R. H. Tromp, P. Postorino, G. W. Neilson, M. A. Ricci, and A. K. Soper, J. Chem. Phys. **101**, 6210 (1994).

[13] A. Botti, F. Bruni, S. Imberti, M. A. Ricci, and A. K. Soper, J. Chem. Phys. **121**, 7840 (2004).

[14] M. Krack, A. Gambirasio, and M. Parrinello, J. Chem. Phys. **117**, 9409 (2002).

[15] J. M. Sorenson, G. Hura, R. M. Glaeser, and T. Head-Gordon, J. Chem. Phys. **113**, 9149 (2000).

[16] Y. Marechal, J. Mol. Struct. **700**, 217 (2004).

[17] A. K. Soper, G. W. Neilson, J. E. Enderby, and R. A. Howe, J. Phys. C: Solid State Phys. **10**, 17931801 (1977).

[18] S. R. Dillon and R. C. Dougherty, J. Phys. Chem. A **106**, 7647 (2002).

[19] A. K. Soper, J. Phys.: Cond. Matt. **9**, 2717 (1997).

[20] P. Postorino, R. H. Tromp, M. A. Ricci, A. K. Soper, and G. W. Neilson, Nature **366**, 668 (1993).

[21] R. Leberman and A. K. Soper, Nature **378**, 364 (1995).

[22] G. Hura, D. Russo, R. M. Glaeser, T. Head-Gordon, M. Krack, and M. Parrinello, Phys. Chem. Chem. Phys. **5**, 1981 (2003).

[23] T. Head-Gordon and G. Hura, Chem. Rev. **102**, 2651 (2002).

[24] M. L. Cowan, B. D. Bruner, N. Huse, J. R. Dwyer, B. Chugh, E. T. J. Nibbering, T. Elsaesser, and R. J. D. Miller, Nature **434**, 199 (2005).

[25] N. Huse, S. Ashihara, E. T. J. Nibbering, and T. Elsaesser, Chem. Phys. Lett. **404**, 389 (2005).

[26] S. Woutersen and H. J. Bakker, Nature **402**, 507 (1999).

[27] P. Wernet, D. Nordlund, U. Bergmann, M. Cavalleri, M. Odelius, H. Ogasawara, L. A. Näslund, T. K. Hirsch, L. Ojamäe, P. Glatzel, et al., Science **304**, 995 (2004).

[28] R. Wang, H. Kreuzer, and M. Grunze, Phys. Chem. Chem. Phys. **8**, 4744 (2006).

[29] M. Cavalleri, M. Odelius, D. Nordlund, A. Nilsson, and L. Pettersson, Phys. Chem. Chem. Phys. **7**, 2854 (2005).

[30] J. Smith, C. Cappa, K. Wilson, B. Messer, R. Cohen, and R. Saykally, Science **306**, 851 (2004).

[31] Y. Mantz, B. Chen, and G. J. Martyna, J. Phys. Chem. B **110**, 3540 (2006).

[32] R. Bukowski, K. Szalewicz, G. Groenenboom, and A. van der Avoird, Science **315**, 1249 (2007).

[33] J. Smith, C. Cappa, K. Wilson, R. Cohen, P. Geissler, and R. Saykally, Proc. Nat. Acad. Sci. U.S.A. **102**, 14171 (2005).

[34] M. Leetmaa, K. T. Wikfeldt, M. P. Ljungberg, M. Odelius, J. Swenson, A. Nilsson, and L. G. M. Pettersson, J. Chem. Phys. **129**, 084502 (2008).

[35] O. Fuchs, M. Zharnikov, L. Weinhardt, M. Blum, M. Weigand, Y. Zubavichus, M. Bär, F. Maier, J. D. Denlinger, C. Heske, et al., Phys. Rev. Lett. **100**, 027801 (2008).

[36] T. Tokushima, Y. Harada, O. Takahashi, Y. Senba, H. Ohashi, L. Pettersson, A. Nilsson, and S. Shin, Chem. Phys. Lett. **460**, 387 (2008).

[37] M. Odelius, Phys. Rev. B. **79**, 144204 (2009).

[38] M. Eigen, Angew. Chem. Int. Ed. Engl. **3**, 1 (1964).

[39] G. Zundel, Adv. Chem. Phys. **111**, 1 (2000).

[40] S. Woutersen and H. J. Bakker, Phys. Rev. Lett. **96**, 138305 (2006).

[41] M. Cavalleri, L.-Å. Näslund, D. C. Edwards, P. Wernet, H. Ogasawara, S. Myneni, L. Ojamäe, M. Odelius, A. Nilsson, and L. G. M. Pettersson, J. Chem. Phys. **124**, 194508 (2006).

[42] C. de Grotthuss, Ann. Chim. **58**, 54 (1806).

[43] P. B. Petersen and R. J. Saykally, J. Phys. Chem. B **109**, 7976 (2005).

[44] R. Vacha, V. Buch, A. Milet, J. P. Devlin, and P. Jungwirth, Phys. Chem. Chem. Phys. **9**, 4736 (2007).

[45] J. K. Beattie, Phys. Chem. Chem. Phys. **10**, 330 (2008).

[46] R. Vacha, V. Buch, A. Milet, J. P. Devlin, and P. Jungwirth, Phys. Chem. Chem. Phys. **10**, 332 (2008).

[47] J. Beattie, A. Djerdjev, and G. Warr, Faraday Discuss. **141**, 31 (2009).

[48] D. Spångberg and K. Hermansson, J. Chem. Phys. **120**, 4829 (2004).

[49] M. Born, Z. Phys. **1**, 45 (1920).

[50] R. Weber, B. Winter, P. M. Schmidt, W. Widdra, I. V. Hertel, M. Dittmar, and M. Faubel, J. Phys. Chem. B **108**, 4729 (2004).

[51] M. Cossi, V. Barone, R. Cammi, and J. Tomasi, Chem. Phys. Lett. **255**, 327 (1996).

[52] K. D. Collins, G. W. Neilson, and J. E. Enderby, Biophys. Chem. **128**, 95 (2007).

[53] D. Chandler, Nature **437**, 640 (2005).

[54] S. Hüfner, *Photoelectron spectroscopy* (Springer Verlag, Berlin, 1995).

[55] J. Stöhr, *NEXAFS Spectroscopy (Springer Series in Surface Sciences)* (Springer Verlag, Berlin, 1992).

[56] A. Einstein, Ann. Phys. **17**, 132 (1905).

[57] G. Öhrwall, R. F. Fink, M. Tchaplyguine, L. Ojamäe, M. Lundwall, R. R. T. Marinho, A. N. de Brito, S. L. Sorensen, M. Gisselbrecht, R. Feifel, et al., J. Chem. Phys. **123**, 054310 (2005).

[58] M. P. Seah and W. A. Dench, Surf. Interface Anal. **1**, 2 (1979).

[59] K. Siegbahn, C. Nordling, A. Fahlmann, R. Nordberg, K. Hamrin, J.Hedman, G.Johansson, T. Bergmark, S. Karlsson, I. Lindgren, et al., *ESCA - atomic, molecular, and solid state structure studied by means of electron spectroscopy* (Almqvist och Wiksells, Uppsala, 1967).

[60] K. Siegbahn, C. Nordling, G. Johansson, J. Hedman, P. Heden, K. Hamrin, U. Gelius, T. Bergmark, L. Werme, R. Manne, et al., *ESCA applied to free molecules* (North Holland, Amsterdam, 1969).

[61] H. Siegbahn and K. Siegbahn, J. Electron. Spectrosc. Relat. Phenom. **2**, 319 (1973).

[62] H. Siegbahn, J. Phys. Chem. **89**, 897 (1985).

[63] M. Faubel, S. Schlemmer, and J. P. Toennies, Z. Phys. D: At., Mol. Clusters **10**, 269 (1988).

[64] M. Faubel, B. Steiner, and J. P. Toennies, J. Chem. Phys. **106**, 9013 (1997).

[65] J.-H. Guo, Y. Luo, A. Augustsson, S. Kashtanov, J.-E. Rubensson, D. K. Shuh, H. Ågren, and J. Nordgren, Phys. Rev. Lett. **91**, 157401 (2003).

[66] J. Forsberg, J. Gråsjö, B. Brena, J. Nordgren, L. C. Duda, and J.-E. Rubensson, Phys. Rev. B. **79**, 132203 (2009).

[67] D. M. Mills, ed., *Third-generation hard X-ray synchrotron radiation sources - Source properties, optics and experimental techniques* (Wiley-Interscience, New York, 2002).

[68] D. Iwanenko and J. Pomeranchuck, Phys. Rev. **65**, 343 (1944).

[69] A. Hofmann, *The physics of synchrotron radiation* (Cambridge University Press, Cambridge, 2004).

[70] G. Margaritondo, *Introduction to synchrotron radiation* (Oxford University Press, New York, 1988).

[71] M. Bässler, J. Forsell, O. Björneholm, R. Feifel, M. Jurvansuu, S. Aksela, S. Sundin, S. L. Sorensen, R. Nyholm, A. Ausmees, et al., J. Electron. Spectrosc. Relat. Phenom. **101-103**, 953 (1999).

[72] H. Bergersen, R. R. T. Marinho, W. Pokapanich, A. Lindblad, O. Björneholm, L. J. Saethre, and G. Öhrwall, J. Phys.: Cond. Matt. **19**, 326101 (2007).

[73] *http://www.microliquids.com/*.

[74] R. Weber, Ph.D. thesis, Freie Universität, Berlin (2003).

[75] B. Winter, R. Weber, W. Widdra, M. Dittmar, M. Faubel, and I. V. Hertel, J. Phys. Chem. A **184**, 2625 (2004).

[76] B. Winter and M. Faubel, Chem. Rev. **106**, 1176 (2006).

[77] B. Winter, Nucl. Instr. Meth. A **601**, 139 (2009).

[78] E. F. Aziz, Ph.D. thesis, Freie Universität, Berlin (2007).

[79] E. F. Aziz, A. Zimina, M. Freiwald, S. Eisebitt, and W. Eberhardt, J. Chem. Phys. **124**, 114502 (2006).

[80] E. F. Aziz, M. Freiwald, S. Eisebitt, and W. Eberhardt, Phys. Rev. B. **73**, 75120 (2006).

[81] D. Coster and R. D. L. Kronig, Physica **2**, 13 (1935).

[82] R. M. P. van der Straten and A. Niehaus, Z. Phys. D: At., Mol. Clusters **8**, 35 (1988).

[83] *http://www.physics.utu.fi/en/research/material_science/fitting.html*.

[84] *http://www.wavemetrics.com/.*

[85] B. J. Finlayson-Pitts, *Chemistry of the upper and lower atmosphere - Theory, experiment, and applications* (Academic Press, San Diego, 2000).

[86] B. Finlayson-Pitts, Chem. Rev. **103**, 4801 (2003).

[87] E. M. Knipping, M. J. Lakin, K. L. Foster, P. Jungwirth, D. J. Tobias, R. B. Greber, D. Dabdub, and B. J. Finlayson-Pitts, Science **288**, 301 (2000).

[88] C. W. Spicer, E. G. Chapman, B. J. Finlayson-Pitts, R. A. Plastridge, J. M. Hubbe, J. D. Fast, and C. M. Berkowitz, Nature **394**, 353 (1998).

[89] K. W. Oum, M. J. Lakin, D. O. DeHann, T. Brauers, and B. J. Finlayson-Pitts, Science **279**, 74 (1998).

[90] J. W. Gibbs, *The collected works of J. Willard Gibbs* (Longmans, New York, 1928).

[91] C. Wagner, Phys. Zeitschr. **25**, 474 (1924).

[92] L. Onsager and N. N. T. Samaras, J. Chem. Phys. **2**, 528 (1934).

[93] P. Jungwirth and D. J. Tobias, Chem. Rev. **106**, 1259 (2006).

[94] L. X. Dang and T. M. Chang, J. Phys. Chem. B **106**, 235 (2002).

[95] P. Jungwirth and D. J. Tobias, J. Phys. Chem. B **105**, 10468 (2001).

[96] L. Vrbka, M. Mucha, B. Minofar, P. Jungwirth, E. C. Brown, and D. J. Tobias, Curr. Opin. Colloid Interface Sci. **9**, 67 (2004).

[97] Y. Levin, A. P. dos Santos, and A. Diehl, Phys. Rev. Lett. **103**, 257802 (2009).

[98] Y. Levin, Phys. Rev. Lett. **102**, 147803 (2009).

[99] V. S. Markin and A. G. Volkov, J. Phys. Chem. B **106**, 11810 (2002).

[100] D. Horinek, A. Herz, L. Vrbka, F. Sedlmeier, S. I. Mamatkulov, and R. R. Netz, Chem. Phys. Lett. **479**, 173 (2009).

[101] A. Akkerman and E. Akkerman, J. Appl. Phys. **86**, 5809 (1999).

[102] D. Emfietzoglou and H. Nikjoo, Radiat. Res. **163**, 98 (2005).

[103] D. Emfietzoglou, F. A. Cucinotta, and H. Nikjoo, Radiat. Res. **164**, 202 (2005).

[104] A. Jablonski and C. J. Powell, J. Electron. Spectrosc. Relat. Phenom. **100**, 137 (1999).

[105] M. Faubel, in *Photoionization and Photodetachment, Part I*, edited by C. Y. Ng (World scientific, Singapore, 2000).

[106] G. Markovich, S. Pollack, R. Giniger, and O. Cheshnovsky, J. Chem. Phys. **101**, 9344 (1994).

[107] S. Ghosal, J. C. Hemminger, H. Bluhm, B. S. Mun, E. L. D. Hebenstreit, G. Ketteler, D. F. Ogletree, F. Requejo, and M. Salmeron, Science **307**, 563 (2005).

[108] A. W. Morris and J. P. Riley, Deep Sea Res. Oceanogr. Abstr. **13**, 699 (1966).

[109] A. K. Covington, T. H. Lilley, and R. A. Robinson, J. Phys. Chem. **72**, 2759 (1968).

[110] D. Asthagiri, L. R. Pratt, J. D. Kress, and M. A. Gomez, Proc. Natl Acad. Sci. USA **101**, 7229 (2004).

[111] P. Jungwirth, Faraday Discuss. **141**, 9 (2009).

[112] M. K. Petersen, S. S. Iyengar, T. J. F. Day, and G. A. Voth, J. Phys. Chem. B **108**, 14804 (2004).

[113] M. Mucha, T. Frigato, L. M. Levering, H. C. Allen, D. J. Tobias, L. X. Dang, and P. Jungwirth, J. Phys. Chem. B **109**, 7617 (2005).

[114] B. Winter, M. Faubel, R. Vácha, and P. Jungwirth, Chem. Phys. Lett. **474**, 241 (2009).

[115] J. K. Beattie, Lab on a Chip **6**, 1409 (2006).

[116] P. Atkins and J. de Paula, *Physical Chemistry* (Freeman, W. H. Ed.; OUP: Oxford, 2001).

[117] E. Avarez, G. Vazquez, M. Sanchez-Vilas, B. Sanjurjo, and J. M. Navaza, J. Chem. Eng. Data **42**, 957 (1997).

[118] K. Granados, J. Gracia-Fadrique, A. Amigo, and R. J. Bravo, Chem. Eng. Data **51**, 1356 (2006).

[119] V. Augugliaro, S. Coluccia, V. Loddo, L. Marchese, G. Martra, L. Palmisano, and M. Schiavello, Appl. Cat. B **20**, 15 (1999).

[120] H. Ågren and H. Siegbahn, J. Chem. Phys. **81**, 488 (1984).

[121] H. Ågren and H. Siegbahn, Chem. Phys. **95**, 37 (1985).

[122] B. Winter, E. F. Aziz, U. Hergenhahn, M. Faubel., and I. V. Hertel, J. Chem. Phys. **126**, 124504 (2007).

[123] H. Ågren and K. V. Mikkelsen, J. Mol. Struct. **243**, 425 (1991).

[124] R. Seidel, M. Faubel, B. Winter, and J. Blumberger, J. Am. Chem. Soc. **131**, 16127 (2009).

[125] J. Moens, R. Seidel, P. Geerlings, M. Faubel, B. Winter, and J. Blumberger, J. Phys. Chem. B **114**, 9173 (2010).

[126] K. Mardia, J. Kent, and J. Bibby, *Multivariate Analysis* (Academic Press, 1979).

[127] D. Ghosh, Cell Mol. Life Sci. **64**, 2013 (2007).

[128] N. Lebrun, P. Dhamelincourt, C. Focsa, B. Chazallon, J. L. Destombes, and D. Prevost, J. Raman Spectrosc. **34**, 459 (2003).

[129] A. P. Hitchcock and C. E. Brion, J. Electron. Spectrosc. Relat. Phenom. **19**, 231 (1980).

[130] I. Ishii and A. P. Hitchcock, J. Chem. Phys. **87**, 830 (1987).

[131] S. G. Urquhart, A. P. Hitchcock, R. D. Priester, and E. G. Rightor, J. Pol. Sci. B **33**, 1603 (1995).

[132] L. S. Cederbaum, J. Zobeley, and F. Tarantelli, Phys. Rev. Lett. **79**, 4778 (1997).

[133] R. Santra, J. Zobeley, L. S. Cederbaum, and N. Moiseyev, Phys. Rev. Lett. **85**, 4490 (2000).

[134] S. Marburger, O. Kugeler, U. Hergenhahn, and T. Möller, Phys. Rev. Lett. **90**, 203401 (2003).

[135] G. Öhrwall, M. Tchaplyguine, M. Lundwall, R. Feifel, H. Bergersen, T. Rander, A. Lindblad, J. Schulz, S. Peredkov, S. Barth, et al., Phys. Rev. Lett. **93**, 173401 (2004).

[136] M. Mucke, M. Braune, S. Barth, M. Forstel, T. Lischke, V. Ulrich, T. Arion, U. Becker, A. Bradshaw, and U. Hergenhahn, Nature Physics **6**, 143 (2010).

[137] O. Björneholm, A. Nilsson, A. Sandell, B. Hernnäs, and N. Mårtensson, Phys. Rev. Lett. **68**, 1892 (1992).

[138] P. Maciejewski, U. Höfer, W. Wurth, and E. Umbach, J. Electron. Spectrosc. Relat. Phenom. **62**, 1 (1993).

[139] J. Schnadt, P. A. Brühwiler, L. Patthey, J. N. O'Shea, S. Södergren, M. Odelis, R. Ahuja, O. Karis, M. Bässler, P. Persson, et al., Nature **418**, 620 (2002).

[140] M. Fahlman, A. Crispin, X. Crispin, S. K. M. Henze, M. P. d. Jong, W. Osikowicz, C. Tengstedt, and W. R. Salaneck, J. Phys.: Condens. Matter **19**, 183202 (2007).

[141] A. Föhlisch, S. Vijayalakshmi, F. Hennies, W. Wurth, V. Medicherla, and W. Drube, Chem. Phys. Lett. **434**, 214 (2007).

[142] A. Föhlisch, P. Feulner, F. Hennies, A. Fink, D. Menzel, D. Sanchez-Portal, P. M. Echenique, and W. Wurth, Nature **436**, 373 (2005).

[143] N. Agmon, Chem. Phys. Lett. **244**, 456 (1995).

[144] N. B. Librovich, V. P. Sakun, and N. D. Sokolov, Chem. Phys. **39**, 351 (1979).

[145] A. Botti, F. Bruni, S. Imberti, M. A. Ricci, and A. K. Soper, J. Chem. Phys. **120**, 10154 (2004).

[146] M. E. Tuckerman, D. Marx, and M. Parrinello, Nature **417**, 925 (2002).

[147] C. Cappa, J. Smith, B. Messer, R. Cohen, and R. Saykally, J. Phys. Chem. A **111**, 4776 (2007).

[148] B. Winter, E. F. Aziz, N. Ottosson, M. Faubel, N. Kosugi, and I. V. Hertel, J. Am. Chem. Soc. **130**, 7130 (2008).

[149] B. Winter, U. Hergenhahn, M. Faubel, O. Björneholm, and I. V. Hertel, J. Chem. Phys. **127**, 094501 (2007).

[150] D. Nordlund, H. Ogasawara, H. Bluhm, O. Takahashi, M. Odelius, M. Nagasono, L. G. M. Pettersson, and A. Nilsson, Phys. Rev. Lett. **99**, 217406 (2007).

[151] P. H. Citrin, G. K. Wertheim, and Y. Baer, Phys. Rev. Lett. **35**, 885 (1975).

[152] D. Nolting, N. Ottosson, M. Faubel, I. V. Hertel, and B. Winter, J. Am. Chem. Soc. **130**, 8150 (2008).

Acta Universitatis Upsaliensis

Digital Comprehensive Summaries of Uppsala Dissertations from the Faculty of Science and Technology 828

Editor: The Dean of the Faculty of Science and Technology

A doctoral dissertation from the Faculty of Science and Technology, Uppsala University, is usually a summary of a number of papers. A few copies of the complete dissertation are kept at major Swedish research libraries, while the summary alone is distributed internationally through the series Digital Comprehensive Summaries of Uppsala Dissertations from the Faculty of Science and Technology. (Prior to January, 2005, the series was published under the title "Comprehensive Summaries of Uppsala Dissertations from the Faculty of Science and Technology".)

Distribution: publications.uu.se
urn:nbn:se:uu:diva-151435

ACTA
UNIVERSITATIS
UPSALIENSIS
UPPSALA
2011